Stability of a eutectic interface during directional solidification

by

Seung Hoon Han

A Dissertation Submitted to the

Graduate Faculty in Partial Fulfillment of the

Requirements for the Degree of

DOCTOR OF PHILOSOPHY

Department: Materials Science and Engineering
Major: Metallurgy

Approved:

Signature was redacted for privacy.

In Charge of Major Work

Signature was redacted for privacy.

For the Major Department

Signature was redacted for privacy.

For the Graduate College

Iowa State University
Ames, Iowa

1995

TABLE OF CONTENTS

	Page
CHAPTER 1: GENERAL INTRODUCTION	1
I. Background	1
II. Dissertation Organization	7
References	9
CHAPTER 2: DIRECTIONAL SOLIDIFICATION OF THE ALUMINA-ZIRCONIA EUTECTIC SYSTEM	10
Abstract	10
I. Introduction	11
II. Experimental	13
III. Results	16
(1) Microstructural Observations	16
(2) Microstructural Scales	22
(3) Effects of Impurity	22
IV. Discussion	26
(1) Microstructures	26
(2) Eutectic Spacing	29
(3) Colony and Dendrite Spacing	32
V. Conclusions	33
Acknowledgments	33
References	34
CHAPTER 3: COLONY FORMATION DURING EUTECTIC GROWTH	37
Abstract	37
I. Introduction	38
II. Experimental	40
III. Results	42
(1) *Morphological Observations*	43
(2) *Two Phase Planar Interface Instability*	46

(3) Mechanisms of the Formation of Two Phase Cellular and Dendritic Interfaces 46
(4) Mechanism of Eutectic Spacing Adjustment 52
(5) Interface Temperature Variation with Velocity 58
(6) Eutectic and Colony Spacings with Velocity 58

IV. Discussion 62
(1) Colony Formation 62
(2) Interface Temperature Variation with Velocity 65
(3) Eutectic Spacing Variation with Velocity 73
(4) Colony Spacing Variation with Velocity 75

V. Conclusion 76

Acknowledgment 78

References 78

CHAPTER 4: STABILITY OF EUTECTIC MICROSTRUCTURES 82

Abstract 82

I. Introduction 83

II. Experimental 85

III. Results and Discussion 93
(1) Oscillatory Behaviors in Hypoeutectic Composition 93
(2) Oscillatory Behaviors in Hypereutectic Composition 101
(3) Banded Structures 114
(4) Morphological Transitions 118
(5) Coupled Zone Concept 128
(6) Comparison with Oscillatory Structures in Other Systems 134

IV. Conclusions 135

Acknowledgments 136

References 136

CHAPTER 5: GENERAL CONCLUSION 138

I. Alumina-Zirconia Eutectic System 138

II. Colony Formation during Eutectic Growth 139

III. Oscillating Microstructures in Eutectic Growth 140

ACKNOWLEDGMENT 142

CHAPTER 1: GENERAL INTRODUCTION

I. Background

Since the first appearance of human beings on the earth, nature has been the object of curiosity and the challenge of our daily life. Great efforts have been made to understand and utilize nature for our conveniences. This role has been played under the name of "Science" or many times, "Experiences" through our human history. This human history was and still is a history of "Materials" in another point of view. Those who discovered a new material ruled the other groups and enjoyed more privileges than those who did not.

With the invention of fire, the first revolution in materials arrived. People started to shape and fabricate the newly found bronze for better weapons from the melts. Iron age was initiated by those who discovered the materials by pure luck and with developed skill in controlling the fire. Therefore, it can be said the field of metallurgy has a long historical background.

Industrial revolution supported by the knowledge from the classical physics triggered massive manufacturing of steel, and the two world wars made a significant progress in material science as well as other technologies. The emergence of semiconductor and microchip which often is called as "a new stone age" required extremely high purity crystals. Almost all the materials used in our daily life including these high quality crystals underwent the solidification process in some stage of their processing. This solidification is the oldest and still the most common trasformation technique in material processing. This process has been taken into as a natural phenomenon for a long time due to its common practices and complexity of the structures developed. It was not until 40 years ago that the solidification processing was studied with the scientific approach. The beauty of solidification is that a variety of microstructures can be developed during non-equilibrium processing. The microstructures formed here are almost permanent and often very difficult to modify

completely even during the post fabrication procedures. Most of the physical and mechanical properties are heavily dependent on the microstructures of the alloys. Therefore, the understanding and the controlling of the microstructures are vitally important.

Studies on solidification have been traditionally made with casting processes in which the molten metal was poured into a designed mold. However, in the casting, the microstructures developed are often influenced by the geometry of the mold and some of the processing parameters are not controlled independently but coupled. Recently, more fundamental questions started to be answered with the key investigations in the directional solidification method where the processing parameters such as temperature gradient, growth velocity, and composition of the alloy are individually controlled. Systematical analysis is usually provided by changing only one parameter with the others fixed and correlating the microstructures developed with the given conditions during the directional solidification. This broad topic of directional solidification has been a powerful tool on the research for directionally grown turbine blades, in-situ composites, laser prosessing of materials, and the development of electronic materials.

Directional solidification develops basically four different types of morphologies. They are planar, cellular , dendritic and eutectic. These are shown in Figure 1. More are possible with the combination of the two, for example, single phase dendrite plus interdendritic eutectic. The critical aspect of forming microstructures has been studied by experiments on the interface pattern evolution. A specific morphology is selected by the system through the interaction of the given parameters under given experimental conditions. The questions were raised as to what physical principles govern the selection of the pattern and how the microstructural scales are determined. These questions and more were examined in transparent, metal analog systems. Organic analog systems have been chosen because they freeze with structures which are similar to metals but with lower melting temperatures. In addition, all the physical properties are known precisely. These organic

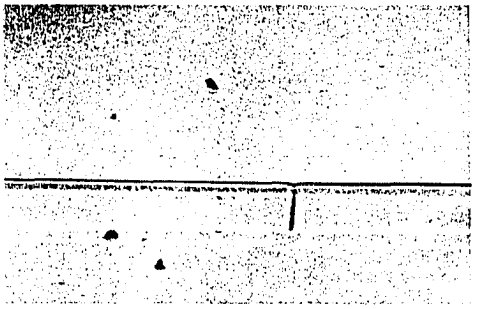

(a)

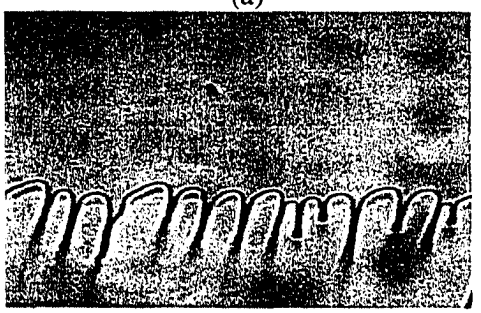

(b)

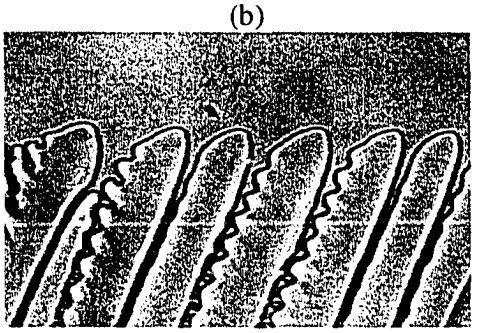

(c)

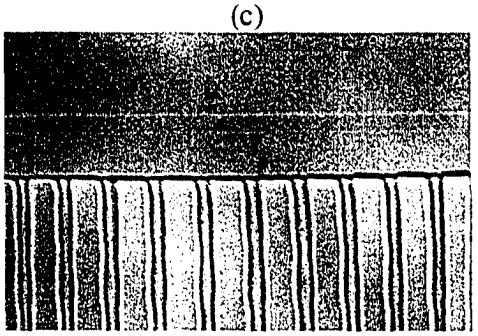

(d)

Figure 1. Four different morphologies formed during directional solidification (a) planar single phase (b) cellular (c) dendritic (d) eutectic interface

systems enhanced our understanding of the dynamic mechanisms of the pattern formation and the selections of microstructural scales with the in-situ observation which is possible due to their transparent property of the systems. In metal systems, this microstructural evolution can only be analyzed after interrupting the growth. Thus, the artificial effect can be involved during the quenching process and dynamic observations are difficult.

In this dissertation, knowledge obtained from single phase solidification studies was extended to eutectic growth which is a simultaneous growth of two different phases. Eutectic microstructures are very important as their potential use as composite materials as well as other applications in the optical and electronic materials. Many experimental work have been made for the steady state growth of lamellar and rod eutectics and theoretical models were proposed for the regular and irregular eutectics. However, most of the previous research has been made on the planar eutectic interface under different experimental conditions. A few studies have been made on the eutectic instabilities from the past.

The objective of this work is to examine the instability problems in eutectic growth during directional solidification. The experimental approach was designed to study the dynamical mechanisms by which the instabilities set in and how the subsequent selections in the microstructures were made. The use of transparent organic analog enables us to observe all the dynamical effects during the solidification process. The system of carbontetrabromide-hexacloroethane (CBr_4-C_2Cl_6) was chosen because this system has been known to produce lamellar eutectics, and has been well characterized by Kaukler [1].

There are three different types of instability problems in the eutectic growth in general. One of the instability is the small wave length instability during the growth. This is mainly caused by the interdiffusion betwen the two phases during the eutectic growth and finally leads to the spacing selection. Dynamical studies by Seetharaman et al. [2, 3] on the lamellar eutectic growth in the same model system revealed that the spacing selection is not very sharp and a band of stable interlamellar spacings is distributed under a given condition.

A stability analysis was performed by Dayte and Langer [4] based on the well-known Jackson and Hunt model on eutectic growth [5]. They showed that within the class of short wave length instabilities the basic microstructures of the binary eutectic growth can be categorized into three different structures. They are (a) steady state structures (b) tilted structures (c) oscillating structures. These structures are shown in Figure 2. The oscillating structures were predicted at off-eutectic compositions and single phase formation from the eutectic was also expected to be related to the finite amplitude of these structures. Recently, morphological instabilities in the binary eutectic system were examined rigorously using the boundary integral technique by Karma and Sarkissian [6]. They mapped out these three structures from their numerical analysis as a function of spacings and compositions. Our experimental work ascertains all these structures and showed general agreement with their prediction.

The second instability involves the formations of single phase cells or dendrites in the presence of interdendritic eutectics. This instability is attributed to the compositional effect on the eutectic microstructures because off-eutectic compositions destabilize the eutectic interface into single phase cells or dendries with interdendritic eutectics under certain conditions. This instability problem has been characterized by many researchers [7~12] based on the Competitive Growth Model (CGM) in which the leading phase is the one that is growing at higher interface temperature. Hence, many experimental studies done so far were compared to the competitive growth models in which two different growth models (one for single phase dendrite, the other for eutectic growth) from their steady state growth were examined. The CGM was experimentally examined in our studies on this instability problem. Our experimental study showed that these transitions from full eutectics to single phase dendrites plus eutectic structures did not occur in the steady state but in the transient state. Therefore, these CGM could not be applied directly to the transitional case.

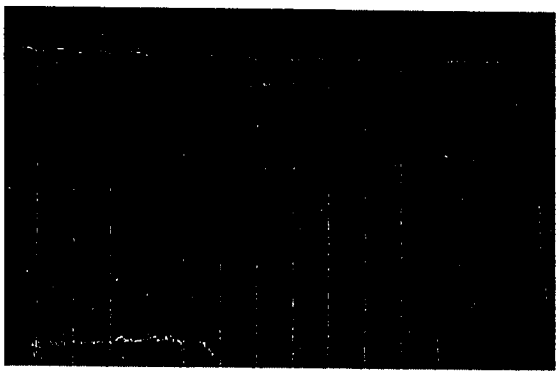

(a)

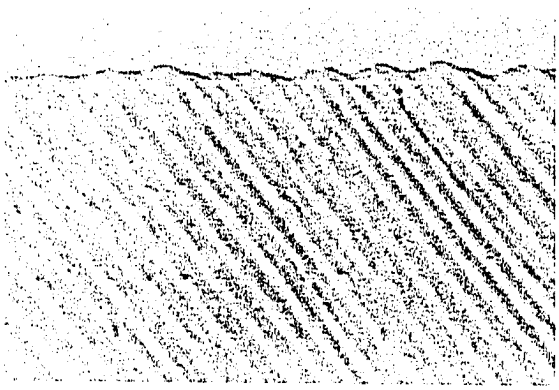

(b)

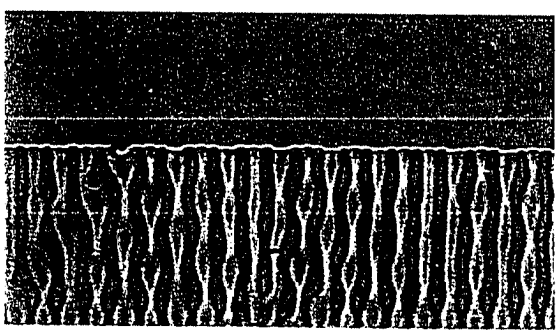

(c)

Figure 2. Three basic eutectic morphologies in the binary system (a) planar eutectics (b) tilted eutectics (c) oscillating eutectic structure

The third instability in the eutectic growth appeared with long wave length which resulted in the breakdown of the planar eutectics into cellular eutectics. This instability was due to the effect of a third impurity. The presence of a third impurity causes a long range diffusion in contrast to the other two instabilities (caused by short range diffusion) mentioned above. Two different morphologies of the colonies were observed and the features of the eutetic cells (colonies) and eutectic dendrites were studied through the experimental approach.

The emphasis in the present work was on the second and third instaibility problems during the eutectic growth. Therefore, the major goal of this work was to characterize the instabilities of planar eutectics relative to the cellular/dendritic structures of a single phase and of two-phase. The precise mechanisms of these instabilities were not understood fully, and especially no quantitative characterizations were made in two-phase cellular/dendritic eutectics before. This work will present the dynamic mechanisms on those two instabilites and the reorganizations of the unstable interface into steady -state structures. The variations in the interface temperatures as well as the spacings (of eutectics and colonies) of two-phase cellualr/dendritic structures from the steady state structures were characterized as a function of veloicty for the first time.

II. Dissertation Organization

This dissertation is written in an alternate format composed of three original manuscripts, preceeded by a general introduction. References cited within each manuscript are placed immediately after the manuscript.

The first manuscript in Chapter 2, "Directional Solidification of the Alumina-Zirconia Eutectic System" will be submitted to *The Journal of Material Science and Engineering* in 1995. The system of Alumina-Zirconia (Al_2O_3-ZrO_2) was chosen because it is a simple eutectic system and the two components are the most commonly studied ceramic materials.

An alternative method of ceramic processing, rather than the conventional sintering of ceramic powders was investigated with directional solidification of a ceramic alloy melt in the Bridgman method. It was thought that through directional solidification, higher density materials could be attained decreasing porosity and improving mechanical properties. Furthermore, directional solidification of the eutectic can provide well aligned composite microstructures, a desirable feature potentially useful for high temperature engine components. Critical experiments have been carried out in hypo (ZrO_2-lean), hyper (ZrO_2-rich), and eutecitc compositions with large velocity range. The microstructures obtained showed colony (eutectic cellular/dendritic) structures almost in all cases. These colony structures, corresponding to the third type of instability , were closely related to the impurities present in initial materials. Poor directionality was also observed due to low thermal conductivities of the materials.

The colony structures observed in the previous chapter led us to studies for understanding the cause of these structural formations and the mechanisms of their formations. This work is presented in Chapter 3, "Colony Formation during Eutectic Growth" and it will be submitted for publication in *The Journal of Metallurgical and Materials Transactions* in 1995. The precise mechanisms of colony formations were studied in a model organic analog system (CBr_4-C_2Cl_6). The interface temperatures of eutectic cells and eutectic dendrites were measured as a function of velocity under a constant temperature gradient. Similar analogy in interface temperature change was found between the eutectic cells and dendrites and those from single phase. Colony spacings were also measured as a function of growth velocity as well as eutectic spacings from the center of the colonies. The experimental results were compared with the existing models and a new model was proposed.

In Chapter 4, the instability of eutectic to single phase cells/dendrites was studied. The manuscript of "Microstructure Selection in Eutectic Growth" will be submitted to *The Journal of Metallurgical and Materials Transactions* in 1995. The commonly used

"Competitive Growth Model" was re-examained in the transitional regime after calculating the coupled zone boundary in the same organic analog system. It was observed that the transitions underwent oscillations between the two different stable morphologies rather than jumping from one stable morphology to the other when the conditions were closer to the threshold value. The actual velocities measured from the dynamical observations were found to fluctuate and their amplitudes were a strong function of compositions. More fluctuations in the actual velociy were observed as the alloy composition deviated further from the eutectic composition under constant velocities. The mechanisms of dendrite appearance and disappearance were closely examined and these mechanisms confirmed the hysterisis effect in the transition.

References

1. Kaukler, W. F. Ph.D. Thesis, University of Toronto, Toronto, ON, Canada, 1981
2. Seetharaman, V.; Trivedi, R. in "Solidification Processing of Eutectic Alloys", D. Stefanescu and G. J. Abbaschian, eds., AIME, Warrendale, PA, 1988.
3. Seetharaman, V.; Trivedi, R. Metall. Trans. 1988, 19A, 2955.
4. Dayte, V.; Langer, J. S. Phys. Rev. 1981, 24B, 4155.
5. Jackson, K. A.; Hunt, J. D. Trans. Metall. Soc. AIME 1966, 236, 1129.
6. Karma, A.; Sarkissian, A. Metall. Trans. 1995, To be published.
7. Hunt, J. D.; Jackson K. A. Trans. Metall. Soc. AIME 1967, 239, 864.
8. Jackson, K. A. Trans. Metall. Soc. AIME 1968, 242, 1275.
9. Mollard, F.; Flemings, M. C. Trans. Metall. Soc. AIME 1967, 239, 1526.
10. Burden, M. H.; Hunt, J. D. J. Cryst. Growth 1974, 22, 328.
11. Kurz, W.;Fisher, D. J. Int. Met. Rev. 1979, 177.
12. Trivedi, R.; Kurz, W. in "Solidification Processing of Eutectic Alloys", D. Stefanescu and G. J. Abbaschian, eds., AIME, Warrendale, PA, 1988.

CHAPTER 2:

DIRECTIONAL SOLIDIFICATION OF THE ALUMINA-ZIRCONIA EUTECTIC SYSTEM

A manuscript to be submitted to the *Journal of Crystal Growth*

S. H. Han, T. Ellis, C. Boldt, and R. Trivedi

Ames Laboratory US-DOE and the Department of Materials Science and Engineering

Iowa State University, Ames, IA 50010

Abstract

Directional solidification experiments have been carried out in Al_2O_3 (alumina)-ZrO_2 (zirconia) system near eutectic compositions by using the Bridgman and the laser scanning techniques. The compositions investigated were 30 wt%, 50 wt%, and 42.5 wt% of ZrO_2 (eutectic composition) and solidification studies were carried out over a wide range of velocity, 2 to 10000 μm/s. In all studies nonplanar eutectic structures were formed which showed the presence of two-phase cellular and dendritic colonies. Different microstructural scales, such as eutectic spacing, colony spacing, and primary cellular/dendritic spacings were examined for different compositions and growth velocities. The formation of different microstructures of stable and metastable phases, over the range of velocities studied, is discussed. The eutectic spacing variation with growth rate is found to show a departures from the existing model based on a planar front growth [20], and this deviation was found to be more singnificant in the higher velocity regime. The colony spacing was found to decrease with increasing velocity in a manner analogous to the variation in the single phase dendrite spacing with velocity. Experimental results on microstructures and spacings are analyzed by using appropriate theoretical models.

I. Introduction

Ceramic materials are potential candidates for application in high temperature components, and microstructural control is critical for engineering applications [1, 2]. In this respect, oxide ceramic eutectics are important since they exhibit very high melting temperatures, usually of the order of 2000 °C, and they also tend to resist oxidation and high temperature creep, and perform well in some corrosive environments [2].

Directional solidification of the Al_2O_3-ZrO_2 system has been carried out previously, and these results are given in Table 1. Most of these studies have centered around utilizing Bridgman and modified Bridgman growth techniques [3-7], in which only a narrow range of the growth rates, between 0.75 and 15.56 cm/hr (2.08 μm/s-43.22 μm/s), were investigated with temperature gradients in the region of 20.0 K/mm [3, 5]. Reported microstructure were eutectic colonies consisting of ZrO_2 rods in a Al_2O_3 matrix [3-7]. The eutectic spacing was somewhat uniform in the center of colonies, but increased towards the boundary with a very coarse structure at the boundaries. Colony spacing and eutectic spacing at the center of colonies were measured, and found to decrease with increasing velocity. The limited data on eutectic spacing were fitted to the planar growth theoretical model of Jackson and Hunt [20].

The major objective of this research was to carry out a more detailed investigation of microstructure formation in ceramic systems. For this study, the Al_2O_3-ZrO_2 system was selected in order to extend previous studies in this system. Also, the phase diagram and physical properties of these materials are well characterized. We have carried out experimental studies over a very wide range of velocities, i.e. 2~10000 μm/s, which includes the range studied previously (2.0~40 μm/s). In our work, additional experiments have also been carried out at V=200 μm/s by using the directional solidification technique, and at V=10^4 μm/s by using the laser scanning technique. Al_2O_3 dendrites at low velocity were found to be highly faceted, whereas ZrO_2 dendrites were found to be nonfaceted.

Table 1. Compilation of data from the literature review concerning Al_2O_3-ZrO_2.

Composition	Method	Velocity µm/sec	Temperature Gradient K/mm	Structures	Reference
Al_2O_3-37 mol% ZrO_2	Bridgman	3.58-43.22	22	colonies w/ ZrO_2 rods	3
Al_2O_3-37 mol% ZrO_2	gradient furnace	2.08 and 2.78	120	no colonies w/ lamellar eutectic	4
Al_2O_3-42 wt.% ZrO_2	flame press. atomization	_____	>1000	amorphous eutectic	5
Al_2O_3-ZrO_2	E.F.G.	3.86, 35.28, and 141.11	_____	colonies w/ rod eutectic	22
Al_2O_3-ZrO_2-Y_2O_3 eutectic	float zone r.f. heating	2.22, 5.56, and 55.56	100	~20, colonies ~0.8, none	17
Al_2O_3-ZrO_2 eutectic	Bridgman	2.22, 11.11	20	colonies w/ ZrO_2 rods Al_2O_3 to ZrO_2 (001)//{100} (110)//<100>	6, 16
Al_2O_3-42.7 wt% ZrO_2-4.4 wt% Y_2O_3	Stepanov	5.56-27.78	_____	colonies	7
"	Verneuil	1.39-5.56	_____	colonies	7
Al_2O_3-34.5 mol% ZrO_2-3.5 mol% Y_2O_3	"	2.78-5.56	_____	" [2110]//[100] faceting along these planes	8, 9
Al_2O_3-ZrO_2-0,1.2,2.1,5.3 mol% Y_2O_3	float zone w/Xe arc	2.78-25	60	colony growth only w/ higher Y_2O_3 additions	10, 11
Al_2O_3-34 wt% ZrO_2-10 wt% Y_2O_3	Bridgman	<3.03	_____	Colony growth w/ rods ZrO_2	12
Al_2O_3-17 wt%, and 42.5 wt% ZrO_2	electrohydro dynamic rapid solidification	_____	$> 10^3$	Amorophous and eutectic structures	23

A transition from faceted to nonfaceted dendrites was observed for Al_2O_3 as the velocity was increased. The spacing of eutectics, colonies, and single phase dendrites were measured as a function of composition and velocity. The measured eutectic spacings showed deviations from the existing theoretrical model which is based on the planar eutectic interface model [20]. The colony spacing was found to decrease with velocity as $V^{-1/4}$, which is analogous to the variation in the single phase dendrites with velocity. Experimental results on eutectic, colony and dendrite spacings are analyzed with more appropriate theoretical models.

II. Experimental

Al_2O_3 and ZrO_2 powders (5-20μm in diameter) of commercial purity were used for this experimental study, and impurity levels were reported to be of 99.8% Al_2O_3 and 99.0% for the ZrO_2. Analysis of the powders showed typical impurities for Al_2O_3 to be Na, Fe, and Si with each registering under 300 ppm level. The ZrO_2 showed impurities of less than 1% corresponding to HF, while other impurities were listed as Ti, and Si, each below 550 ppm. Experiments were also carried out by using higher grades of powders with reported purities of 99.999% for Al_2O_3 and 99.9975% for ZrO_2. The physical properties of Al_2O_3 and ZrO_2, obtained from the literature, are given in Table 2.

The reported eutectic composition is about 58.5 wt% Al_2O_3 and 41.5 wt% ZrO_2 as shown in Figure 1 [24]. Thus, we studied three different compositions which were hypoeutectic (30 wt % zirconia), eutectic, and hypereutectic (50 wt % zirconia). The detailed experimental conditions are shown in Table 3.

The directional solidification of Al_2O_3-ZrO_2 in Ta crucibles was carried out with the Bridgman technique under the rates varying between 2 and 200μm/s. The system was first evacuated and then back filled with argon gas to a pressure of 5 psi, to reduce the chances of arcing within the furnace during the runs. Each sample was first heated to approximately

Table 2. Physical properties of Al_2O_3-ZrO_2 system

Physical properties	Alumina (Al_2O_3)	Zirconia (ZrO_2)	Reference
Crystal structure	Hexagonal (α-Al_2O_3)	Cubic, T>1000°C Monoclinic, T<1000°C	27
Thermal expansion coefficient	8.3×10^{-6}/°C	7.6×10^{-6}/°C	27
Thermal conductivity	0.0181 cal/cm°Csec (at 1800°C)	0.004 cal/cm°Csec	28 27
Melting temperature	2050°C	2677°C	27
Entropy of fusion, ΔS_f	339.652 J/Kmol	248.093 J/Kmol	29
Distribution coefficient, k	0.05	0.133	24
Thermal diffusivity	0.019 cm^2/sec at 800°C	0.0053 cm^2/sec at 750°C	28
Diffusion coefficient	$1.85 \times 10^{-5} cm^2$/sec	———	
Solid density	3.96g/cm^3 at 25°C	5.56 g/cm^3 (Monoclinic)	33
Liquid density (calculated with 44.6 wt% ZrO_2 addition)	3.455 g/cm^3 at 1935°C	———	30

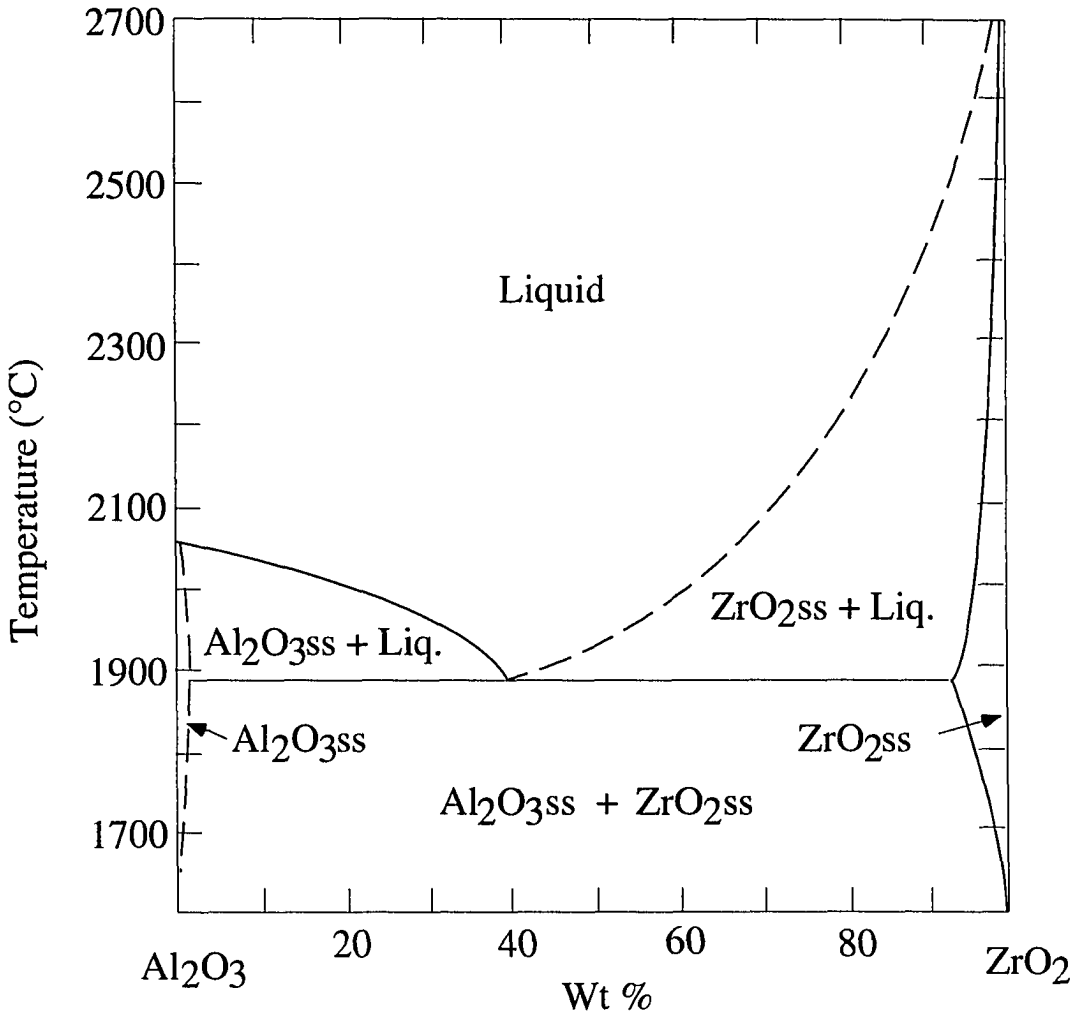

Figure 1. The phase diagram for the alumina-zirconia eutectic system. SS represents solid solution of each phase [24].

Table 3. Experimental conditions in the directional solidification of Al_2O_3-ZrO_2.

Composition*	Technique	Velocity, μm/s	Temperature gradient, K/mm (estimated)
30 wt% ZrO_2	Bridgman	2, 20, and 200	20
	Laser Scanning	10000	
42.5 wt% ZrO_2	Bridgman	2, 10, 20, and 200	"
50 wt% ZrO_2	Bridgman	2, 20, and 200	"

*Nominal compositions of 99.8% Al_2O_3 and 99.0% ZrO_2.

2100°C, and then directionally solidified at an appropriate withdrawal rate. The solidified samples were then examined by optical microscope and SEM, to measure eutectic, colony, and dendrite spacing variation with velocity.

Rapid solidification studies were carried out by using the laser scanning technique. A thin sample of 30 wt% ZrO_2 was made by the slip casting technique and the laser beam of 0.26 mm in diameter, 50W power, was scanned on this sample at the velocity of 0.01m/s (10000μm/s). The laser treatment made a pool that was 640μm wide, and 345μm deep. The microstructures from these experiments were studied with TEM on a thin longitudinal slice (11 mil) of this sample sectioned along the center line of the pool.

III. Results

(1) Microstructural Observations

Several runs were initially made using the lower purity materials. These experiments encompassed off-eutectic as well as eutectic compositions at withdrawal rates of 2, 10, 20, and 200μm/s. In all cases, extensive colony growth was noted. Typical microstructures from

different velocities are shown in Figure 2 for hypereutectic composition (ZrO_2 rich composition), and the scales of both the eutectic and the colony were found to become finer as the velocity was increased. Similar behavior was also observed for eutectic and hypoeutectic compositions. The colonies contained a very fine rod type eutectic structure in the center, while a coarser structure was found at the colony boundaries. The center region of colonies showed a very uniform spacing of rods, as shown in Figure 3, and eutectic spacings were measured from these areas only. At lower velocities, the colony strtucture consisted of two-phase cellular structure, while at a higher velocity, i.e. V=200μm/s, a dendritic colony structure was observed as shown in Figure 2(b) and (c). A cellular colony was again observed at very high velocity in the laser experiment.

The off-eutectic experiments also yielded both Al_2O_3 and ZrO_2 dendrites in addition to eutectic colonies. The 50 wt% ZrO_2 samples contained ZrO_2 dendrites while the samples at 30 wt% ZrO_2 demonstrated considerable Al_2O_3 dendrite growth. Micrographs depicting these dendrites are shown in Figure 4. It was noted that the Al_2O_3 dendrites exhibited a strongly faceted behavior while ZrO_2 dendrites were nonfaceted in nature. Also, hypereutectic samples (50wt% ZrO_2) showed no ZrO_2 dendrites at withdrawal rates of 20μm/s or less, as can be seen in Figure 2(b), but single phase ZrO_2 dendrites were found at a higher velocity (200μm/s) indicating that this growth condition lies outside the coupled zone. Since faceted Al_2O_3 and non-faceted ZrO_2 primaries were observed in off-eutectic compositions at low rates, a coupled zone that is skewed towards Al_2O_3 side is expected in this system [26, 35]. It should be noted that dendrite shaped colonies were also observed at 200μm/s as can be viewed in Figure 2(c)

The microstructures observed in the high velocity experiment carried out by using a laser are shown in Figure 5. Two-phase cellular eutectics (colonies) can be seen in Figure 5(a), whereas Figure 5(b) shows the formation of nonfaceted Al_2O_3 dendrites from a different region. This is a marked contrast to the faceted dendrites found at lower solidification velocity.

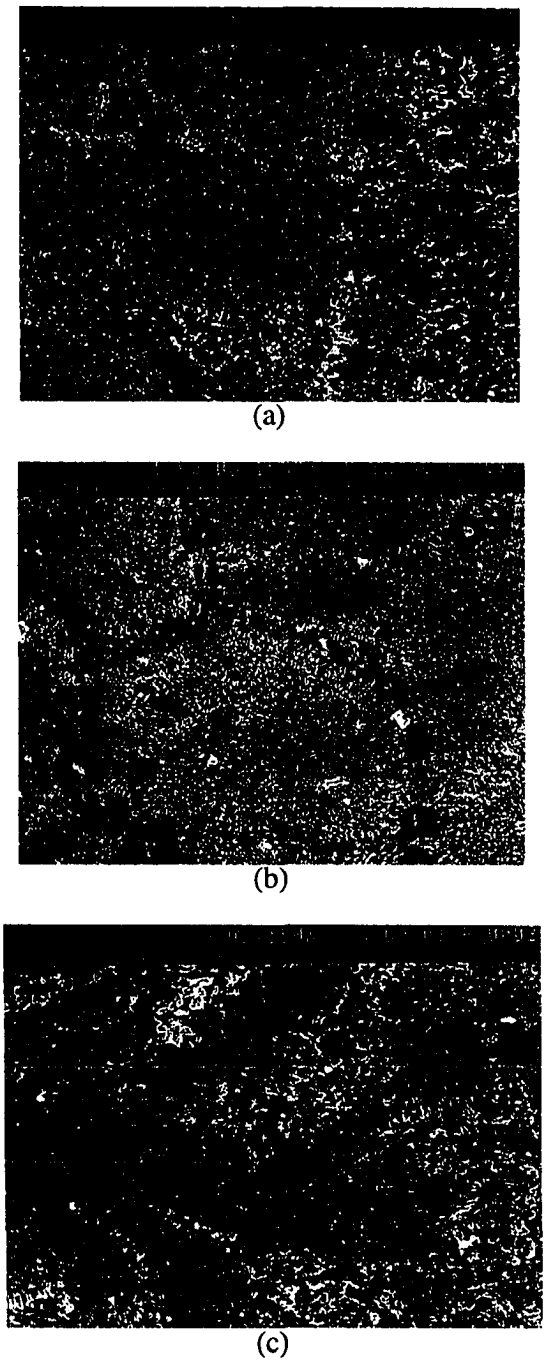

Figure 2. Micrographs from transversal section of Al_2O_3 + 50 wt% ZrO_2 withdrawn from the furnace at (a) 2, (b) 20, and (c) 200μm/s.

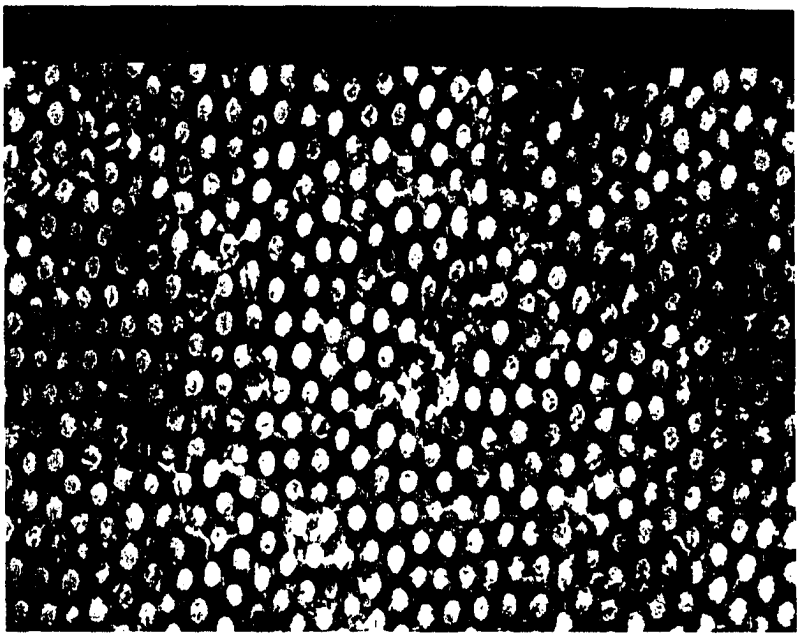

Figure 3. Rod eutectics from the transversal section grwon at V=2μm/s in 30wt% ZrO_2. White phase is the ZrO_2 and the matrix (darker phase) is the Al_2O_3 phase.

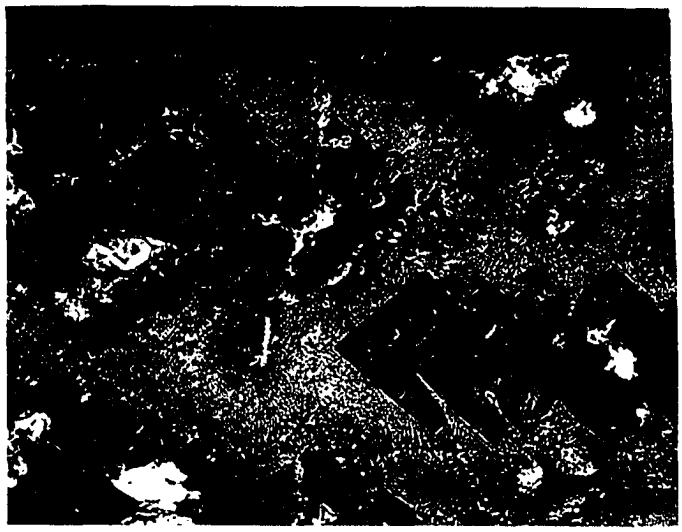

(a)

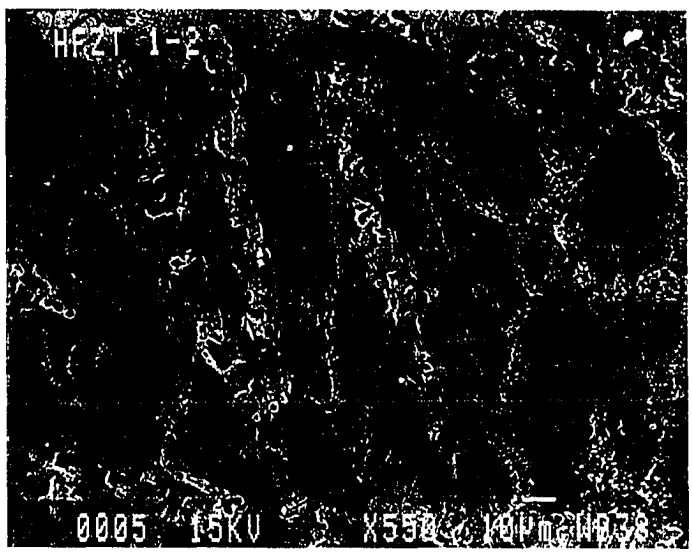

(b)

Figure 4. Micrographs depicting (a) faceted Al_2O_3 dendrites resulting from the hypo eutectic samples (30 wt% ZrO_2), and (b) non-faceted ZrO_2 dendrites resulting from the hyper eutectic samples (50 wt% ZrO_2).

(a)

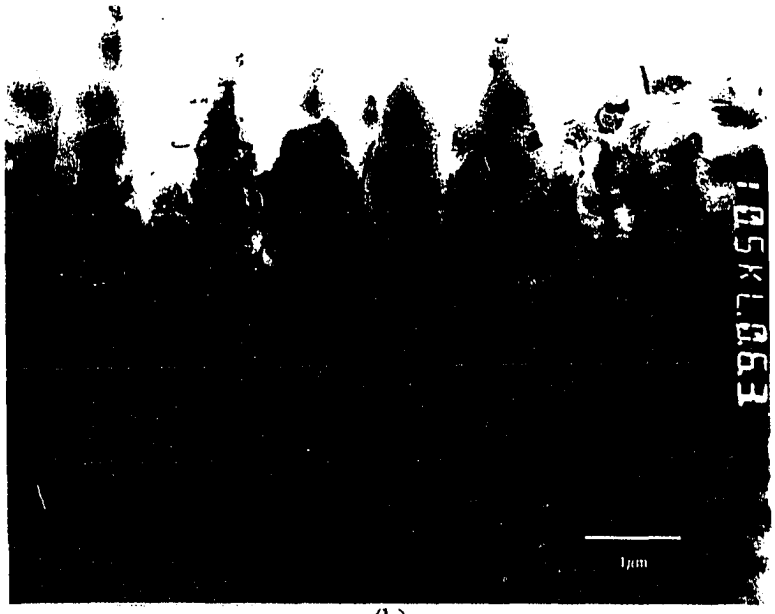

(b)

Figure 5. Microstructures from the rapid solidification with laser melting at V=1cm/s in a thin sample of 30 wt% ZrO_2. (a) Cellular eutectics at high velocity, (b) Non-faceted Al_2O_3 dendrites.

(2) Microstructural Scales

During the present experimental work, different morphologies such as single phase dendrites, eutectic colonies, and eutectics were observed for all compositions examined. Eutectic, colony and primary dendrite spacings were measured for samples solidified at different velocities, and all these results are shown in Figure 6. Also shown on this plot are the eutectic spacings reported by Minford [16], and colony spacings reported by Borodin et al. [14]. Figure 6(c) shows that the eutectic spacing decreases with growth rate, although at smaller rate than the $V^{-1/2}$. The variation in colony spacings with velocity show close to $V^{-1/4}$ relationship. The results of the present work also show agreement with previous results in low velocity range. The primary dendrite spacing in Figure 6(a) shows the largest microstructural scale, and the slopes of the colony and the dendrite spacings with respect to the growth rate appear to be quite analogous to each other.

(3) Effects of Impurity

Since colony structures form due to the presence of a third element, experiments were also carried out with the high purity Al_2O_3 and ZrO_2 powder and with the addition of Ta, Y_2O_3 (Yttria), and Sc (Scandium). Experiments in high purity powders with eutectic composition, carried out at V=5μm/s, showed that the colony formation was reduced significantly. A coarse microstructure at the boundaries was not observed, as shown in Figure 7(a). The eutectic structure was found to be somewhat irregular, and was not a distinctly rod-type euetectic. In contrast, the addition of Y_2O_3 and Sc showed enhanced tendency for colony formation. An example of colony structures with the addition of Sc is shown in Figure 7(b). Also, we used Ta crucible, and at very low velocities, some Ta contamination from the crucible was observed near the contained wall. Thus, a range of 50 ppm to 0.1wt% of Ta was added to the sample to examine the effect of the Ta on the microstructure. Two different types of interactions were observed as shown in Figure 8. An experimental result at V= 5μm/s shows a large Ta dendrite

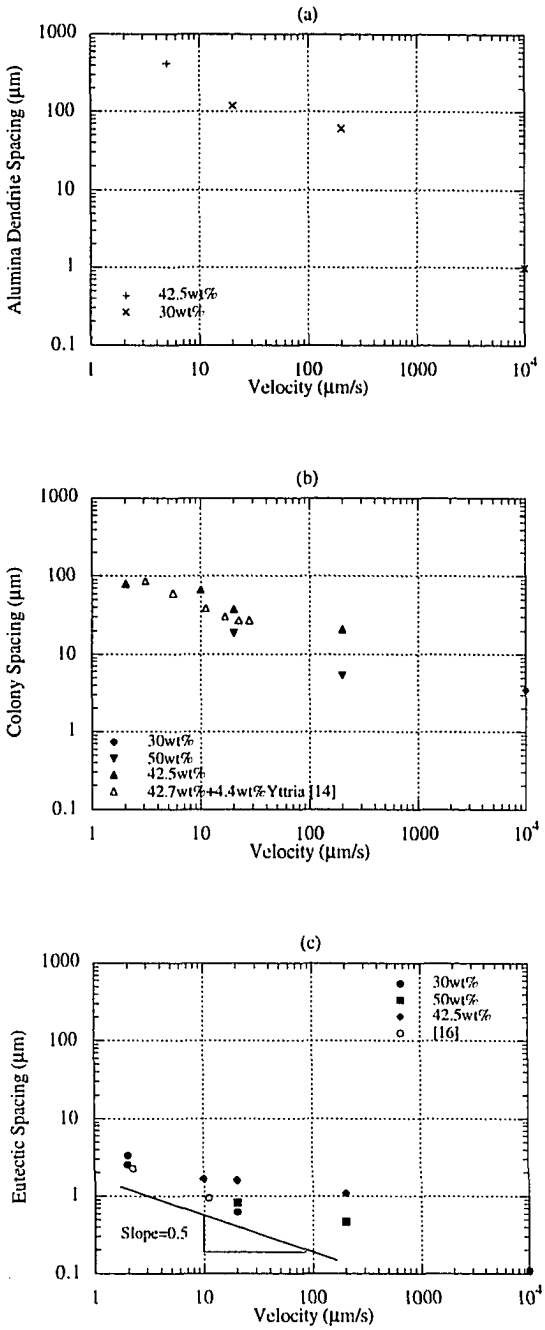

Figure 6. Microstructural scales depicting (a) dendrites (b) colonies (c) eutectics from various compositions as a function of growth velocity.

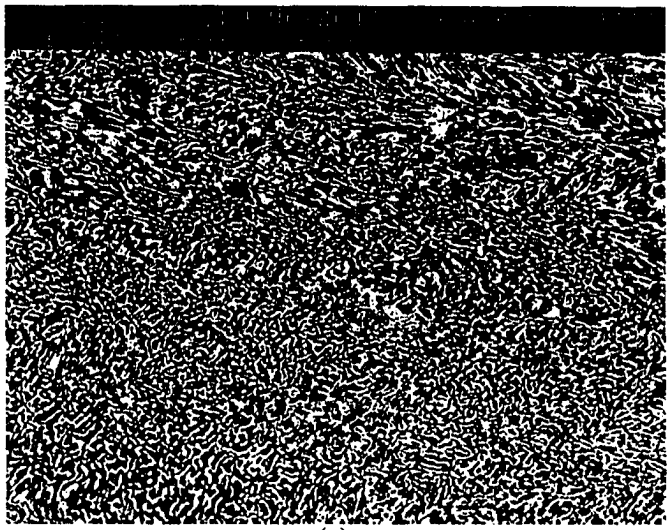

(a)

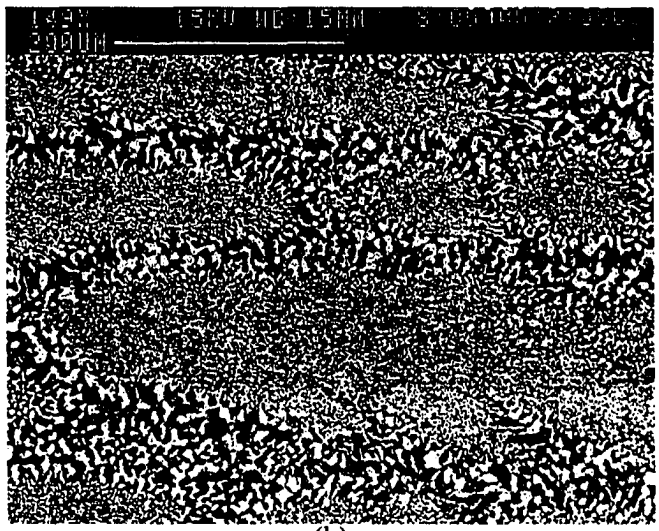

(b)

Figure 7. (a) Micrograph showing the lack of significant colony formation with the high purity powder ceramic. Velocity was at 5μm/s. (b) Micrograph showing colony formation and resulting microstructure due to the addition of 20 vol% of Sc. A withdrawal rate of 5μm/s was used.

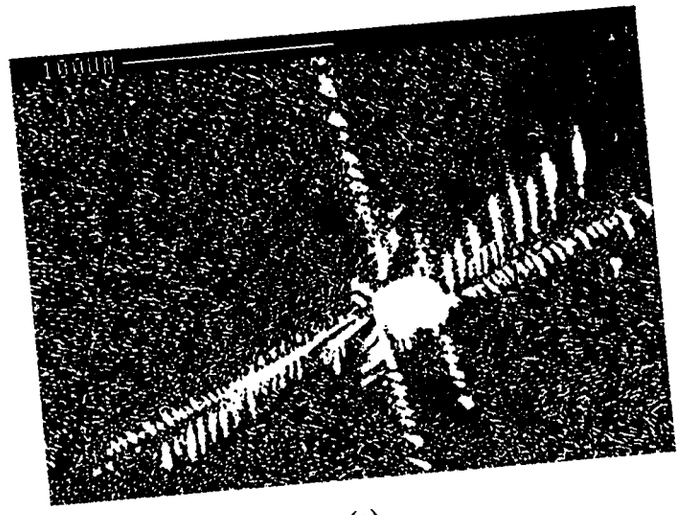

(a)

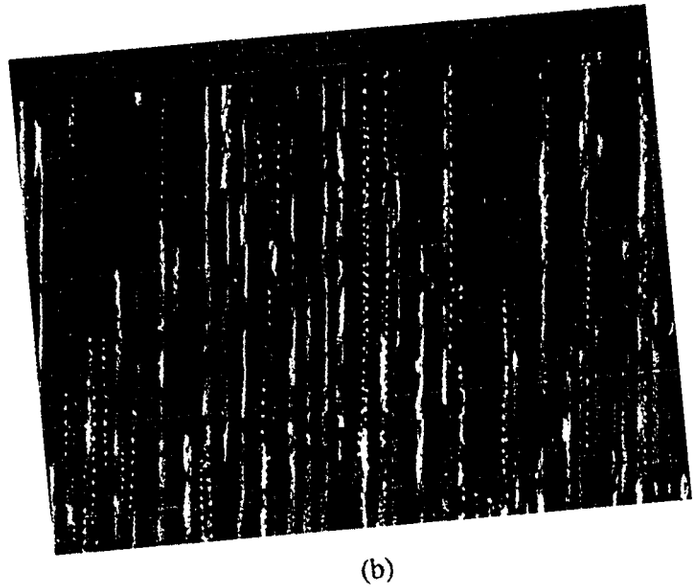

(b)

Figure 8. Ta contaminations into the matrix (a) forming dendrite at the velocity of 5μm/s (b) forming small beads along the eutectics at the velocity of 2μm/s.

(white phase) surrounded by a eutectic microstructure as in Figure 8(a). Ta is insoluble in solid phases of Al_2O_3 and ZrO_2, so that the increased concentration of Ta causes nucleation of Ta ahead of the solid:liquid interface. In contrast to this observation, a small amount of Ta dissolved from the container exhibited an interesting feature, as shown in Figure 8(b), for V=2μm/s. Since Ta is not soluble in either of the two solid phases, it gets incorporated at the solid:solid interface of the eutectiic. It is thought that Rayliegh instability causes the thin layer of Ta to form tiny elongated spheres along the Al_2O_3-ZrO_2 eutectic boundaries. The presence of a small metallic phase at the boundary may increase the toughness of the ceramic since it will tend to blunt off any crack propagation.

IV. Discussion

We shall first examine different microstructures that are observed in the Al_2O_3-ZrO_2 system, and then discuss the effect of velocity of microstructural spacings.

(1) Microstructures

The basic eutectic microstructure was found to consist of ZrO_2 rods in the Al_2O_3 matrix. The formation of rod eutectic is governed by the volume fraction of the minor phase and by the interface energy between the two solid phases in the eutectic. If the solid:solid interface energies for rod and lamellar eutectics is assumed to be the same, a rod eutectic will form when the volume fraction of the minor phase, $f_{(ZrO_2)} < 0.30$. In general, it is difficult for a rod phase to have good matching over all orientations, whereas the solid:solid interface in a lamellar eutectic can have a planar low energy orientation. Thus, rod eutectic formation will require $f_{(ZrO_2)}$ to be significantly less than 0.3. From the phase diagram shown in Figure 1, the volume fraction of ZrO_2, $f_{(ZrO_2)}=0.352$, which is higher than the maximum theoretical value of 0.3 for rod formation [34]. The formation of rod-type eutectic may be due to the uncertainty in the phase diagram. The calculation for $f_{(ZrO_2)}=0.3$ gives the eutectic composition

of 36.3 wt% of ZrO_2. Or formation of rod eutectic may also be due to the effect of impurity on the interface energy. A careful observation of Figure 7(a) shows that the eutectic structure tends to become lamellar as the purity of the component is increased.

The formation of colonies has been shown to occur due to the presence of nonplanar eutectic growth interface. The instability of a planar eutectic is caused by the presence of third element which is an impurity element. In order to examine the nature of nonplanar solid:liquid interface which lead to colony formation, we shall look at the colony formation in an organic analog system (CBr_4-C_2Cl_6) whose transparent property allows one to look at the shape of the advancing interface. Different types of interfaces have been observed in this system, as shown in Figure 9 [32]. At low velocities, a planar eutectic growth is observed, as shown in Figure 9(a). However, as the velocity is increased, the planar interface becomes unstable and forms two-phase cellular structure. Two different morphologies of cellular colonies can form: a "fan" colonies, Figure 9(b), and "needle" colonies, Figure 9(c). Fan colonies are named such that they show fanning or rotating of lamellae at the boundaries, and the term "needle" colonies refers to the fact that all lamellae are aligned in a specific direction even if the macroscopic interface is curved. At higher velocities, the two-phase cellular structure transforms to a two-phase dendritic structure, as in Figure 9(d). Needle colonies form due to the presence of anisotropy in this system. The colony structures observed in the Al_2O_3-ZrO_2 system can be understood by examining the needle colonies growing in the longitudinal direction, Figure 9(c), whose transverse section will appear as in Figure 2. The regions with smaller eutectic spacings in Figure 2 correspond to the leading part of the colonies in Figure 9(c).

The morphological fetures of colony and primary dendrite, observed under high rate of solidification in a laser experiment show very different microstructures. The eutectic colony which exhibits a needle like cellular structure at low velocities, and a needle like dendritic structure at V=200 μm/s, transforms into a very distinct fan morphology at high rates. In a similar manner, the primary Al_2O_3 dendrites, which were highly faceted at low velocities

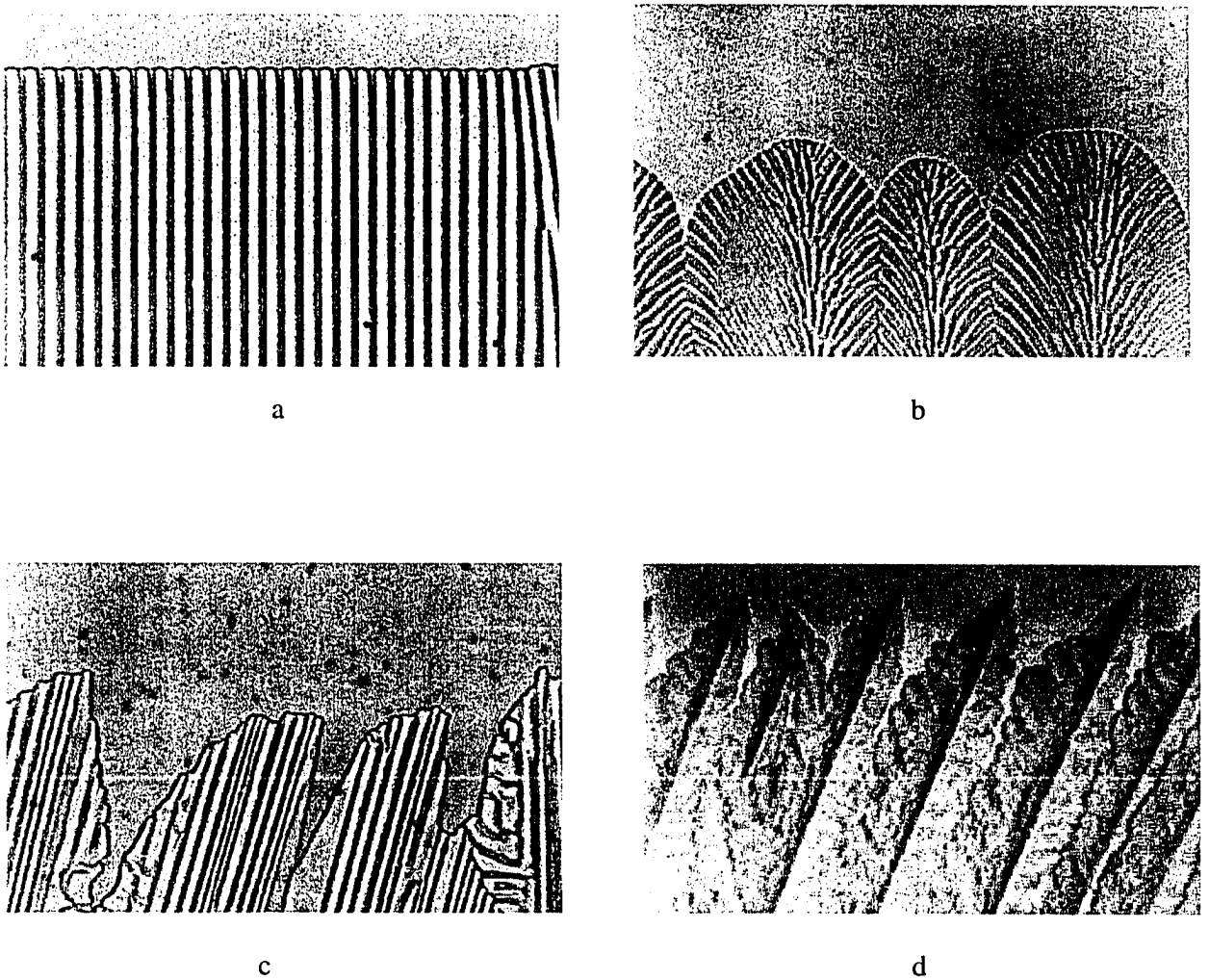

Figure 9. Various microstructures according to different velocities (from lower to higher) (a) planar eutectic (b) cellular: fan type (c) cellular: needle type (d) eutectic dendrites.

(Figure 4) show nonfaceted dendrites at high velocities. These changes in morphologies occur due to the formation of metastable Al_2O_3 phase at high undercoolings. This is evident from Figure 5(b) which show that the primary Al_2O_3 dendrites form sidebranches with a four fold symmetry indicating that a cubic form of Al_2O_3 is formed at high growth rates compared to the hexagonal structure that forms at low growth rates.

(2) Eutectic Spacing

Earlier studies on the oxide eutectic solidifications were carried out over a small velocity regime and the measured average eutectic spacings were assumed to follow Jackson and Hunt model [20]. Minford [16] and Stubican and Bradt [21] fitted their experimental data in the Al_2O_3-ZrO_2 system to the J-H model, which gave $\lambda^2V=1.13\times10^{-17}m^3/s$ [16] and $\lambda^2V=1\times10^{-17}m^3/s$ [21]. Their data are shown along with the results of the present study in Figure 6. The results at higher growth rates, i.e. at V=200 μm/s, show a departure from the predicted slope as the velocity increases. The result obtained from the laser studies also shows significant departure, although this result is influenced by the formation of a metastable phase. We shall thus examine the theoretical model to assess how the eutectic spacing variation with the growth rate alters when the eutectic interface is nonplanar.

The basic idea for the variation in interface temperature with velcoty are shown in Figure 10. The reference temperature for undercooling was taken as the binary eutectic temperature, T_E, in which the total undercooling at the leading tip of a colony is divided into three processes, such that

$$\Delta T = T_E - T_i = \Delta T_P + \Delta T_E + \Delta T_{cd} \qquad (1)$$

where T_E is the binary eutectic temperature, and T_i is the interface temperature. The undercooling from the binary eutectic temperature is composed of the following: (i) the

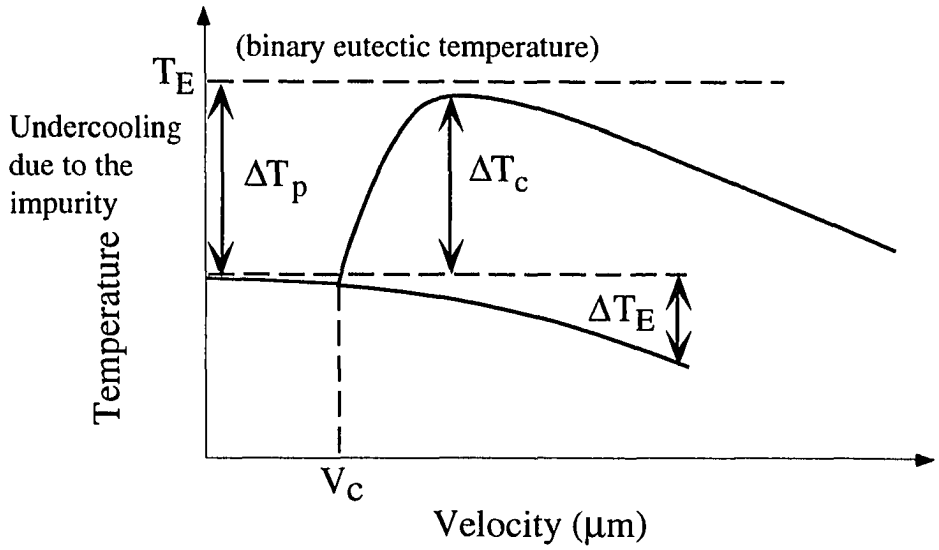

Figure 10. Schematic representation of the variation in the interface temperature as a function of velocity under a constant temperature gradient for a two-phase structure [31].

undercooling at a planar eutectic interface due to the presence of a third element (ΔT_p), (ii) the undercooling for the eutectic growth (ΔT_E), and (iii) the undercooling for the cell or the dendritic growth (ΔT_{cd}). Thoeretical model for the colony undercooling in a ternary system was developed by McCartney et al. [31] who used the analogy of the single phase cellular and dendritic growth to evaluate the undercooling ΔT_{cd}. Their result can be written as

$$T_i = [\, T_E + M_C C_{\infty C}] - \left[\frac{GD}{V}\right] - 2\left[\frac{-2aV}{D}\left(M_c(1-k_c)C_{\infty c}\right)+\frac{k_c}{V}DG\right]^{1/2} - \Delta T_E \qquad (2)$$

Where T_E is the binary eutectic temperature and T_i is the actual interface temperature, $M_c=dT/dC^L{}_c$ is the slope of the eutectic valley, $C^E{}_C=C_{\infty c}/k_c$ is the average liquid composition at the interface, and k_c is the weighted eutectic distribution coefficient for the third element, c, which is defined as

$$k_c = \frac{k_{\alpha c} S_\alpha}{S_\alpha + S_\beta} + \frac{k_{\beta c} S_\alpha}{S_\alpha + S_\beta} \qquad (3)$$

The first term on the right hand side in equation (2) gives the effect of the third component on a planar interface growth. McCartney et al. [31] also assumed that the eutectic undercooling is the same for colonies as that for a planar interface, and assumed $\Delta T_E = A'V^{1/2}$. A' is approximately a constant even though there is a small dependency of $C_{\infty c}$ through M [31].

Recently, the present authors [32], through experimental studies in a transparent model organic system, have shown that the eutectic undercooling can alter significantly due to the curvature of the interface. The effect of curvature on eutectic interface temperature will also influence the relationship between the eutectic spacing and velocity.

Figures 9(b)~9(d), and Figure 5(a) show that a significant change in eutectic interface from planarity occurs near the center region of the colony. This will influence both the

diffusion and surface energy effects, and lead to an increase in eutectic spacing as the planar interface becomes nonplanar [32]. For, fan-type colonies, the lamellae become tilted, and it is now established that a tilted structure has a larger spacing than the lamellae growing in the heat flow direction. Thus, one would expect the eutectic spacing to increase slightly as the transition from a planar to cellular interface occurs. The spacing will finally decrease as dendritic colonies are formed [32]. This leads to growth rate dependence of eutectic spacing to be less than that predicted by the planar eutectic growth model near the transition point, which is shown by the present experimental results. The above conclusion has recently been tested by the authors [32] through experimental studies in a model transparent system, in which an initial increase in the eutectic spacing at the planar to cellular transition condition was observed. The spacing was then found to decrease in the dendritic range with a growth rate dependence that was small than the $V^{-1/2}$ scaling law. The results in the ceramic system have also been found to exhibit this trend.

(3) Colony and Dendrite Spacing

The formation of colonies occurs through the insability of the eutectic interface with respect to the third impurity element. The impurity element piled up ahead of the interface gives rise to constitutional supercooling. Thus, as a first approximation, one can assume that the impurity does not influence the diffusion of binary elements, so that the process of instability is analogous to that for a single phase with the third element causing the instability. One would thus expect the colony spacing to be analogous to the cellular and dendrite spacing in a single phase growth. In the nonplanar regime, the colony spacing should thus follow $V^{-1/4}$ dependence which is observed in our experimental study, as shown in Figure 6.

The primary dendrite spacing, shown in Figure 6, also follows the same variation with velocity as the colony spacing. However, the values of the constants for the two cases are different so that there is a shift in the curve.

V. Conclusions

Directional solidification studies in Al_2O_3-ZrO_2 eutectic system shows the eutectic microstructures to consist of rods of ZrO_2 in an Al_2O_3 matrix. Colony growth was found to be prevalent in all samples and it resulted from the presence of third components such as Ta, Y_2O_3, and Sc or impurities. In addition to colony formations, faceted Al_2O_3 dendrites and non-faceted ZrO_2 dendrites were observed when the ceramic sample was solidified outside the coupled zone. When the velocity was extended to the rapid solidification regime, the Al_2O_3 dendrties were found to grow in a non-faceted manner due to the formation of metastable Al_2O_3 at large undercoolings. A similar transition in colony structure was also observed in that the colonies became fan like at high velocities.

Eutectic spacings at the center of the colony, measured from the extended velocity regime, also showed deviations from the existing model. This departure comes due to the nonplanar eutectic interface which alters the eutectic spacing in the center of the colony. The colony spacing was found to be at least about 10 times larger in size than that of eutectic, and showed an analogous trend to the spacing variation for the single phase dendrite. This is because both these spacings are governed by the long range diffusions of solutes around nonplanar interfaces. The general trend in eutectic, colony and primary dendrite spacing variation with velocity was found to be similar, and detailed theoretical models are required to quantitatively assess the magnitude of these changes.

Acknowledgments

The authors wish to thank Wilfred Kurz for carrying out the laser experiments and Fran Laabs for the TEM studies. Appreciation is also extended to Drew Delaney and Thomas Lograsso for their technical support. This work was carried out at Ames Laboratory, which is operated for U.S. Department of Energy by Iowa State University under contract No. W-7405-

ENG-82. This work was supported by the Office of Basic Energy Sciences, Division of Materials Sciences.

References

1 R. L. Ashbrook, *J. Am. Ceram. Soc.*, 60 (1977) 428.

2 S. N. Lakiza, *Poroshkovaya Metallurgiya,* 28 (1990) 637.

3 F. Schmid and D. Viechnicki, *J. Mat. Sci.*, 5 (1970) 470.

4 F. Schmid and D. Viechnicki, *Advanced Materials: Composites and Carbon,* Symposium of American Ceramics Society, Chicago, Il, ACS, Columbus, (1973) 96.

5 N. Claussen, G. Lindemann, and G. Petzow, *Ceram. Int.*, 9 (1983) 83.

6 W. J. Minford, R. C. Bradt, and V. S. Stubican, *J. Am. Ceram. Soc.*, 62 (1979) 154.

7 V.A. Borodin, A. G. Reznikov, M. Yu. Starostin, T. A. Steriopolo, V. A. Tatarchenko, L. I. Chernyshova, and T. N. Yalovets, *J. Cryst. Growth*, 82 (1987) 177.

8 L. Mazerolles, D. Michel, and R. Portier, *J. Am. Ceram. Soc.*, 69 (1986) 252.

9 D. Michel, L. Mazerolles, J. P. Dallas, M. Stucky, and R. Portier, *Physical Chemistry of the Solid State: Applications to Metals and their Compounds*, Elsevier Science Publishers, Amsterdam, 1984, 397.

10 J. Echigoya, Y. Takabayashi, H. Suto, and M. Ishicame, *J. Mat. Sci. Let.*, 5 (1986) 150.

11 J. Echigoya, Y. Takabayashi, and H. Suto, *J. Mat. Sci Let.*, 5 (1986) 153.

12 V. N. Batog, V. G. Karabutov, B. B. Morozov, Yu. I. Smirnov, and A. V. Logunov, *Inorg. Mat.*, 22 (1986) 1631.

13 S. Brandon and J. Derby, *J. Cryst. Growth*, 121 (1992) 473.

14 V. A. Borodin, M. Yu. Starostin, and T. N. Yalovets, *J. Cryst. Growth*, 104 (1990) 148.

15 F. L. Kennard, Ph.D. Thesis, Pennsylvania State University, 1973.

16 W. J. Minford, Ph.D. Thesis, Pennsylvania State University, 1976.

17 C. O. Hulse and J. A. Batt, *Final Tech. Rept.*, UARL-N910803-10, 1974.

18 C. C. Sorrell, M.S. Thesis, Pennsylvania State University, 1980.

19 V. Seetharaman and R. Trivedi, *Metall. Trans. A.*, 18A (1988) 2955.

20 K. A. Jackson and J. D. Hunt, *Trans. AIME*, 236 (1966) 1129.

21 V. S. Stubican and R. C. Bradt, *Ann. Rev. Mater. Sci.*, 11 (1981) 267.

22 F. H. Cocks, *Conference on In Situ Composites*, Tech. Rept. NMAB-308-Vol. 1, 1973, 141.

23 T. Whitney, V. Jayaram, C. G. Levi, and R. Mehrabian, *Solidification Processing of Eutectic Alloys*, The Metallurgical Society, 1988, 199.

24 A. M. Alper, R. C. Doman, R. M. McNally, and H. C. Yeh, *Phase Diagrams*, edited by A. M. Alper, Academic Press, London and New York, 1970, 117.

25 R. Trivedi and W. Kurz, *Acta metall.*, 42 (1994) 15.

26 R. Trivedi and W. Kurz, *Solidification Processing of Eutectic Alloys*, D. Stefanescu and G. J. Abbaschian, eds., AIME, Warrendale, PA, 1988, 3.

27 F. Galasso, *Structure and Properties of Inorganic Solids*, 1st Edition, Pergamon, Oxford, New York, 1970.

28 E. Ryshkewitch and D. Richerson, *Oxide Ceramics*, Academic Press Inc, Orlando, 1985.

29 M. W. Chase, C. A. Davies, J. R. Downey, D. J. Frurip, R. A. McDonald, and A. N. Syverud, *J. Phys. Chem. Ref. Data*, 14 (1985) suppl. 1.

30 J. M. Lihmann and J. S. Haggerty, *J. Am. Ceram. Soc.*, 68 (1985) 81.

31 D. G. McCartney, J. D. Hunt, and R. M. Jordan, *Metall. Trans. A.*, 11A (1980) 1243.

32 S. H. Han and R. Trivedi, *Metall. Trans.*, to be submitted.

33 J. D. Cawley and W. E. Lee, *Materials Science and Technology*, vol 11, R. W. Cahn, P. Haasen, and E. J. Kramer, eds., VCH, New York, NY, 1994.

34 R. Trivedi, J. T. Mason, J. D. Verhoeven, and W. Kurz, *Metall. Trans. A.*, 22A (1991) 2523.

35 W. Kurz and D. J. Fisher, *Fundamentals of Solidification*, Trans Tech Publications, Aedermannsdorf, 1992.

CHAPTER 3:
COLONY FORMATION DURING EUTECTIC GROWTH

A manuscript to be submitted to the *Journal of Metallurgical and Materials Transactions*

S. H. Han and R. Trivedi

Ames Laboratory US-DOE and the Department of Materials Science and Engineering
Iowa State University, Ames, IA 50011

Abstract

Directional solidification studies in a eutectic system have been carried out to study the formation of nonplanar eutectic structures which give rise to two-phase eutectic colonies. Experiments have been carried in a model transparent system of carbon tetrabromide and hexachloroethane so that the mechanisms of colony formation can be observed in situ and the temperature of the two-phase cellular and dendritic interfaces can be measured precisely. A detailed dynamical study was carried out to examine the coupling between the macroscopic curvature of the interface caused by the presence of a third component and the adjustment in eutectic structure required to maintain a two-phase structure. The mechanisms by which planar to cellular, and cellular to dendritic transitions occurred in the two-phase structure have been established. Quantitative measurements on the variation in interface temperature, eutectic spacing, and colony spacing with velocity have been carried out over the two-phase planar, cellular and dendritic structures. Interface temperature and eutectic spacing were found to decrease initially with velocity in the planar eutectic regime. However, as the planar interface became unstable, the interface temperature, the eutectic spacing at the center of colonies and the colony spacing were all found to increase initially, went through maximum, and then decreased

as the cellular structure transformed into the two-phase dendritic structure. These experimental results have been analyzed by using appropriate theoretical models of cellular, dendritic and eutectic growth.

I. Introduction

An extensive study on eutectic growth has been carried out in the past because of their potential applications to mechanical and electronic components. Theoretical models of the eutectic growth have also been developed, based on a macroscopically planar eutectic interface, to correlate the microstructural scales with the operating parameters. However, eutectic growth at higher growth rates often show the formation of a two-phase cellular or a two-phase dendritic structure, which is often referred to as the *eutectic colony structure*. Several experimental studies have been carried out to understand the colony structure formation in metallic systems [1-16], ceramic systems [17] and transparent organic systems [18]. Colony formation has also been observed in highly undercooled droplets of ultra high purity metals [19] and in laser processing of ceramics at high growth rates [17].

The formation of the two-phase cellular or dendritic colony structure has been associated with the presence of a ternary impurity element which leads to the constitutional supercooling at the interface [2, 3]. Tiller [2] applied the constitutional supercooling criterion to the planar eutectic interface instability to establish the conditions for the colony formation. More detailed linear stability analysis has also been carried out to predict the condition for the onset of instability. The predictions of these models have been compared with experimental studies in several systems [1-12], and a good agreement was found.

Most of the studies on colony so far have been concentrated on the condition for the onset of instability in the two-phase system, and no detailed quantitative experimental work has been carried out on the dynamics of the process of reorganization of the unstable interface into a regular two-phase cellular and dendritic interface, and the establishment of steady-state

microstructural scales of the colony structure. McCartney et al. [36] have proposed a model for the interface temperature variation with velocity by using an analogy with the single-phase cellular and dendritic growth, and they have shown that the interface temperature which initially decreases with velocity in the planar interface regime will increase as the cellular two-phase structure forms, and then decrease with velocity as the cellular structure transforms into a dendritic structure. The eutectic spacing at the center of the colony, however, has not been examined, and is generally believed to follow the same scaling law as that for a planar eutectic interface.

The main objective of this work was to investigate the mechanisms of the colony formation, and to quantitatively characterize two-phase cellular and dendritic microstructures in terms of the variation in interface temperature, eutectic spacing and colony spacing with velocity. For this study, the organic analog system (CBr_4-C_2Cl_6) was chosen whose transparency enables one to observe the dynamical processes of colony formation, and it allows accurate measurements of interface temperature. We have examined the dynamical processes that lead to the instability of the interface and observed the mechanisms that were operative during the formation of colonies. In addition, we have also characterized the interface temperature, eutectic spacing and colony spacing as a function of velocity. The interface temperature was found to increase initially as the planar eutectic structure becomes unstable and form cellular and dendritic structures, but it then went through a maximum as the velocity was increased further. A theoretical model is examined to describe this variation in interface temperature with velocity.

The eutectic spacing was found to follow the established model only for the planar eutectic interface growth. At the threshold of instability, the eutectic spacing was found to increase slightly and then decrease slowly with further increase in velocity. This departure from the planar eutectic growth model comes due to the deviation in the lateral diffusion field due to the curvature of the interface or the tilting of the lamellae. The colony spacing

measurements also showed a maximum with velocity, and its variation was analogous to that for the single phase cell-dendrite spacing. Experimental results on colony microstructures are analyzed by using an analogy with the existing models for the single phase cellular and dendritic growth models for the third element.

II. Experimental

As received carbon tetrabromide and hexacloroethane were first sublimated separately to remove impurities, and then mixed under an inert atmosphere to obtain required compositions. Because of the high vapor pressure of hexachloroethane, a small amount of additional hexacloroethane was added to obtain the desired composition. In this system, carbon tetrabromide decomposes slightly into bromine which serves as a third element that causes the planar eutectic interface to become unstable. The sample was made by the procedure described by Seetharaman et al. [20], but a sample about twice as long was used in the present study to examine long term dynamics. The thickness of the sample was 50~70 μm, and it was controlled by the use of Pt sheets as spacers between the glass slides. Eutectic composition, 8.4 wt% of C_2Cl_6, as well as off-eutectic compositions were examined. The alloy composition was determined by measuring the thickness of the single phase layer ahead of the eutectic plane after the cell had been stabilized using the known temperature gradient value. Compositions were also checked from the volume fraction measurements when planar eutectic interface was observed.

The temperatures of the hot and cold baths were controlled to give temperature gradient, G=1.80 K/mm. Interface temperature measurements were made from CBr_4-C_2Cl_6 with the calibrated K-type thermocouple. The temperature was read through the Keithley scanner every 3 seconds with the computer program during the actual run. The change in the temperatures with the distance is shown in Figure 1 with a schematic view of the growing interface and the tip of the thermocouple. The interface temperature was thus measured by monitoring the

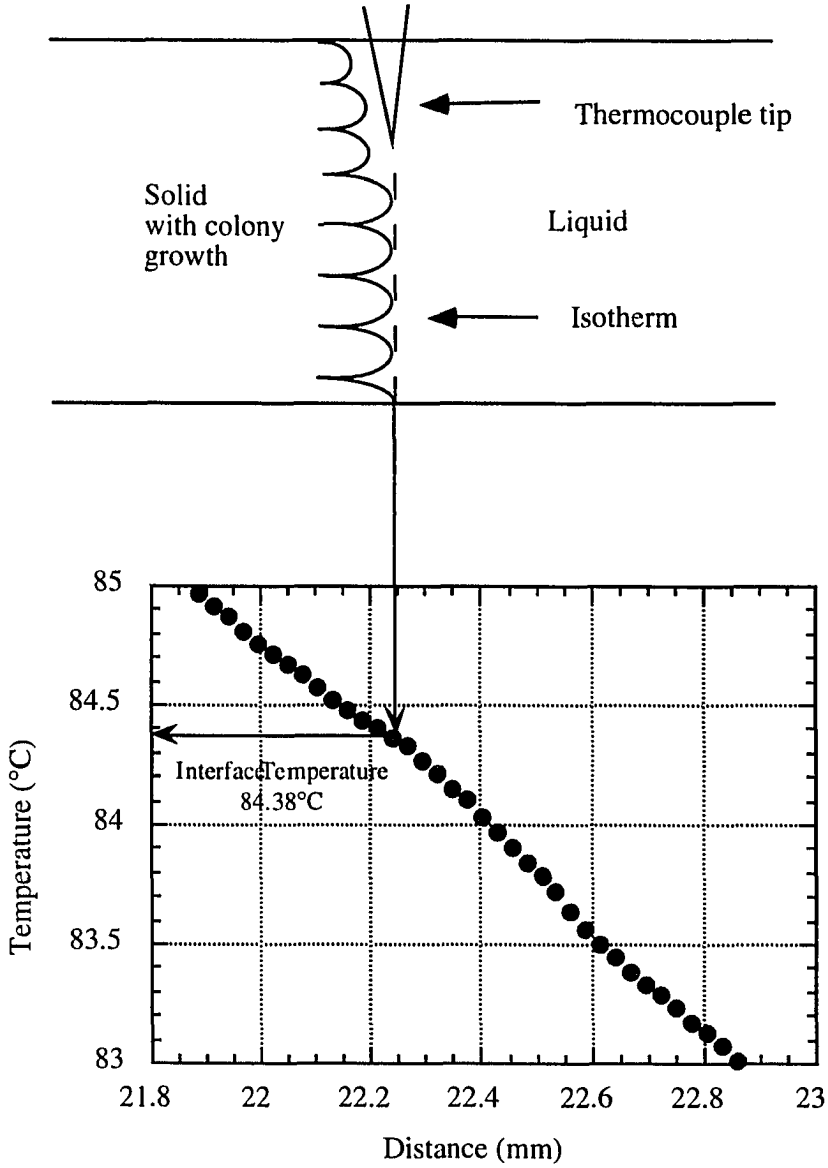

Figure 1. Schematics of actual interface measurement procedure and the results for the experiment at V=9 μm/s.

position of the interface front which was parallel to the tip of the thermocouple junction away from the interface, since the presence of the thermocouple perturbed the interface around the thermocouple region. The temperature reading was taken in the ranges of 0.003 mV (0.072 °C) at most. The minimum value was taken when the reading was made with the ranges in the temperature.

The growth velocity was examined in the range of 0.5μm/s~100μm/s, and about 4.3 cm of the sample was solidified each time after stabilizing the sample. The same sample was used throughout a given set of experiments. Photographs were taken at definite time intervals or the dynamic changes were recorded on a video tape for the further investigation. Detailed experimental method can be found elsewhere [21].

Eutectic spacings as well as those of the colony growth were measured as a function of velocity. Eutectic spacings were taken only from the central part of the colonies after the planar eutectic interface broke down into cellular and dendritic eutectics because the eutectic spacing is generally nonuniform, i.e. it increases from the center to the boundary of the colony. Colony spacings were measured from the micrographs of cellular and dendritic eutectics. Since eutectic dendrites were found to grow in the specific growth direction, spacings were measured for colonies that were growing in the same direction, close to the heat flow direction. For both, eutectic and colony spacing, average values along with minimum and maximum values were determined.

III. Results

Experiments were carried out over a range of velocity, 0.5~100μm/s, with temperature gradients varying from 1.64 to 1.88K/mm. These results are divided into different aspects of two-phase microstructures that include (1) morphological observations, (2) two phase planar interface instability, (3) mechanisms of the formation of two phase cellular and dendritic

interfaces, (4) interface temperature variation with velocity, and (5) eutectic and colony spacings as a function of velocity.

(1) Morphological Observations

Different interface morphologies observed in this study are shown in Figure 2. Planar eutectics were observed at lower velocities, whereas eutectic dendrites were observed at higher velocities. In the intermediate velocity range, two different types of cellular colonies were observed, and they are termed as "fan" and "needle" colonies according to their morphological features. The difference in their shapes came from the orientation effect such that if the growing colony assumed a nonpreferred orientation, it formed a fan colony in which the lamellae became curved and grew normal to the macroscopic interface. If the lamellae were aligned along the preferred orientation, a needle type colony was formed in which the lamellae were straight even for a curved two-phase cellular or dendritic growth front. In the dendritic growth regime only needle colonies were observed.

In the cellular range, both fan and needle colonies were often observed to be present next to each other. In this case, the needle type colonies were always leading so that the interface temperature of the needle colony was higher than that of the fan type colony, i.e. the interface undercooling for the needle colony was smaller. This is because the preferred orientation has a lower kinetic undercooling than the other orientations. If the experiments were carried out long enough, most of the fan type cellular colonies were observed to die out leaving needle colonies along the entire interface.

At higher velocities, the side branch formation became evident resulting in eutectic dendrites. As can be seen in Figure 2(d), the characteristics of these morphologies were similar to those of the needle type colonies near the tip region. The tip region consisted of a few lamellae and was found to become sharp as the velocity was increased. This change in the tip region was analogous to that occurring in the single phase growth at the cell-dendrite

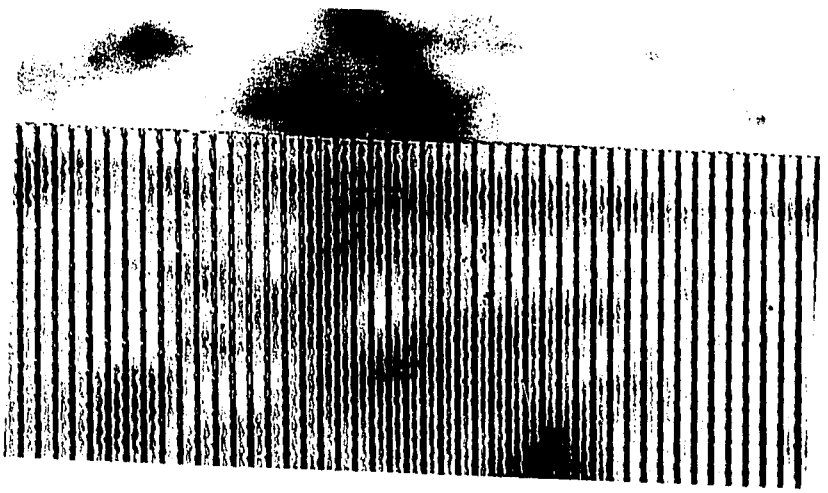

(a)

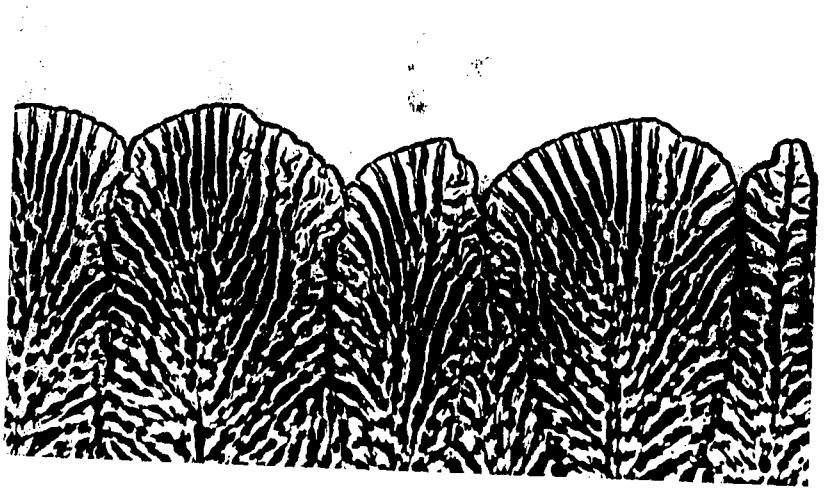

(b)

Figure 2. Basic microstructures according to different velocities (from lower to higher) (a) planar eutectic (b) cellular eutectic: fan type (c) cellular eutectic: needle type (d) eutectic dendrites.

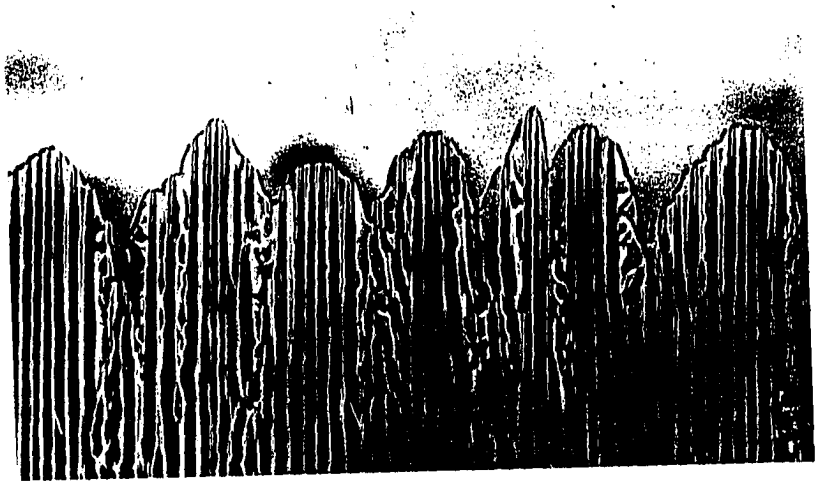

(c)

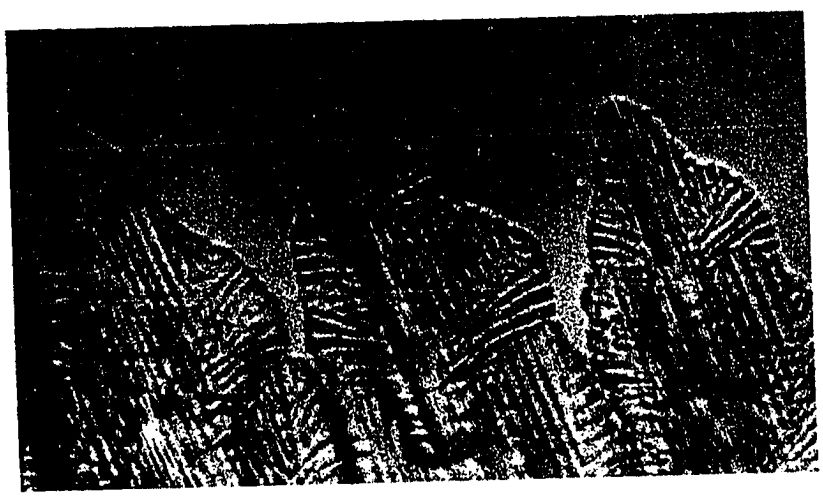

(d)

Figure 2. Continued.

transition condition. The mechanism of the side branch formation, however, was quite different from that of the single phase dendrites. First, the α phase at the side was observed to show a branching instability and one of the branches grew away from the growth direction. β phase was then nucleated between the branched α phase instabilities. This mechanism of side branch formation was observed above the two-phase cellular to dendritic transition condition (V>5-6 μm/s at G=1.8K/mm).

(2) Two Phase Planar Interface Instability

A series of experiments was carried out on the same sample in order to determine the critical velocity for the planar eutectic interface instability. The velocity range investigated was from 2-6μm/s at G=1.8K/mm. The interface was observed to become unstable at 2.5μm/s, giving the critical condition for the planar interface instability as $(G/V)_{cr} = 7.2 \times 10^4$ Ks/cm^2.

Before the interface was perturbed into colony structures, an "incubation time" was observed during which the planar eutectic interface remained stable. This incubation time was required for the impurity atoms to develop a sufficient concentration gradient ahead of the interface to attain the constitutional supercooling condition. The incubation time, τ, decreased with an increase in velocity, as shown in Figure 3. The basic relationship was obtained as $\tau = A/V^2$, where $A = 1.67 \times 10^{-4}$ cm^2/s, which is proportional to the diffusion coefficient of the impurity in the liquid.

(3) Mechanisms of the Formation of Two Phase Cellular and Dendritic Interfaces

Once the interface became unstable, the colony formation occurred through the process of wave length selection, as shown in Figure 4. The basic process of interface instability and the subsequent reorganization of the macroscopic interface shape into a periodic array of cellular colony was found to be very analogous to the formation of cellular structures in single phase alloy. However, for the eutectic front, this long range instability was controlled by the

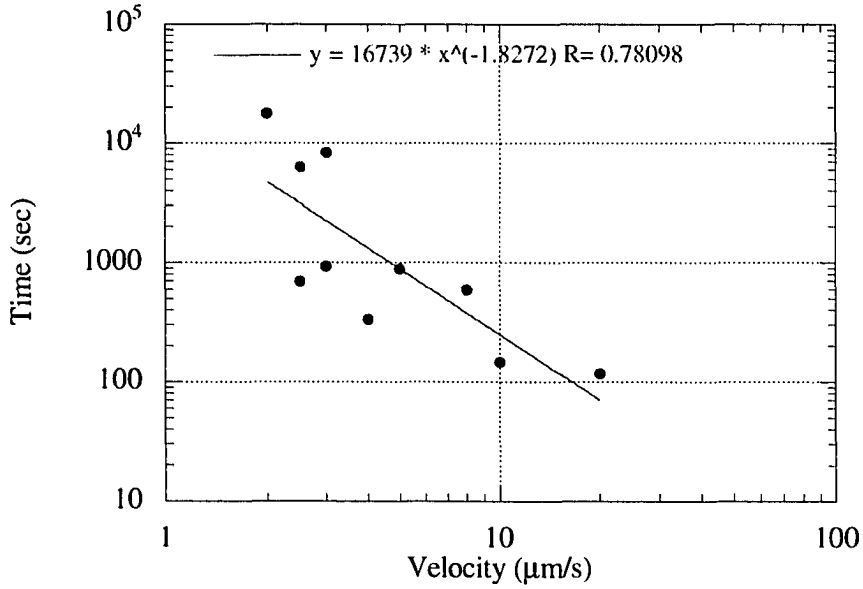

Figure 3. The incubation time measured as a function of velocity.

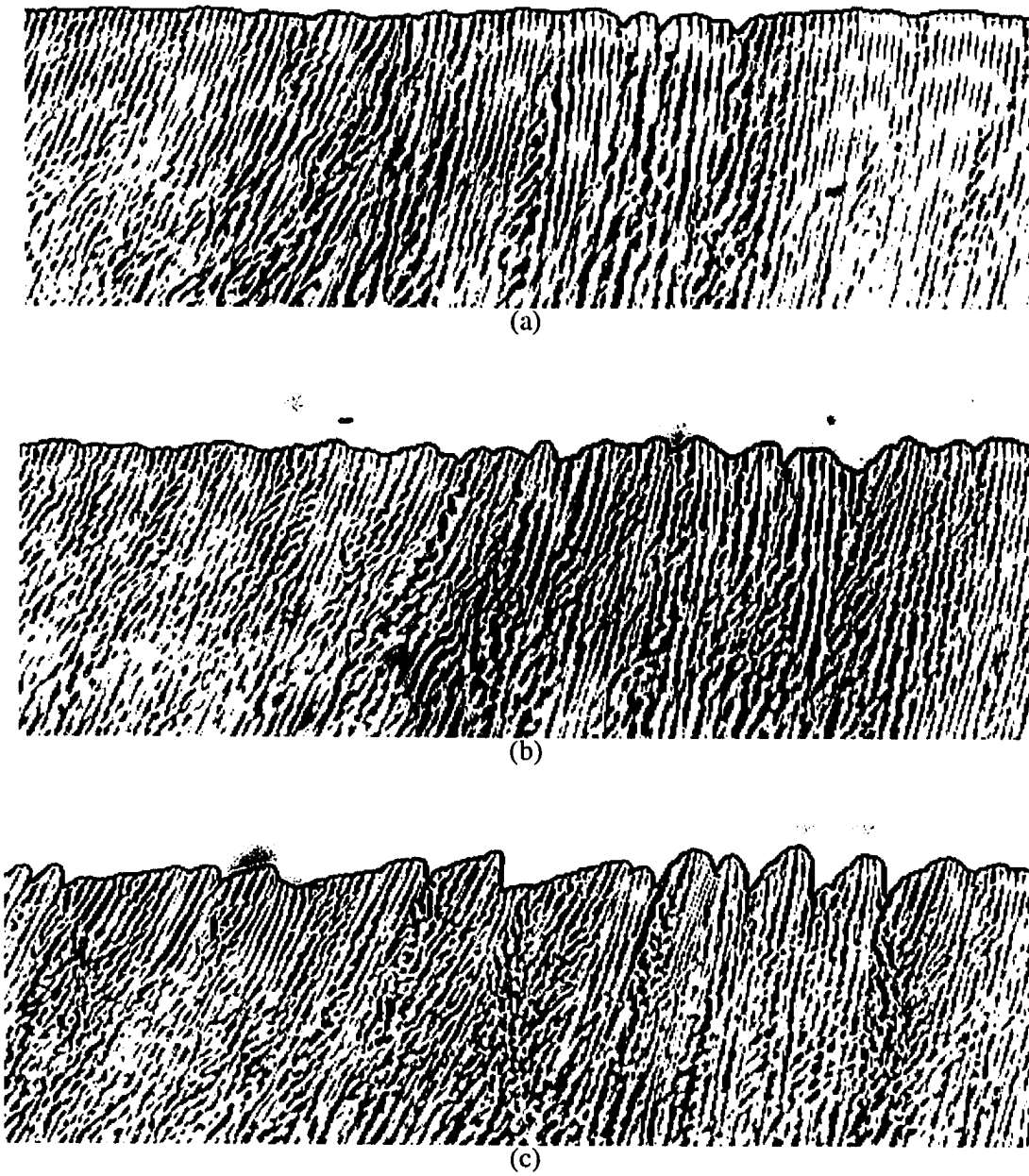

Figure 4. Time sequence of gradual interface perturbation into colony structure after the velocity change from V_1=2μm/s to V_2=4μm/s at times; (a) at 23m 20s (b) at 23m 50s (c) at 24m 50s.

diffusion of the third component. The major difference for the instability of a eutectic front is that the eutectic structure must also go through the readjustment process to conform to the macroscopically curved interface, if the eutectic structure is to remain stable. Thus, the mechanism by which the eutectic structure adjusts is crucial in determining the difference in eutectic characteristics, such as the eutectic spacing, between a planar and a nonplanar eutectic.

In order to examine the dynamics of the colony interface, a set of five separate experiments was carried out at velocities ranging from 1~5μm/s. Each experiment was held long enough to make sure that steady state was reached, and the results are shown in Figure 5 for V=1, 3 and 5μm/s. The interface was planar at V=1μm/s during the entire run, whereas colonies were observed at velocities of 3 and 5μm/s. For V=3μm/s, the instability was triggered at t=17.3 min and formed a cellular eutectic at t=23.7 min. When the interface became unstable, a sharp change in the relative position was observed. The relative positions of the leading colony interface at V=3μm/s, and V=5μm/s show more jagged behavior with larger amplitudes compared to the one from a planar eutectic. Some of these large fluctuations in the relative position came from the oscillations in the tip velocities of the colonies, as the tip temporarily becomes unstable and forms a single phase dendrite since the initial composition of this alloy is off-eutectic (8.26wt% C_2Cl_6). As soon as the single phase appears, the local velocity is reduced due to the local compositional changes, and the coupled growth is resumed.

Some long range oscillations are also seen at V=1 and 2μm/s, and these can correlated with the formation of tilted eutectic grains in which lamellae were growing with some angle with respect to the heat flow direction. The effect of tilting on the average eutectic spacings at V=2μm/s is shown in Figure 6. A tilted eutectic was formed after some initial transient at around t=120 min, and it reverted to a normal eutectic around t=200 min. We note that a significantly larger spacing was observed in the tilted regime than in the regime of straight lamellae.

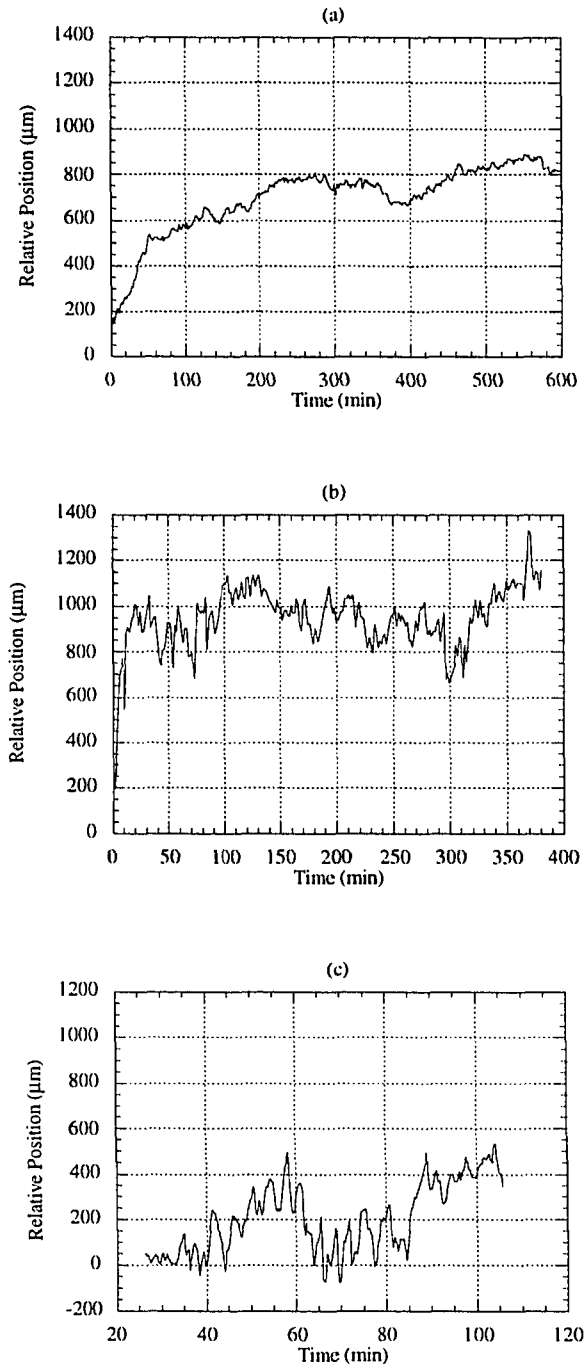

Figure 5. Relative positions with time at different velocities (G=1.8K/mm, C=8.26wt% C_2Cl_6) (a) V=1μm/s, (b) V=3μm/s, and (c) V=5μm/s.

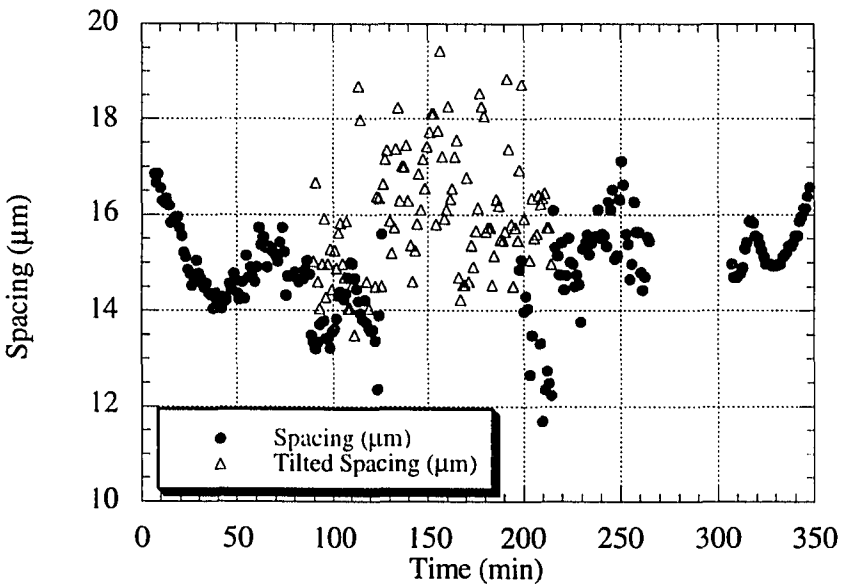

Figure 6. Average eutectic spacings with planar eutectic interface at V=2μm/s.

(4) Mechanism of Eutectic Spacing Adjustment

Since colonies are formed by the presence of a third impurity element, the long range instability of the interface is determined by the impurity element. As in the case of single phase instability [50], grain boundaries play a crucial role in the initiation of the instability in the eutectic system. As the interface region near the grain boundary begins to amplify rapidly, the eutectic structure must also cooperate and alter its characteristics if the two-phase structure is to remain stable. We shall thus examine how the coupling between the macroscopic change in the interface shape and the microscopic adjustment in eutectic spacing occurs.

There are two possible ways by which the eutectic structure can conform to a curved interface. Since the curved interface increases the solid:liquid interface area, either the eutectic spacing needs to be increased or new lamellae (or rod) need to be created. In fact, both these processes were observed to be operative in our experimental studies. The most common mechanism by which eutectic structure increased its spacing was through the process of tilting, since the tilted eutectics are stable at larger spacings [23-25]. The tilting mechanism was particularly operative for fan type colonies. The creation of new lamellae occurred through the tip splitting of the major phase and the subsequent nucleation (or growth) of the second phase in the grooves. In fact, for fan colonies both the tip splitting and tilting were observed to occur simultaneously, and the spacing adjustment was quite complex, as we shall now discuss.

The dynamical process of the change in the eutectic structure during the formation of fan type colonies is shown in Figure 7. As the interface near the grain boundary became curved, the eutectic structure responded with the tilting of the lamellae. As shown in Figure 7(a), the tilted lamellae formed with a larger local spacings. In the process of tilting of eutectic lamellae to confirm to the macroscopic interface shape change, an overshoot in the tilting process occurred so the spacing of the tilted lamellae became larger than the stable spacing. These tilted lamellae thus became unstable to tip-splitting, and small depressions were formed in the major phase, as seen in Figure 7(b). These tip-splitting instabilities then propagated

(a)

(b)

Figure 7. Time sequence of tiltings and splittings in the lamellae which result in curving of lamellae to colony formation (a) t=3 hrs 0.24 min (b) t=3 hrs 5.69 min (c) t=3 hrs 10.23 min (d) t= 3 hrs 15.22 min.

(c)

(d)

Figure 7. Continued.

laterally towards the inside of the eutectic grain, causing neighboring lamellae to split. The second phase was then formed in the groove, thereby creating additional two-phase structure to accommodate the curvature of the macroscopic interface. Once a new lamellar is created, the overall adjustment of spacing goes through a complex dynamical process. The new lamellar interacts with the neighboring lamellae, which becomes smaller, and then readjusts to give rise to wavy (or oscillatory) mode, as seen in Figure 7(c).

Once the initial curved interface was established, the subsequent adjustment of the interface curvature was often coupled with the creation of new lamellae through a series of repeated splittings of lamellae at the same location of the interface, as shown in Figure 8. Whenever splitting occurred, the newly formed lamellae extended slightly further out and caused lateral translation of the neighboring lamellae to establish stable eutectic spacing, causing the lamellae to become curved with time. These repeated splitting events thus played a crucial role in the formation of fan type colonies, both by providing additional lamellae and by bending of the lamellae to allow the interface to assume the shape that was dictated by the impurity element. As the lamellae became curved, a larger value of eutectic spacing was found.

A somewhat different mechanism was observed for the formation of needle colonies. Although the formation of these colonies was also initiated with a long wavelength instability, they were not accompanied by an array of depressions of the lamellae as was observed for the fan type colonies. Instead, the branching of the lamellae was observed from one of the lamellae at the side that was growing near the eutectic grain boundary, as seen in Figure 9. These branched lamellae grew out faster with a certain orientation causing the neighbors to be bent to the boundary area. As in the single phase cellular growth, when the size of the needle colony became large, the splitting of the colony was observed which allowed the colony to adjust to the steady state colony spacing value.

Experimental observations show that fan and needle morphologies coexisted under the same conditions. Due to the anisotropy effects, the needle type colonies were often observed

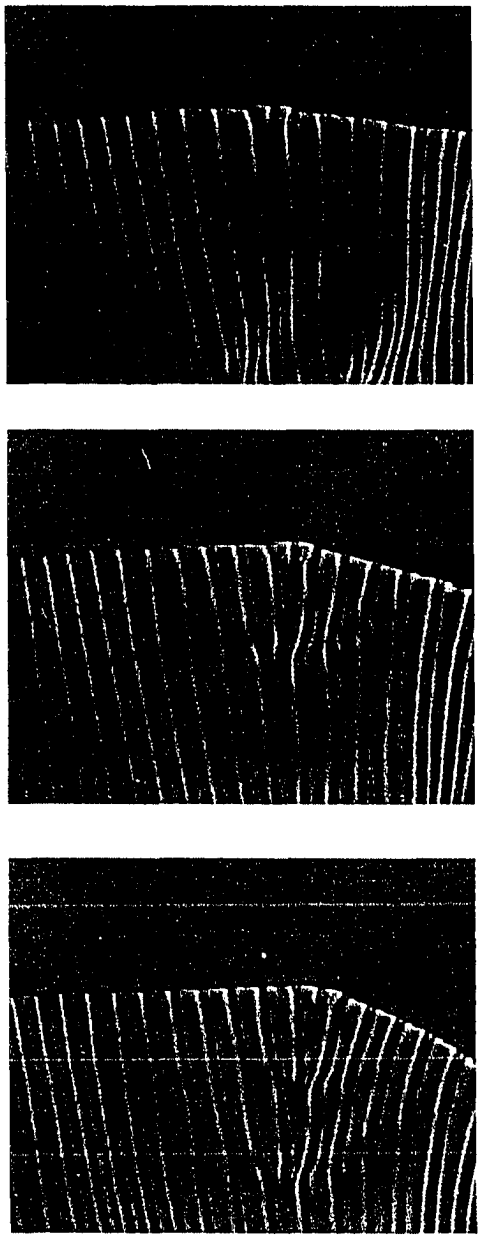

Figure 8. Time sequence of the repeated splitting at V=7μm/s. Lamellar bending can be observed with continued splittings of minor phase in the similar area from (a) to (c)

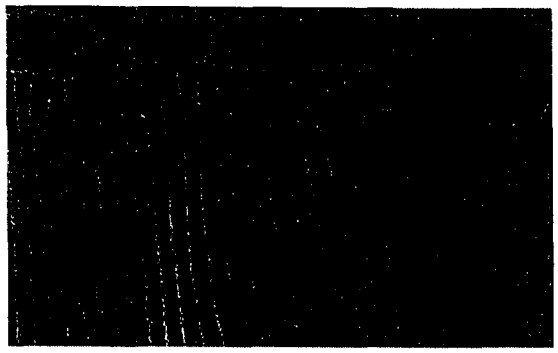

(a)

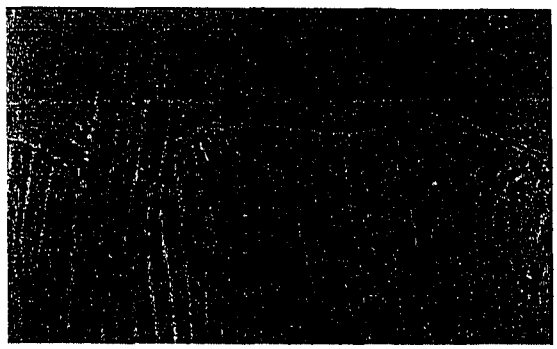

(b)

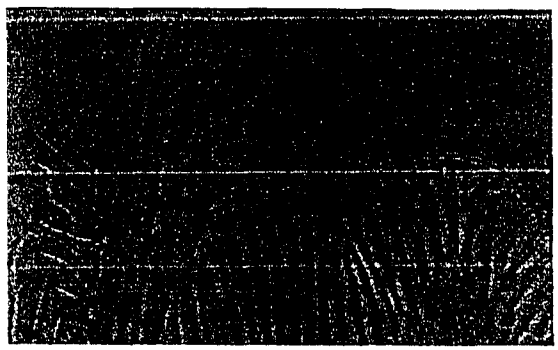

(c)

Figure 9. Sequence of branching mechanism in the formation of the needle colonies at V=5μm/s (a) t=17.4 min (b) t=18 min (c) t=18.7 min.

to form first. Since these needle colony regions were leading the unperturbed planar eutectic interface, the impurity rejection from these needle regions reduced the growth of the planar interface in the vicinity of the needle colony, which in turn led to a curved fan type colony next to the growing needle colony. Figure 10 shows the resultant microstructure in which the needle colony at the right hand side was formed first and it led to the formation of a fan colony at the left side.

(5) Interface Temperature Variation with Velocity

A series of experiments was carried out in order to examine the changes in interface temperature with velocities. Figure 11 shows the variation in interface temperature with velocity. The interface temperature increased at first with the increases in the velocity when colony formation occurred, it then showed a maximum around V=8μm/s, and finally decreased as the velocity was increased. The temperature increases in the cellular eutectic (up to V=5μm/s) were observed to be large in scale compared to the changes in the region of the eutectic dendrites that formed at higher velocities. This observation is qualitatively very analogous to the interface temperature variation in a single phase.

(6) Eutectic and Colony Spacings with Velocity

Eutectic spacings were measured from the planar eutectic interface as well as from the colony structures. When the eutectic spacings were measured from the perturbed structures, the spacings from the middle part only were measured. The result is shown in Figure 12, in which the error bars show the standard deviation. It can be seen that the average eutectic spacing (solid circle) decreases with velocity at first before the breakdown. As soon as the planar eutectic interface becomes unstable, an increase in eutectic spacing was found. As velocity was increased further, the spacing started to decrease. Figure 12(b) shows the maximum and minimum values measured over several colonies. Measurements from a

Figure 10. A mcirograph of fan and needle colony that were present next to each other at V=3μm/s.

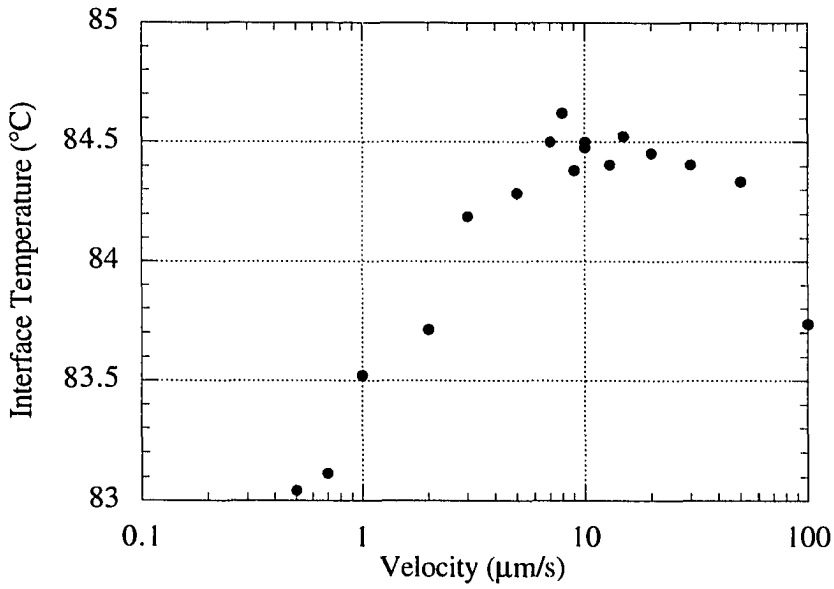

Figure 11. Interface temperature variation with velocity under constant temperature gradient (G=1.8 K/mm).

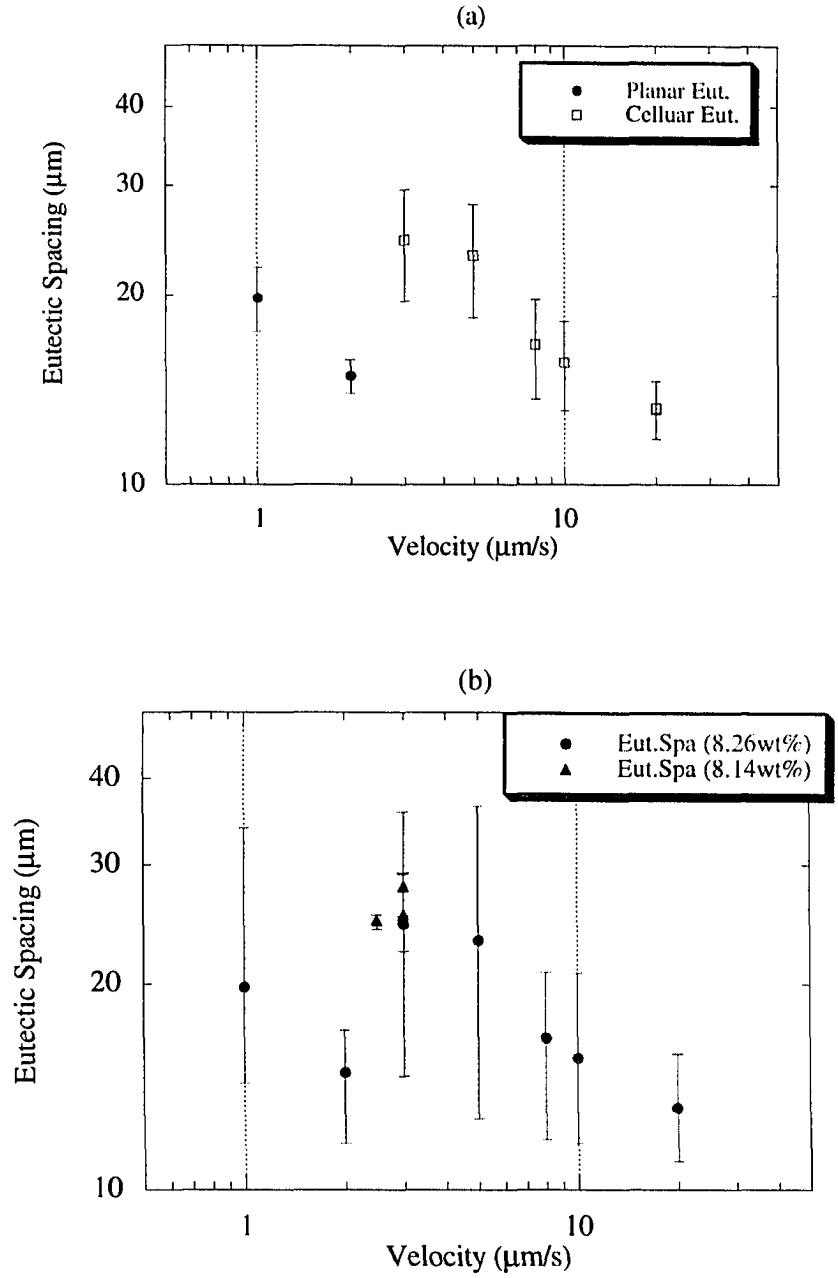

Figure 12. Eutectic spacings from planar and colony eutectics as a function of velocity. (a) Average eutectic spacing with standard deviation (C=8.26wt%) (b) Maximums and minimums (in error bars) with average eutectic spacings.

different composition (8.14 wt%) also illustrate slight increase in the eutectic spacing with an increases in the velocity at the threshold of planar interface instability.

Colony spacings were also measured as a function of velocity. The spacing variation with the velocity is shown in Figure 13, with open and filled circles showing the average spacings for two different compositions. The error bars in Figure 13(a) represent the standard deviations in the average spacing measurements. The same data are also shown in Figure 13(b) with the maximum and the minimum values of colony spacings. The colony spacing was found to increase initially with velocity, reached a maximum value at V=8μm/s, and then started to decrease with further increase in velocity when side branches developed.

IV. Discussion

(1) Colony Formation

A possible origin of the eutectic colonies was suggested by Tiller [2] who showed that constitutional supercooling ahead of the planar eutectic interface could result in the formation of a stable cellular interface. For a binary eutectic growth, the diffusion field does not produce enough supercooling to promote cell formation. Thus, the instability of eutectic structures was proposed to occur because of the present impurity atoms which led to the constitutional supercooling condition. From the solution of the steady state diffusion equation in the liquid, Tiller obtained for the solute profile in the liquid as

$$C_L = C_0 \left[1 - \{(1 - k_c) / k_c\} e^{-Vz/D} \right] \qquad (1)$$

where

$$k_c = \left[\lambda_\alpha k_{\alpha c} + \lambda_\beta k_{\beta c} \right] / \lambda$$

and C_0 is the concentration of the third element. $k_{\alpha c}$ and $k_{\beta c}$ are the distribution coefficients of the solute in the α and β phases respectively. λ is the eutectic spacing, and λ_α and λ_β are the

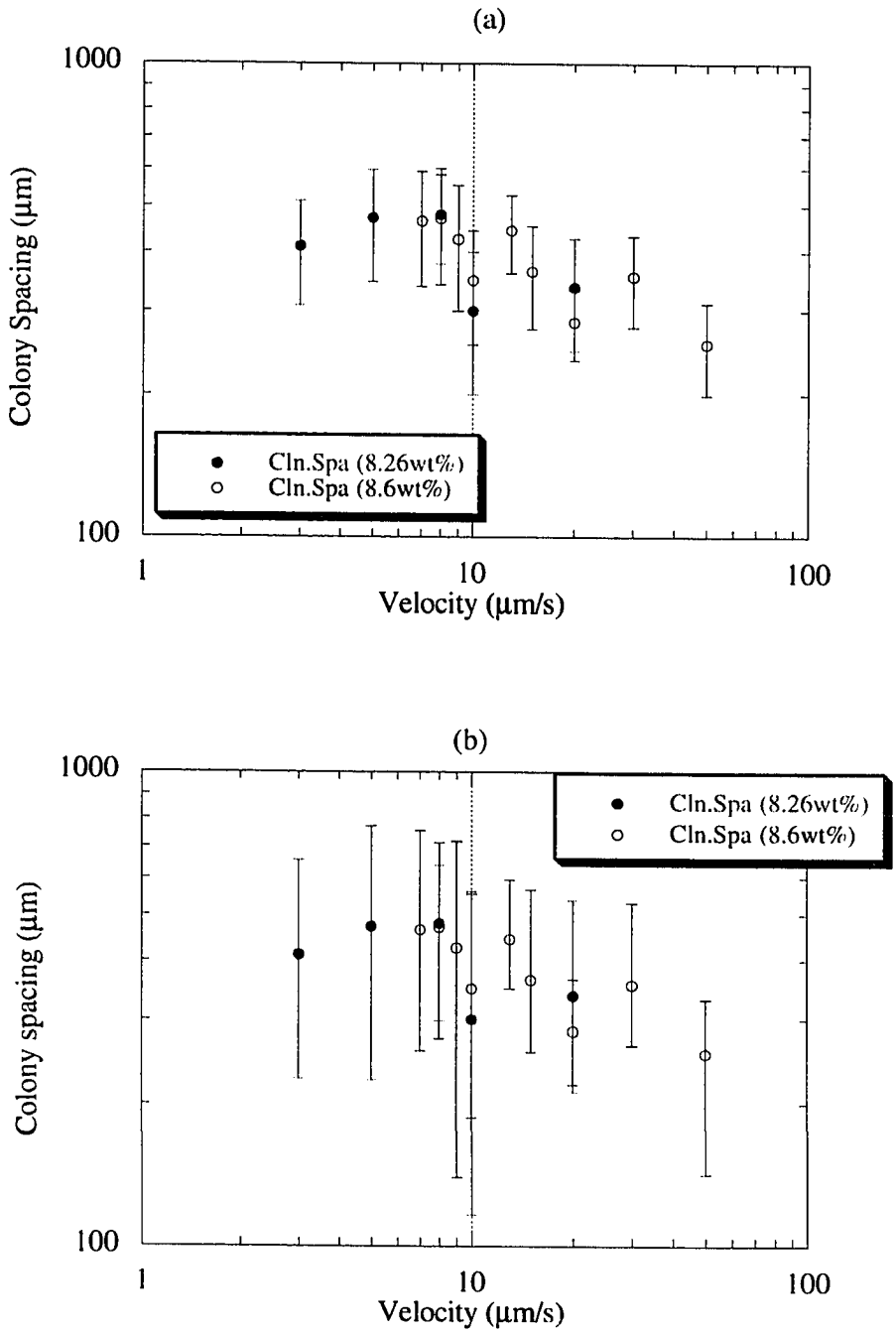

Figure 13. Colony spacings as a function of velocity from two different compositions. Error bars represent (a) standard deviations (b) maximums and minimums.

width of the α and β lamellar.

The above result is analogous to the one for solute concentration ahead of a planar interface during the growth of a single phase. The only difference is that the k value is the weighted average from the both phases in the eutectic growth. In the transition from a planar to a cellular interface only the plane wave term was considered to be appreciably affected since the presence of a cellular interface will create lateral diffusion fluxes over distances that are large compared to the lamellar spacing. The constitutional supercooling criterion for the stability of a planar two-phase growth in presence of an impurity was then obtained as

$$\frac{G}{V} = \frac{m_c C_0 (k_c - 1)}{k_c D} \qquad (2)$$

It is apparent from the above equation that the probability of colony formation would be increased with an increase in V, or a decrease in G or an increase in impurity concentration (C_0).

Weart et al. [1] carried out directional solidification in Al-Zn, Sn-Zn and Al-Cu systems, and showed that colony formation is characterized by growth parameters V and G in the same manner as those for the planar interface instability in single phase alloys. Gruzleski and Winegard [9, 10] studied colony formation in the Sn-Cd system and found some deviation from the constitution supercooling criterion. Kraft and Albright [4] also examined the critical condition for eutectic colony formation in the Al-$CuAl_2$ system. They found that pronounced eutectic colonies were formed only when the ratio of G/V was below a certain critical value (10Khr/cm^2). Furthermore, pronounced colony structures were evident either near the thermocouple bead where impurity atoms were segregated or in the last top part of the sample where larger amount of impurities were present. The need for impurity to form colonies was demonstrated by Chilton and Winegard [3] by showing the suppression of colonies when zone

refined lead and tin alloys were used, and by Kerr et al. [7] by adding 0.5 wt% Bi in the Sn-Cd system.

More detailed theoretical models, based on the Mullins-Sekerka [31] approach, to study the stability of a planar eutectic structures have been developed by Strassler and Schneider [49], Hurle and Jakeman [30], and Cline and Tarshis [34]. A more rigorous stability analysis on the two dimensional lamellar eutectic was carried out by Datye and Langer [40]. Unlike the previous works [30, 33] in which they treated the eutectics as a single phase by averaging over the properties of the two different solid phases, they allowed the variations in lamellar spacings, and they also released the assumption of a flat solidification front. Starting from the J-H model with dimensionless parameters, perturbation analysis was carried out in which the triple point was allowed to move arbitrarily in two directions. The results showed two limits of stability. One of the limits of instability was found to occur exactly at the point of minimum undercooling, so that eutectic growth becomes unstable for spacings less than the minimum undercooling value. This instability was first proposed intuitively by J-H [22] and predicted by the model of Strassler and Schneider [49]. Datye and Langer also found oscillatory and tilting instabilities for off-eutectic compositions. Datye and Langer [40] also showed that the boundary layer in a pure binary system does not induce Mullins-Sekerka type long-wavelength instability even for off-eutectic compositions. The system rather was found to be stabilized by the local variations in the volume fractions of each phases, giving rise to oscillating modes. This oscillatory instability was found to depend upon the thermal gradient value. From the rigorous theoretical analysis, it is now well-established that colony formation is possible only when a third component (or impurity) is present in the system.

(2) Interface Temperature Variation with Velocity

We shall examine the variation in interface temperature with velocity by considering planar, cellular and dendritic interface of the two phase structure. In order to examine the

physics that lead to the establishment of the interface temperature, we shall first divide the undercooling into different terms as:

$$\Delta T = T_E - T_i = \Delta T_P + \Delta T_E + \Delta T_{cd} \tag{3}$$

where T_E is the binary eutectic temperature, and T_i is the interface temperature. The undercooling, with respect to the binary eutectic temperature, is composed of: the planar interface undercooling due to the presence of third element (ΔT_p), the undercooling for the two-phase cell or the dendritic growth (ΔT_{cd}) due to the presence of an impurity, and the undercooling for the planar or nonplanar eutectic growth (ΔT_E) which is controlled by the diffusion field of the binary alloy. The general effects of these undercoolings on the interface temperature is shown schematically in Figure 14. We shall now examine each contribution separately.

For a planar eutectic interface, the steady-state growth occurs at the solidus temperature in the ternary system, which gives

$$T_i = T_E + m_c \left[\frac{C_0}{k_c}\right] - \Delta T_E \tag{4}$$

Where T_E is the binary eutectic temperature and T_i is the actual interface temperature, $m_c = dT/dC^L_c$ is the slope of the eutectic valley, C_0/k_c is the average liquid composition at the interface. The second term on the right hand side in equation (4) gives the effect of the third component on a planar interface growth. The third term is the eutectic undercooling which, for a planar eutectic front, is given by the Jackson and Hunt model [22] as $\Delta T_E = A'V^{1/2}$. A' is approximately a constant even though there is a small dependency of C_0 through m_c [36].

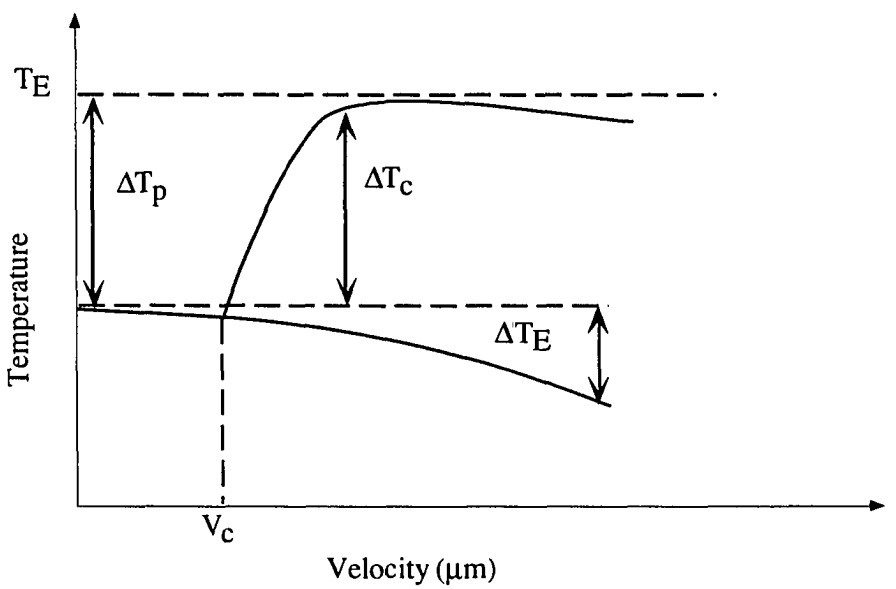

Figure 14. Schematic representation of the each terms for the colony undercooling.

When the planar two phase eutectic breaks down to a cellular two phase eutectic, the undercooling at the colony tip will change. The temperature of the cell tip will initially rise due to radial rejection of the impurity element and then decrease with increasing velocity when cellular eutectic transforms into a dendritic eutectic. By direct analogy with single phase cell model, we assume that the cell tip assumes the temperature for which the constitutional supercooling vanishes, which gives

$$T_i = [T_E + m_c\ C_0 / k_c] + \left[m_c C_0 (k_c - 1) / k_c - \frac{GD}{V} \right] - \Delta T_E \qquad (5)$$

or

$$T_i = [T_E + m_c\ C_0] - \left[\frac{GD}{V} \right] - \Delta T_E \qquad (6)$$

Note that for a cellular eutectic, the interface temperature is composed of three terms: the first term is the liquidus temperature of the ternary alloy, the second term is the cellular undercooling, and the third term is eutectic undercooling. The eutectic undercooling for nonplanar front will deviate from that for the planar front.

At higher velocities, when dendritic structure forms, the change in interface temperature is controlled by the boundary layer of the impurity element. A more detailed model of dendrite growth, based on the Ivantsov solution, can be used to calculate the dendrite tip undercooling. However, we shall use a simplified model of Burden and Hunt [41, 42] which captures the basic physics of the model, and which gives a simpler relationship, as [36]

$$T_i = [\ T_E + m_c C_0] - \left[\frac{GD}{V} \right] - 2\left[\frac{-2aV}{D} (m_c (1 - k_c) C_0) + \frac{k_c}{V} DG \right]^{1/2} - \Delta T_E \qquad (7)$$

The above equation includes the interface undercooling due to the formation of dendrites and cells. The simple addition of cellular and dendritic undercooling at interface is justified since the dendritic undercooling in the cellular range and the cellular undercooling in the dendritic range are negligible. Equation (7) was developed by McCartney et al. [36] under the assumption that the eutectic undercooling for a nonplanar interface is the same as that for a planar eutectic interface.

Experimental results on the interface temperature variation with velocity show the general trend predicted by the model, Figure 14. The precise quantitative comparison, however, is difficult since one requires the knowledge of several system parameters that are not available accurately, and one needs a model of nonplanar eutectic that has not been developed as yet. Nevertheless, we can get a reasonable estimate by approximating the eutectic undercooling as that for a planar interface [36], and evaluating system constants by using the experimental results.

If the eutectic undercooling is small compared to the term (GD/V) at low velocities in the cellular range, one can use planar eutectic undercooling. In this case, equation (6) can be rearranged as

$$T_i + \left[A' V^{1/2}\right] = \left[T_E + m_c C_0\right] - \left[\frac{GD}{V}\right] \qquad (8)$$

where $\Delta T_E \approx A' V^{1/2}$ for a planar eutectic. The constant A' was evaluated for the binary eutectic case. The values of the diffusion coefficient and the $m_c C_0$ can now be obtained from the slope and intercept of a plot of $T_i + A'\sqrt{V}$ versus 1/V, as shown in Figure 15. Using the value, $T_E = 84.7°C$, which is the maximum limit of the binary eutectic temperature reported by Mergy et al. [27], and the known value of G, the diffusion coefficient of the ternary element was obtained as 6.55×10^{-6} cm^2/s. The intercept on the y axis, (84.638°C), which corresponds

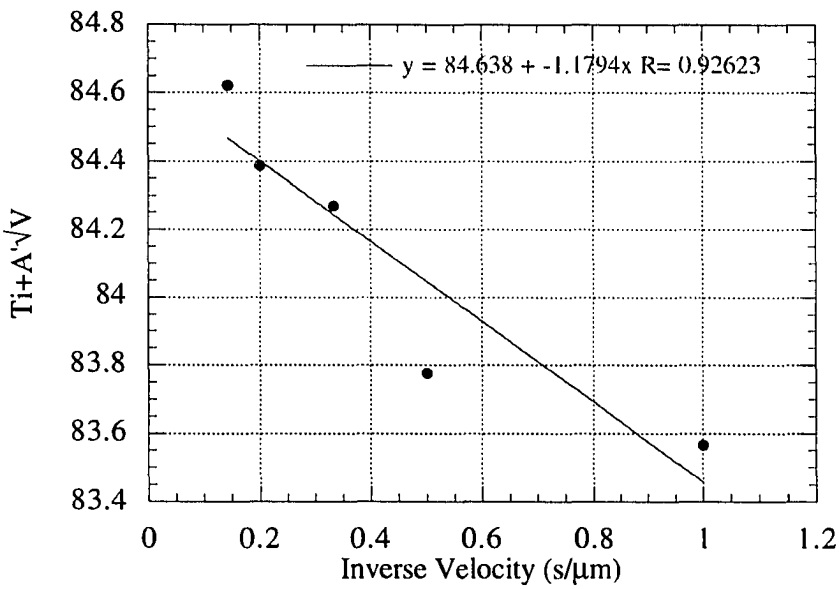

Figure 15. Interface temperature ($T_i + A'\sqrt{V}$) versus inverse of velocity for lower velocity region (1~7μm/s) for obtaining the diffusion coefficient.

to the liquidus temperature of the ternary alloy, $T_E + m_c C_0$, gives $m_c C_0 = -0.062$ °C. The distribution coefficient (k_c) of the third component was estimated from the measured value of the interface temperature at V=1μm/s with the planar eutectic and using the equation (4) above. The value of k_c was calculated as 0.054. Now that the basic system parameters are known, the available theoretical models could be examined. Using the above estimated values, the interface temperature was calculated as a function of velocity in the planar and cellular regime by using equation (6), and the results are shown in Figure 16. The interface temperature was found to decrease with the velocity in the planar eutectic regime, but it increased with the formation of cellular eutectics.

Note that the maximum in interface temperature can occur in the cellular regime, since as the cellular undercooling becomes zero, the eutectic interface undercooling increases with velocity. Also, in the dendritic colony regime the dendrite tip undercooling, in equation (7), can be approximated as $A_d V^{1/2}$, which gives a similar relationship as the eutectic undercooling. The value of A_d, however, was found to be a factor 5 smaller than the value of A' so that eutectic undercooling will become dominant at higher velocities, within the range of the validity of the dendrite undercooling model. Thus, it is important to properly characterize the eutectic undercooling for a nonplanar interface. The interface undercooling should be higher for a nonplanar interface, so that the calculated results overestimate the interface temperature values. This is shown by the interface temperature result at the highest velocity which is significantly lower than the value predicted by the planar eutectic significantly below the calculated result based on the planar eutectic model. The effect of nonplanarity of the interface also influences the eutectic spacing variation with velocity which we shall now discuss.

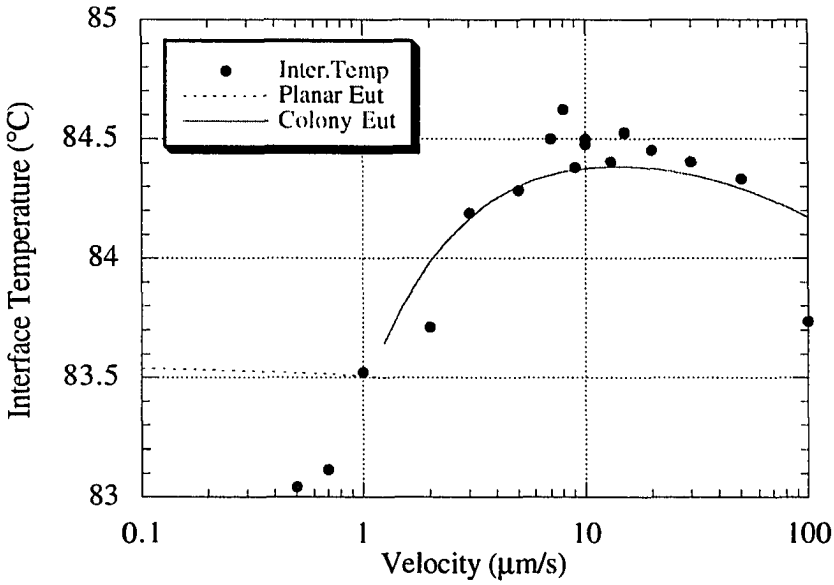

Figure 16. Comparison of the experimental data with the model from McCartney et al. [36].

(3) Eutectic Spacing Variation with Velocity

Eutectic spacings were measured from the planar as well as the perturbed eutectic interfaces. Spacing measurements were taken only from the central part when the colonies were developed at higher velocities. The spacings measured did not show linear decreases with the increases in the velocity as predicted by the planar eutectic interface model, but a small increase in the spacing was observed above the threshold velocity of instability. Figure 17 shows average eutectic spacing values in the measurements from the two different compositions (8.14 and 8.26 wt% of C_2Cl_6) along with the data from Seetharaman and Trivedi [20] that characterized average spacing in the velocity range 0.2-2μm/s. Our results for V=1, and 2μm/s for planar eutectic interface agree with the earlier results [20], and they can be described by the J-H model to give $V\lambda^2 = 3.80\pm0.8\times10^{-7}$ mm^3/s. However, the experimental data in the nonplanar eutectic regime show significant deviations from the planar eutectic growth model. Also shown in Figure 17 are the measurements from a sample with a different composition (8.14wt% C_2Cl_6) at V=2.5 and 3μm/s. These measurements confirm the increases in the eutectic spacings when the interface undergoes the morphological instability. After the break-down into the colonies, the eutectic spacings were found to decrease with an increase in velocity. The same phenomenon has been observed in earlier studies in the Al_2O_3-ZrO_2 system [17].

The deviation in the eutectic spacings from the planar interface model will now be examined. Figure 2 shows that the characteristics of eutectics are significantly different for a curved interface compared to the planar interface even at the center of the colony. For a fan-type colony, the curvature of the interface shows that the normal velocity of the interface decreases, and thus the spacing will increase, with the distance from the center. This effect, however, would be small in the center region of the colony. The major effect on the spacing occurs due to the rotation of the lamellae which gives rise to tilting. The diffusion field around a tilted eutectic is significantly different, and theoretical models have shown that the tilting

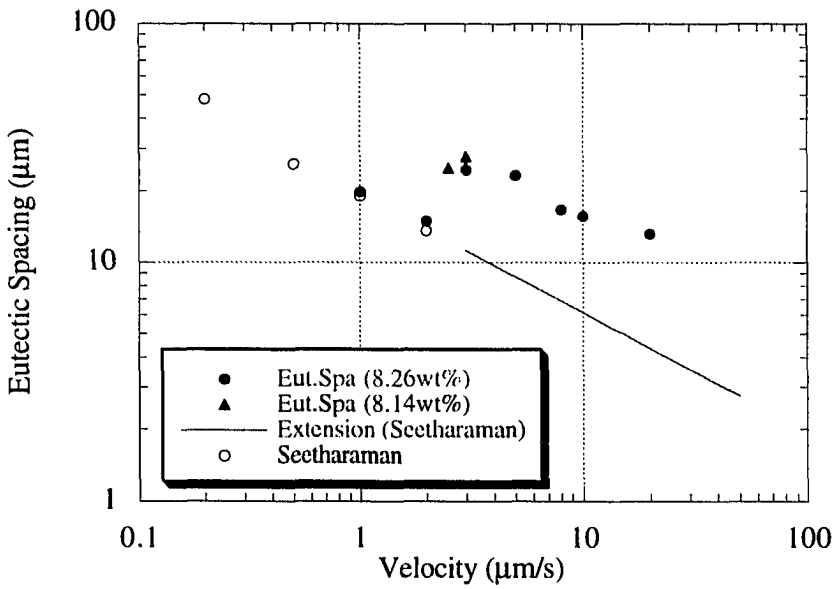

Figure 17. Average eutectic spacings from two different compositions as a function of velocity. Previous work by Seetharaman et al. [20] is shown for comparison.

mode is accompanied by an increase in undercooling and an increase in the spacing. Our dynamical studies have consistently shown that the spacing increases whenever tilting of the lamellae occurs. Thus, as the macroscopic interface becomes curved, the lamallae will tilt and increase the spacing. For needle-like colonies, the curvature of the interface at the tip is quite sharp, and it is of the order of lamellar spacing so that the diffusion field will be significantly perturbed, and coupling will become weaker which will increase the eutectic spacing. The effect of nonplanar interface will result in a spacing larger than that predicted by the planar interface model under a given velocity condition. A detailed theoretical model, based on the nonplanar eutectic needs to be developed to examine quantitatively the scaling law for nonplanar eutectics.

(4) Colony Spacing Variation with Velocity

The average colony spacings were measured at different velocities under constant temperature gradient. The results from the colony spacing measurements shown in Figure 13, and they show the following similarities to the single phase primary cell and dendrite spacing: 1) The order of magnitude is close between the colonies and single phase cells and dendrites. 2) Both growth patterns show maximum in their spacings as the velocity is increased. 3) The variation in the spacing with the growth rate follows a linear trend in the log-log plot. Thus, a similar governing equation can be used even for the two phase cellular and dendrites if the formation of colonies is controlled by the diffusion of the third element. Since the diffusion by ternary element is the key to the formation of colonies, the primary spacing model for the single phase can be applied to colony growth with the diffusion coefficient and the distribution coefficient values for the third element.

Different analytical models [44, 47, 48] show the basic variation in spacing to be given by the expression [47]

$$\lambda_1 = A\left[\{m_c(k_c-1)/k_c\}C_0 - GD/V\right]^{1/4} V^{-1/4} G^{-1/2} \qquad (9)$$

All the terms are the same as defined before, and λ_1 is the primary spacing. The equation (9) can be simplified by neglecting the second term in the bracket in the dendrite region. The value of the constant A is a function of k_c, D and Γ, where Γ is the Gibbs-Thomson parameter.

The colony spacing was examined with the model described above, and the growth parameters for the ternary element were inserted into the equation (9), and the result shown in Figure 18. The experimental values shown here are the average colony spacings from the two different compositions. A best fit was obtained for A = 330 $(cm^3K/s)^{1/4}$. The velocity dependence was found to be close to the exponent value of (-1/4) rather than (-1/2) that was suggested earlier [11, 12].

V. Conclusion

The formation of two-phase colony structure in eutrectic system was examined in a transparent organic analog system, and the mechanisms by which a planar two-phase interface evolved into a cellular and dendritic two-phase structures were characterized. Two different types of colonies were observed in the cellular regime: fan type and needle type. Needle type colonies were found to form along the preferred orientation.

Colony structures evolve due to the presence of a third element in the binary eutectic system which causes the instability of the interface. It was shown that the eutectic structure must reorganize to conform to the macroscopic curvature of the interface. Mechanisms through which the coupling between the macroscopic interface shape and the microscopic eutectic lamellae adjustment process were identified. The macroscopic curvature of the interface initiated from the grain boundary area, and the eutectic structure adjustment process was shown to occur through the tilting of the lamellae and the repeated splitting of the major phase to create

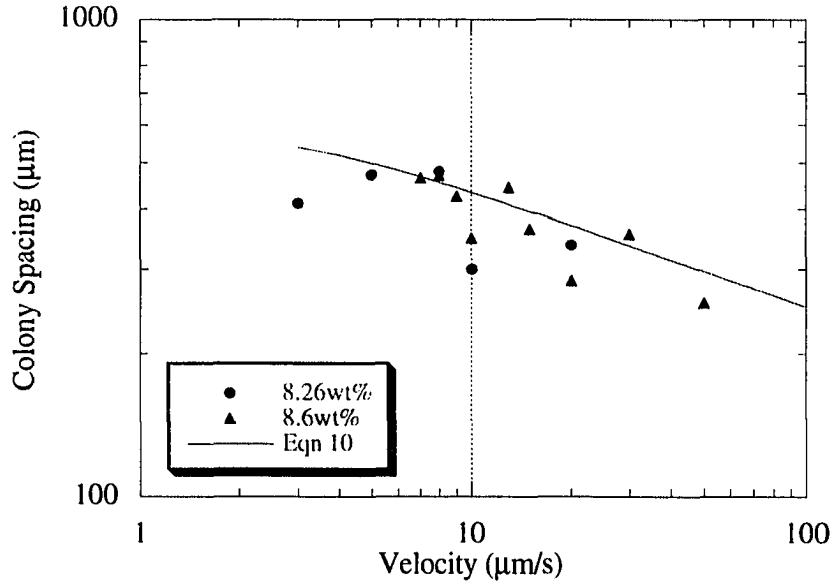

Figure 18. Comparison of the experimental data in colony spacings with the existing model on spacings in single phase cells and dendrites.

new lamellae. The process of tilting and nucleation of lamellae was shown to give rise to larger eutectic spacing.

In order to characterize colony growth, the interface temperatures, eutectic spacing at the center of the colony and colony spacings were measured as a function of growth velocity. The interface temperature and eutectic spacing were shown to decrease with velocity in the planar eutectic growth regime. However, they were found to increase as the planar interface reorganized into a cellular interface. As the eutectic became nonplanar, the interface temperature, the eutectic spacing and the colony spacing all increased with velocity, then went through their maximum values, and finally decreased when the two-phase dendritic structure was formed. Appropriate theoretical models were examined to explain the variation in interface temperature and colony spacing with velocity.

Acknowledgment

This work was carried out at Ames Laboratory, which is operated for U.S. Department of Energy by Iowa State University under contract No. W-7405-ENG-82. This work was supported by the Office of Basic Energy Sciences, Division of Materials Sciences.

References

1. H. W. Weart and D. J. Mack: *Trans. AIME*, 1958, vol. 212, pp. 664-670.
2. W. A. Tiller: *Liquid Metals and Solidification*, Ed. by ASM, Cleveland, pp. 276-318.
3. J. P. Chilton and W. C. Winegard: *J. Inst. Metals*, 1961, vol. 89, pp. 162-164.
4. R. W. Kraft and D. L. Albright: *Trans. AIME*, 1961, vol. 221, pp. 95-102.
5. L. M. Hogan: *J. Australian Inst. Metals*, 1961, vol. 6, pp. 279-288.
6. J. A. E. Bell and W. C. Winegard: *J. Inst. Metals*, 1964, vol. 93, pp. 318-319.
7. H. W. Kerr, J. A. Bell and W. C. Winegard: *J. Australian Inst. Metals*, 1965, vol. 10, pp. 64-69.

8. R. W. Kraft: *J. Metals*, 1966, vol. 18, pp. 192-200.

9. J. E. Gruzleski and W. C. Winegard: *J. Inst. Metals*, 1968, vol. 96, pp. 304-307.

10. J. E. Gruzleski and W. C. Winegard: *Trans. AIME*, 1968, vol. 242, pp. 1785-1791.

11. P. K. Rohatgi and C. M. Adams: *Trans. AIME*, 1969, vol. 245, 1609-1613.

12. W. M. Rumball: *Metallurgia*, 1968, vol. 78, pp. 141-145.

13. J. B. Bullock, C. J. Simpson, J. A. Eady, and W. C. Winegard: *J. Inst. Metals*, 1971, vol. 99, pp. 212-214.

14. M. D. Rinaldi, R. M. Sharp and M. C. Flemings: *Metall. Trans.*, 1972, vol. 3, pp. 3133-3148.

15. H. W. Weart: Ph. D. Thesis, University of Wisconsin, 1957.

16. F. L. Kennard: Ph. D. Thesis, Pennsylvania State Universiry, 1973.

17. S. H. Han, C. W. Boldt, and R. Trivedi: Unpublished Work at Iowa State University, 1993.

18. V. Seetharaman: Unpublished Work at Iowa State University, 1987.

19. T. Whitney, V. Jayaram, C. G. Levi, and R. Mehrabian: *Solidification Processing of Eutectic Alloys*, The Metallurgical Society, 1988, 199.

20. V. Seetharaman and R. Trivedi: *Metall. Trans. A.*, 1988, vol. 19A, pp. 2955-2964.

21. S. H. Han: M. S. Thesis, Iowa State University, 1991.

22. K. A. Jackson and J. D. Hunt: Trans. *Metall. Soc. AIME*, 1966, vol. 236, pp. 1129-1142.

23. G. Faivre, S. De Cheveigne, C. Guthmann, and P. Kurowski: *Europhys. Lett*, 1989, vol. 9(8), pp. 779-784.

24. G. Faivre and J. Mergy: *Phys. Rev. A*, 1992, vol. 45, p. 7320.

25. G. Faivre and J. Mergy: *Phys. Rev. A*, 1992, vol. 46, p. 963.

26. W. F. S. Kaukler: Ph. D. Thesis, University of Toronto, Toronto, ON, Canada, 1981.

27. J. Mergy, G. Faivre, C. Guthmann, and R. Mellet: *J. Crystal Growth*, 1993, vol. 134, pp. 353-368.

28. R. M. Jordan and J. D. Hunt: *Metall. Trans.*, 1971, vol. 2, p. 3401.

29. D. E. Coates, S. V. Subramanian, and G. R. Purdy: *Trans. AIME*, 1968, vol. 242, pp. 800-809.

30. D. T. J. Hurle and E. Jakeman: *J. Crystal Growth*, 1968, vol. 3, p. 574.

31. W. W. Mullins and R. F. Sekerka, *J. Appl. Phys.*, 1964, vol. 35, p. 444.

32. F. R. Mollard and M. C. Flemings: *Trans. AIME*, 1967, vol. 239, p. 1526.

33. H. E. Cline: *Trans. Metall. Soc. AIME*, 1968, vol. 242, p. 1613.

34. H. E. Cline and L. A. Tarshis: *Trans. Metall. Soc. AIME*, 1969, vol. 245, p. 422.

35. R. M. Sharp and M. C. Flemings: *Metall. Trans.* 1974, vol. 5, p. 823.

36. D. G. McCartney, J. D. Hunt and R. M. Jordan: *Metall. Trans.*, 1980, vol. 11A, p. 1243.

37. J. D. Holder and B. F. Oliver: *Metall. Trans.*, 1974, vol. 5, p. 2423.

38. T. F. Bower, H. D. Brody and M. C. Flemings: *Trans. Metall. Soc. AIME*, 1966, vol. 236, p. 624.

39. S. De Cheveigne, C. Guthmann, P. Kurowski and E. Vicente: *J. Crystal Growth*, 1988, vol. 92, pp. 616-628.

40. V. Datye and J. S. Langer: *Phys. Rev. B*, 1981, vol. 24, p. 4155.

41. M. H. Burden and J. D. Hunt: *J. Cryst. Growth*, 1974, vol. 22, p. 99.

42. M. H. Burden and J. D. Hunt: *J. Cryst. Growth*, 1974, vol. 22, p. 109.

43. V. G. Smith, W. A. Tiller, and J. W. Rutter: *Canadian Journal of Physics*, 1955, vol. 33, p. 723.

44. R. Trivedi: *Metall. Trans.*, 1984, vol. 15A, p. 977.

45. R. Trivedi and W. Kurz: *Int. Met. REV.*, 1994, vol. 39, p. 49.

46. W. Kurz and D. J. Fisher: *'Fundamentals of solidification'*; 1992, Aedermannsdorf, Switzerland, Trans Tech Publications.

47. J. D. Hunt: *Solidification and Casting of Metals*, The Metals Society, Book 192, London, 1979, p. 3.

48. W. Kurz and D. J. Fisher: *Acta Metall.*, 1981, vol. 29, p. 11.

49. S. Strassler and W. R. Schneider: *Phys. Cond. Matter*, 1974, vol. 17, p. 153.

50. S. R. Coriell and R. F. Sekerka: *J. Crystal Growth*, 1973, vol. 19, pp. 285-293.

CHAPTER 4:
STABILITY OF EUTECTIC MICROSTRUCTURES

A manuscript to be submitted to the *Journal of Metallurgical and Materials Transactions*

S. H. Han and R. Trivedi

Ames Laboratory US-DOE and the Department of Materials Science and Engineering
Iowa State University, Ames, IA 50011

Abstract

The instability of eutectics to the single phase formation has been examined through critical experiments in the vicinity of the transition conditions. The role of the dynamical processses during the process of the selection of eutectic or a single phase was critically evaluated. Away from the transition condition, the phase selection occurred through the nucleation of the appropriate phase. However, close to the transition, an oscillating mode was found in which the system oscillated between the two steay-state morphologies. The transition from a eutectic to a single phase was thus observed not to be sharp but it occurred over a finite band of velocities in which an oscillating or a banded structure was formed. The effects of the imposed velocity and composition on this oscillatory mode were examined. It was found that, as the conditions were farther from the transition point, the oscillations damped out and the system selected one of stable morphologies. The alloy composition had a significant influence on the oscillation behavior, and the oscillations were found to increase as the compositions deviated from the eutectic composition. The regime of banded structures was established for the carbon tetrabromide-hexachloroethane system. Also, the mechanisms by which the eutectic-single phase dendrite transition occurred outside the oscillating regime have been quantitatively characterized.

I. Introduction

Eutectic growth has been studied extensively because of its unique properties and possible applications in many fields. The characteristics of eutectic alloys are that they have lower melting temperatures compared to the pure elememts, and a zero freezing range which gives excellent flow properties which are valuable in casting, welding, and soldering processes. In addition, eutectic microstructures are much finer than those of dendrites, so that improved mechanical properties can be attained. The possibility of forming in situ composites having desired two or three different phases growing simultaneously has also attracted much interest in eutectic growth. Several studies have thus been carried out to establish the growth condition under which uniform eutectic microstructures can be attained. Two critical microstructural aspects are the eutectic spacing which is controlled by the growth rate and the relative volume fraction of the two phases which is controlled by the alloy composition. In order to control the volume fractions, the conditions which give rise to eutectic microstructures in an off-eutectic alloy need to be properly identified. A proper model requires the study of the stability of the eutectic interface with respect to the single phase growth, and it is this study that will be critically examined in this paper.

The stability of eutectic structures against single phase formation is generally described by a coupled zone, which represents a regime of composition and undercooling (or velocity) conditions in which a eutectic microstructure can be formed. The basic model for the coupled zone was developed by Tammann and Botschwar [1], who characterized the coupled zone as the region in which eutectics grew faster than the primary phases under given undercooling conditions. This approach is known as the Competitive Growth Model (CGM). The velocities of different microstructures, for comparison, were determined from the steady state growth model for each possible morphology, and the regime of composition and undercooling where eutectic structure would be selected was plotted on a phase diagram. Kofler [2] extended this

work in binary organic systems and described three different types of coupled zones: regular zone about the eutectic composition, a skew zone and a mixed mode. More quantitative approach was developed subsequentlty by Hunt and Jackson [3] for the selection of eutectic microstructure under directional solidification conditions. In this case, the stability of the eutectic structure was based on the steady-state interface temperatures, the microstructure having a larger interface temperature will be the one selected by the system. Later, Jackson [4] modified the earlier work [3] on the conditions for the dendrite-eutectic transition by taking into account the temperature gradient. The model was then compared with experimental studies on the eutectic stability by Mollard and Flemings [5] and a good agreement was shown. The theoretical models of coupled zone, using more accurate descriptions of dendrite and eutectic growth have been developed by Burden and Hunt [6], Kurtz and Fisher [7, 8] and Trivedi and Kurz [9].

There are several basic concerns about the competitive growth model: (1) The model considers interface temperatures based on the steady-state growth model. In reality, the selection process occurs during the dynamical condition in which the velocity of the interface is changing. These dynamical effects can significantly influence the microstructure or phase selection. (2) The steady-state interface temperatures have been calculated under the assumption that only one morphology (or phase) is present in the system. In general, during the selection process both morphologies (or phases) can be present simultaneouly in which case they will have a significant interaction between them so that the selection condition may not be sharp and the selection could occcur over a range of velocities. (3) The selection condition is based on growth condition only, and it is asssumed that new morphology or phase will nucleate readily.

The main objetive of this work was to investigate the role of dynamics of interface motion on the selection of microstructures in off-eutectic compositions. In order to quantitatively characterize non-steady state effects, experiments were carried out in a model

transparent system of carbon tetrabromide and hexachloroethane in which the interface and the microstructure selection process can be observed in situ. A significantly different selection process was observed in that the dynamical conditions present during the selection process near the transition conditions gave rise to oscillating modes in which the interface was found to oscillate between the eutectic and the single phase. This oscillation mode produced banded microstrucutres consisting of repeated alternating bands of the eutectic and the single phase mcrostructure. These oscillations were found to occur over large distances when the conditions were close to the transition condition. However, the oscillations were found to damp out as the velocity deviated further from the transition condition, resulting in the selection of a specific microstructure. Significantly different oscillating behavior were also observed for hypoeutectic and hypereutectic alloy compositions. The oscillating modes, and the mechanism of formation (or nucleation) of the two phases will be described in this paper, and theoretical ideas which lead to the formation of oscillatory microstructures will be presented. The observations of the oscillating modes in the eutectic system will then be compared with other oscillating modes that have been observed in other systems, which include oscillations between the single phase planar and cellular morphopogies at low [24] and high velocities [10, 11, 12] and the oscillatory modes in peritectic alloys [13, 14] to show that the general existence of oscillating microstructures in directional solidification.

II. Experimental

Directional solidification experiments were carried out in the C_2Cl_6-CBr_4 system, and the procedures used for the purification of the alloy and preparation of the samples were the same as described earlier [21, 25]. The compositions used in this study ranged from 7.64wt% to 10.85wt% of C_2Cl_6, which included the eutectic (8.4wt%), hypoeutectic and hypereutectic compositions.

In order to select velocity ranges that were close to the transition conditions for different compositions, a coupled zone was first determined by using the competitive growth model [9, 15]. An example of a calculation for a given composition is shown in Figure 1, which plots the steady-state temperatures as a function of velocity for both the eutectic and the single phase alloy. These temperature variations were calculated by using a computer program, developed by Gilgien and Kurz [16], for the steady-state dendrite and eutectic growth model, and by using physical parameters given in Table 1. For a given composition, the intersection of these two temperature variations gave the interface temperature and interface velocity conditions for the selection of eutectic or single phase structure. By calculating similar transition conditions for other compositions, coupled zone boundaries were determined, as shown in Figure 2.

Experiments were carried out for a range of compositions, varying from hypoeutectic to hypereutectic compositions, and the temperature gradient was kept constant at G=1.8 K/mm. For each composition, experiments were started with the velocity in the eutectic regime, and then the velocity increased in steps until the eutectic interface became unstable. The velocity ranges selected for the experimental studies are given in Table 2 and 3. All the experiments were recorded on video tapes for further analyses.

Initially, experiments were carried out for different compositions by gradually increasing the velocity in steps over shorter time durations (1-5 hours) to determine the actual range of velocities over which the transition occurred, and to gain an insight into the microstructure transition process. The detailed experimental conditions and the microstructures observed are shown in Table 2. Since several interesting features, including the new oscillating modes were discovered for all samples except the one close to the eutectic coposition, additional experiments of long durations (upto 14 hours) were also carried out to examine whether the oscillations were damped or undamped, and to quantitatively determine the oscillation modes. For these long duration experiments, two compositions from hypoeutectic and two from hypereutectic were selected, and the temperature gradient was kept

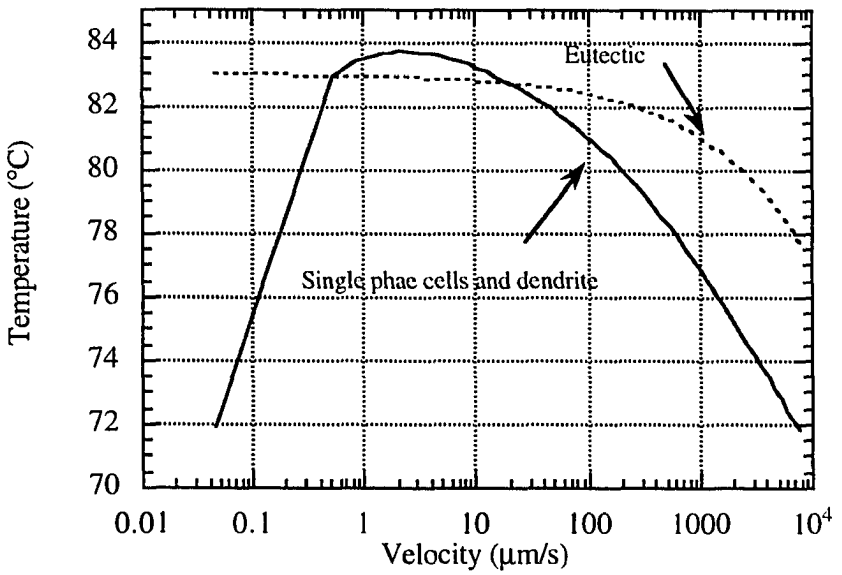

Figure 1. Calculated lines for eutectic and dendrite growth in the composition of 9.5 wt% CBr_4-C_2Cl_6

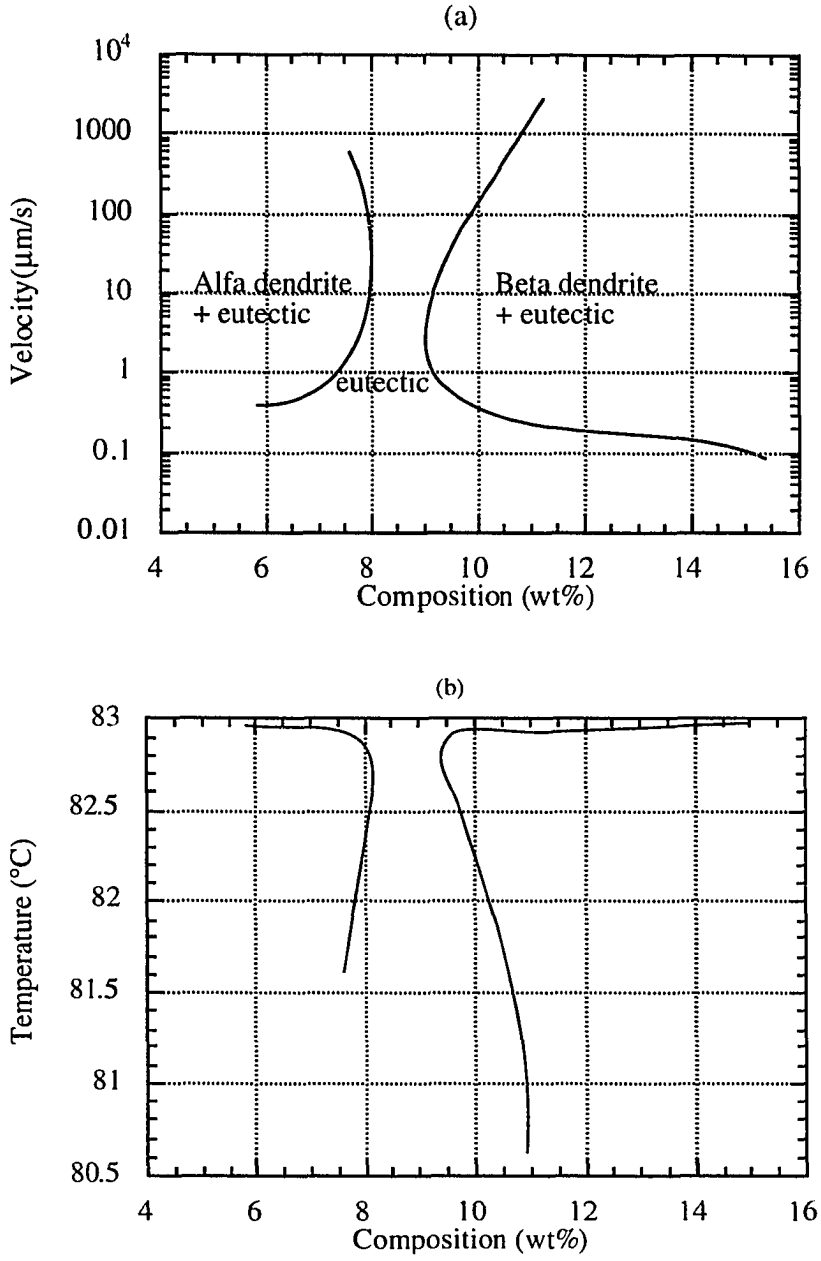

Figure 2. Calculated coupled zone shown (a) in the relation of velocity and composition (b) in the relation of temperature and composition.

Table 1. Numerical values of the physical parameters used for coupled zone calculation for the CBr_4-C_2Cl_6 system.

Parameters	α (CBr_4)	β (C_2Cl_6)	Reference
Ø	1.2		[15]
Temperature gradient	G=1.8K/mm		
Diffusion coefficient	$(0.5\pm0.1)\times10^{-5}cm^2/s$		[19]
R (Tip radius)	$VR^2=978\pm8\mu m^3/s$	$VR^2=124\pm13\mu m^3/s$	[17]
m (Liquidus slope)	-1.482K/wt%	2.164K/wt%	[20]
Density	$3.09g/cm^3$	$2.75g/cm^3$	[20]
Contact angle	$\theta_\alpha=65$	$\theta_\beta=55$	[21]
Γ	$\Gamma_\alpha=8.0\times10^{-8}mK$	$\Gamma_\beta=11.4\times10^{-8}$	[21]
C_0	11.1wt%		[20]

constant at G=1.8 K/mm. The precise composition of each sample was obtained from separate experiments in which steady-state dendritic structure was obtained, and the distance between the tip of the dendrite and the eutectic front was measured. Using the known temperature gradient value, and the calculated values of the dendrite and eutectic undercoolings at known velocity temperature (e.g. the eutectic undercooling was 0.062°C for C=7.83wt% at V=1μm/s), the liquidus temperature of the alloy was determined. The composition value was then obtained from the phase diagram. The compositions of the Exp# 22 was obtained from volume fraction measurements because dendrites were not formed in this composition. About 200 volume fraction data were measured for this composition.

Selected experiments were analyzed carefully in order to understand the variation in the interface temperature and velocity with time for different pulling velocities and initial

Table 2. Experimental conditions and the corresponding microstructures.

Exp#	Temp. Grad (K/mm)	C (initial comp)	V_1 (μm/s)	V_2	V_3
1	1.8	7.64	0.25 for 4hrs50m oscillation	0.5 for 8hrs35m oscillation	5 for 13m dend+eut
2	"	7.91	0.5 for 12hrs30m oscillation	10 for 15min dend+eut	
3	"	7.96	1 for 1hr1m oscillation	2 for 41m dend+eut	4 for 31m dend+eut
4	"	8.09	0.7 for 2hrs30m eut	1 for 1hr dend+eut	4 for 26m dend+eut
5	"	8.56	0.5 for 1hr55m eut (β phase leading)	2 for 25m eut (β phase leading)	8 for 20m colonies
6	"	8.56	1 for 1hr40m eut (β phase leading)	10 for 10m colonies (eut dend)	

Table 2. Continued

7	"	8.93	0.5 for 1hr15m eut (β phase leading)	0.75 for 1hr30m eut+dend (from liquid)	1 dend+eut
8	"	8.93	0.75 for 1hr15m eut (β phase leading)	1 coarsened dend*	
10	"	8.93	0.8 for 1hr30m dend+eut		
11	"	9.92	0.5 for 2hrs36m dend+eut	2 for 13m dend+eut	
12	"	10.85	0.5 for 2hrs16m eut (β phase leading)	2 for 28m eut+dend*	
13	"	10.85	0.7 for 3hrs30m eut+dend*		

*dendrites also nucleated ahead of the interface in the liquid.

Table 3. Experimental conditions and the corresponding microstructures for the long term experiments.

Exp#	Temp. Grad (K/mm)	C (initial comp)	V_1 (μm/s)	V_2	V_3
20	1.8	7.96	0.5 for 14hrs oscillations	0.7 for 1hr30m cells+eut	1 for 1hr10m and 2 for 30m dend+eut
21	1.8	8.09	0.5 for 12hrs oscillations	0.7 for 2hrs50m cells+eut	0.9 for 40m dend+eut
22	1.8	8.56	0.5 for 12hrs eut	0.7 for 1hr30m and 1 for 50m finer eut	2 for 40m colonies
24	1.8	10.85	0.5 for 8hrs10m dend+eut	0.3 for 6hrs52m dend+eut	0.2 for 8hrs25m eut

compositions. The relative interface positions was measured from a reference point fixed on the monitor and the video tapes were analyzed using the image analysis software (Optimas 4.0). In this present work, the reference point was chosen to be located closer to the cold stage, i.e. from the solid side. The decrease in the y values (relative position), thus indicates that the interface is being undercooled during the directional growth.

The oscillating phenomenon gave rise to a banded structure in the transition zone, so that measurements were also carried out on the widths of the bands. The mechanisms by which eutectics became unstable to the single phase cell/dendrite plus interdendritic eutectic were also studied from the video photographs in hypo and hypereutectic compositions. Dendrite appearance and disappearance, as the velocity was increased and decreased, were also examined in the hypereutectic composition.

III. Results and Discussion

As the velocity was changed in the vicinity of the transition condition, the initial eutectic interface did not transform directly into single phase dendrites plus interdendritic eutectics, but it went through oscillations between the eutectic and single phase. We shall now present the results on the oscillatory behavior which leads to the formation of a banded structure near the transition condition, and then describe the mechanisms by which the eutectic to single phase transition occurs. We shall then discuss the formation of a banded structure, and show how this regime of banded structure needs to be included in the coupled zone description. Finally, we shall show that this oscillating phenomena is a very general phenomenon that can occur during the phase selection process.

(1) Oscillatory Behaviors in Hypoeutectic Composition

Near the transition conditions, oscillations between eutectic and single phase were observed for hypo and hypereutectic compositions. However, distinctly different mechanisms

of osciallations were found for hypo and hypereutectic compositions so that we shall describe these oscillations separately.

The time sequence of microstructure formation in hypoeutectic composition is shown in Figure 3 for one experimental run. Similar results were observed for the other experimental runs. As the solidification occurred, the eutectic structure became unstable and a single phase planar front was formed. This planar front, after some time, again became unstable and formed a eutectic structure. The formation of eutectic and single phase band continued with time giving rise to a banded microstructure. The mechanism of the formation of the single phase from eutectic microstructure is observed in Figure 3(a). The α-lamellae slightly outgrew the β-lamellae and this protuded α-lamellae grew laterally such some α-lamellae combined and eliminated some of the the β-lamellae, Figure 3(b). Finally, all the α-lamellae joined and formed a single phase planar interface, Figure 3(c). As the single phase grew a small distance, eutectic nucleated at the grain boundaries, Figure 3(d), and propagated laterally to form a eutectic structure which continued to grow over some distance, Figure 3(e). The α–lamellae once again led and formed a planar single phase interface, Figure 3(f). This process was repeated to form a banded structure.

The formation of eutectic and single phase is controlled by the velocity of the interface, which is not constant, but it oscillates with time. This can be seen in Figure 3, by tracking the position of a speck of dirt that is on the microscope objective, i.e. the speck represents a fixed location in the moving coordinate system. The transition from eutectic to planar front is accompanied by a decrease in the velocity, Figures 3(a) to 3(c), whereas the transition from planar to eutectic front is accompanied by an increase in velocity, Figure 3(d) and 3(e). Thus, the oscillations in the structures can be correlated with the oscillations in interface velocity or interface temperature.

In order to examine the oscillations in interface temperature, which are proportional to the position of the interface in the moving coordinate system, the location of the

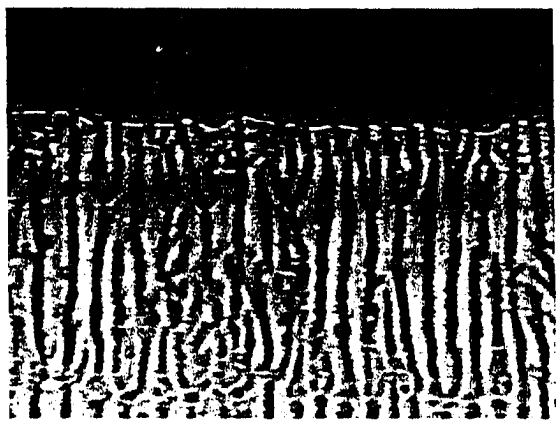

(a) t=471.3 min

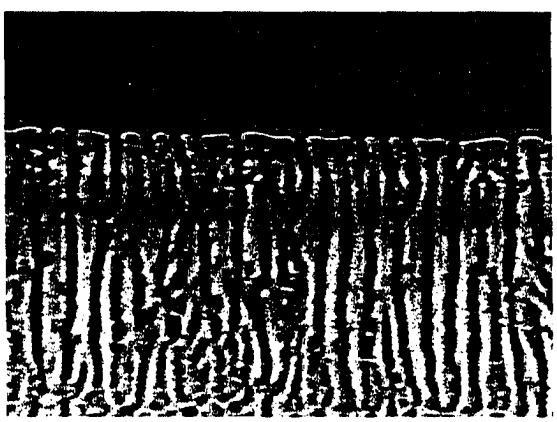

(b) t=472 min

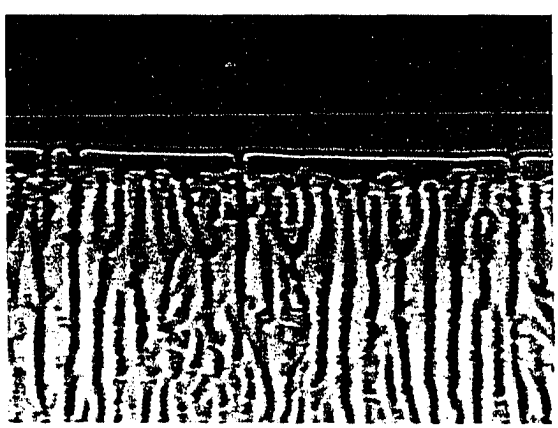

(c) t=473.3 min

Figure 3. Time sequence of oscillations between alfa phases and eutectics in hypo eutectic composition (C=7.96wt%, V=0.5μm/s) (a) t=471.3 min (b) t=472 min (c) t=473.3 min (d) t=480.2 min (e) t=482 min (f) t=484.8 min.

(d) t=480.2 min

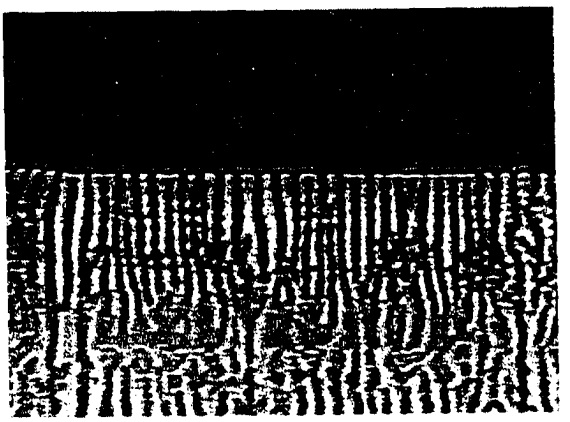

(e) t=482 min

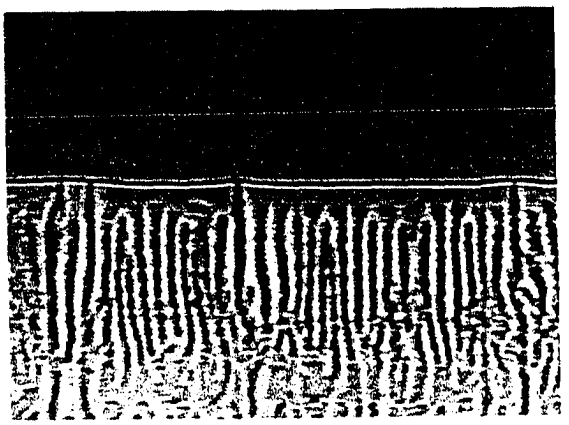

(f) t=484.8 min

Figure 3. Continued.

interface as a function of time was measured. The local velocity of the interface was calculated from the change in interface position with time. The relative positions with time, from experiments in hypoeutectic compositons of C=7.96 and C=8.09wt%, are shown in Figure 4. Although these experiments were held at one velocity for a long time, none of these results show plateau regions indicating that the system did not reach the steady state growth condition in these experiments. As the velocity was increased in steps, the variations in the relative position became larger in amplitude with the emergence of the single phase. The location of single phase (solid circle) and eutectic (open square) in Figure 4 show the oscillations in the leading position between the two morphologies at a lower velocity, and the width of the eutectic and planar phase bands as a function of time are also shown in the figure.

The velocities of the interface were calculated from the derivatives of the relative positions with respect to time and then were averaged over 20 points. The actual velocities from the two hypoeutectic compositions are shown in Figure 5. Although all results showed fluctuations in velocity with time, the amplitudes of fluctuations were smaller when the composition was closer to the eutectic composition. Figure 5 shows that oscillations were more pronounced for the composition C=7.96wt% (Figure 5(a)) than C=8.09wt% (Figure 5(b)). The variations in the velocity with time became accentuated whenever there were the oscillations between the two growth patterns. Some anamolous velocity jumps were observed in Figure 5(b), near t=460 min, which were related to the formation of a doublet-type eutectic at the advancing front, which are shown in Figure 6.

In Figure 5(a), the velocity was increased from V=0.5μm/s to V= 0.7μm/s, and then to V=2μm/s eventually. When the velocity was increased to 0.7μm/s, the oscillations began to damp out, and only the single phase was leading at V=2.0μm/s. The same trend can be observed in Figure 5(b) when the velocity was increased to V=0.9μm/s. This termination in the oscillation indicates that the given condition is outside the coupled zone where the single phase cells or dendrites are leading the eutectics.

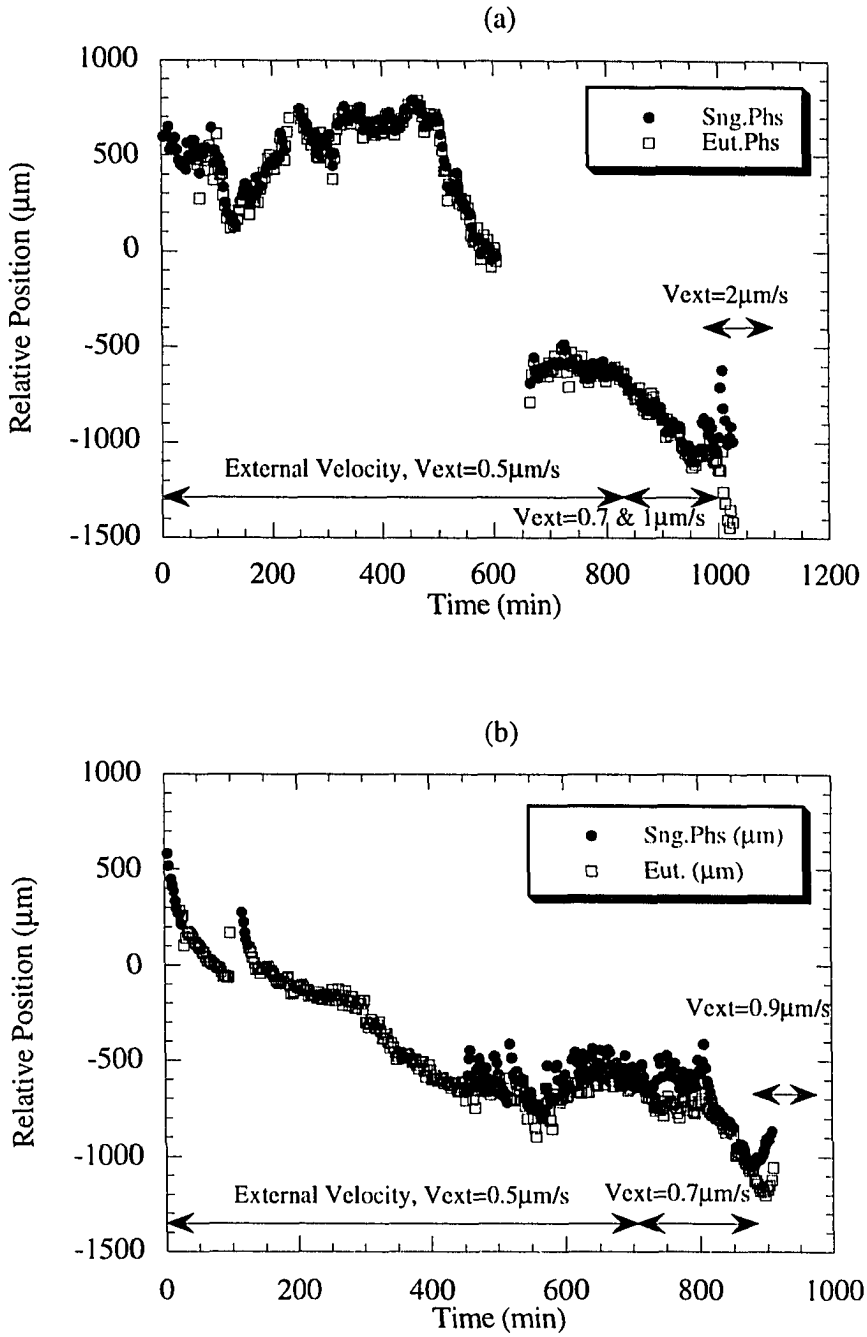

Figure 4. Relative positions with time at the same initial imposed velocity (V=0.5μm/s) in hypoeutectic compositions (a) C=7.96wt% (b) C=8.09wt%.

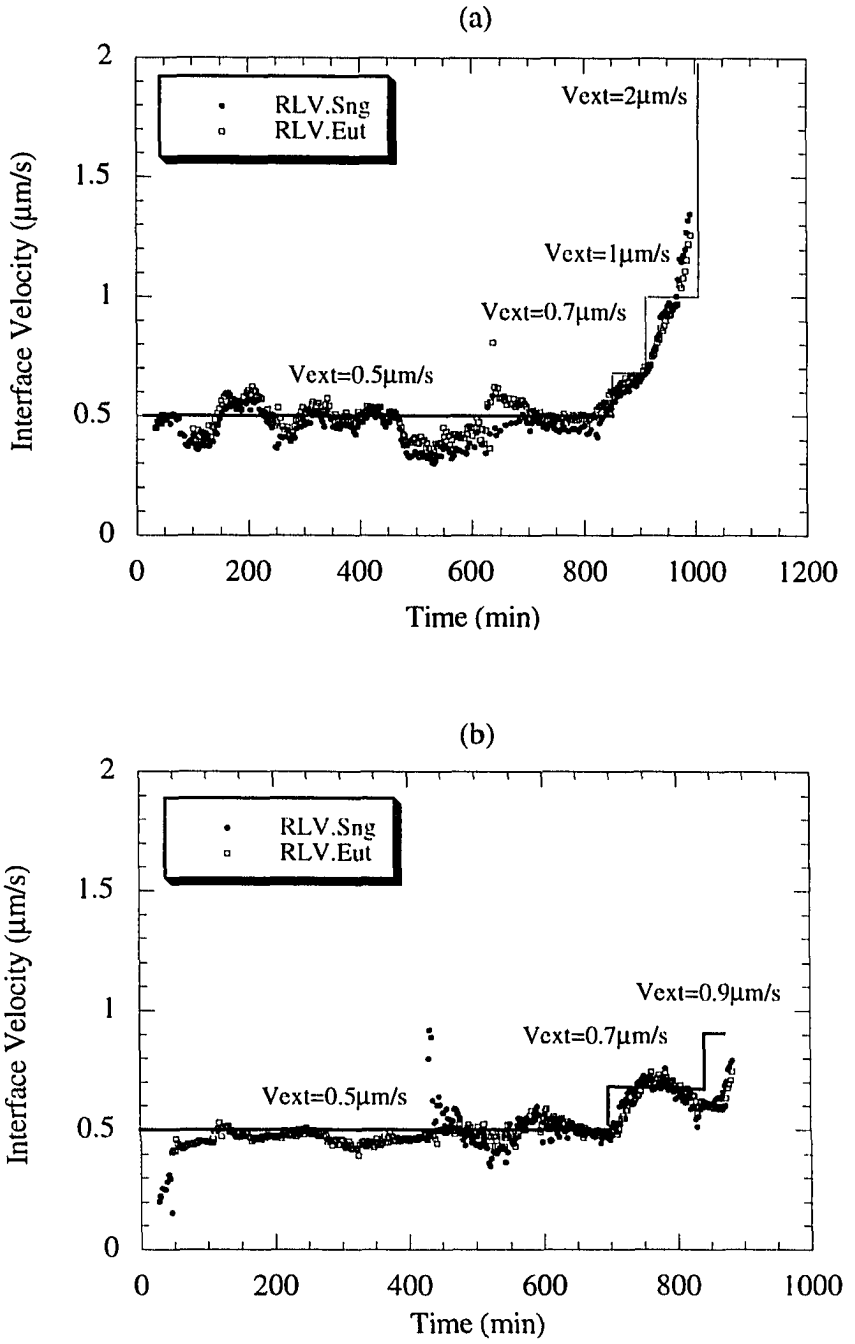

Figure 5. Averaged real velocities with time from the same initial imposed velocities (V=0.5μm/s) in hypo eutectic compositions (a) C=7.96wt% (b) C=8.09wt%. Solid line represents the external velocity changes.

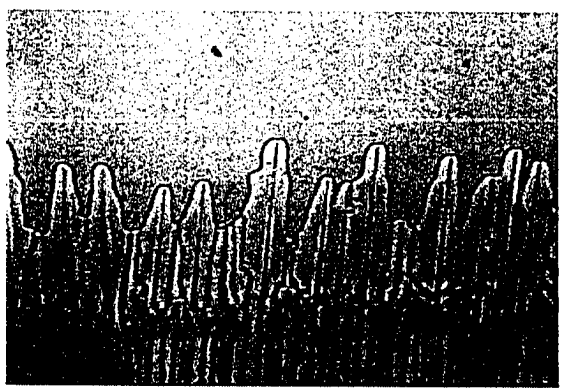

Figure 6. Doublet type microstructures from V=0.5μm/s after 460 minutes (C=8.09wt%).

In order to examine the oscillatory behavior, the results for the hypoeutectic composition (C=7.96wt% C_2Cl_6) are shown in Figure 7 with different time periods at V=0.5μm/s. The analyses show that most of the eutectic growths were observed when the slopes in the relative positions were positive, or the interface was accelerating, and the single phase growth occurs when the interface was decelerating, as shown in the figure. The hatched area stands for the region where the eutectic growth was leading while the other region represents the single phase was going ahead of the eutectics. The variation in interface velocity, obtained from averaging over every five points, is shown in Figure 8. During the early stage, the oscillations were larger in both the single phases and some melting was observed as the local velocity went down below zero around 108 minutes. The oscillations and the velocity variations were found to damped down with time. Similar oscillatory behaviors were observed in other hypo eutectic compositions.

(2) Oscillatory Behaviors in Hypereutectic Composition

In the hypereutectic compositions, two distinctly different types of oscillations were observed depending upon the deviation of composition from the eutectic composition. The time sequence of the micrographs for the first case is shown in Figure 9, C=8.56wt%, in which case the eutectic structure was stable but oscillations between the two phases of the eutectic structure was observed. The β-phase started to lead initially, but α phases were quick in catching up the β front when the leading distance was small. In the second oscillating mode, alternate bands of eutectic and single phase were formed. In this case, the β phases had a long leading distance, and β lamellae were found to merge together forming β single phase layer. In this situation, the coupled growth was recovered with α phase nucleations. We shall first describe the first type of oscillation between the eutectic lamellae. As can be seen in Figure 9(b), the coupled growth was started to become unstable by the β phase leading. These β

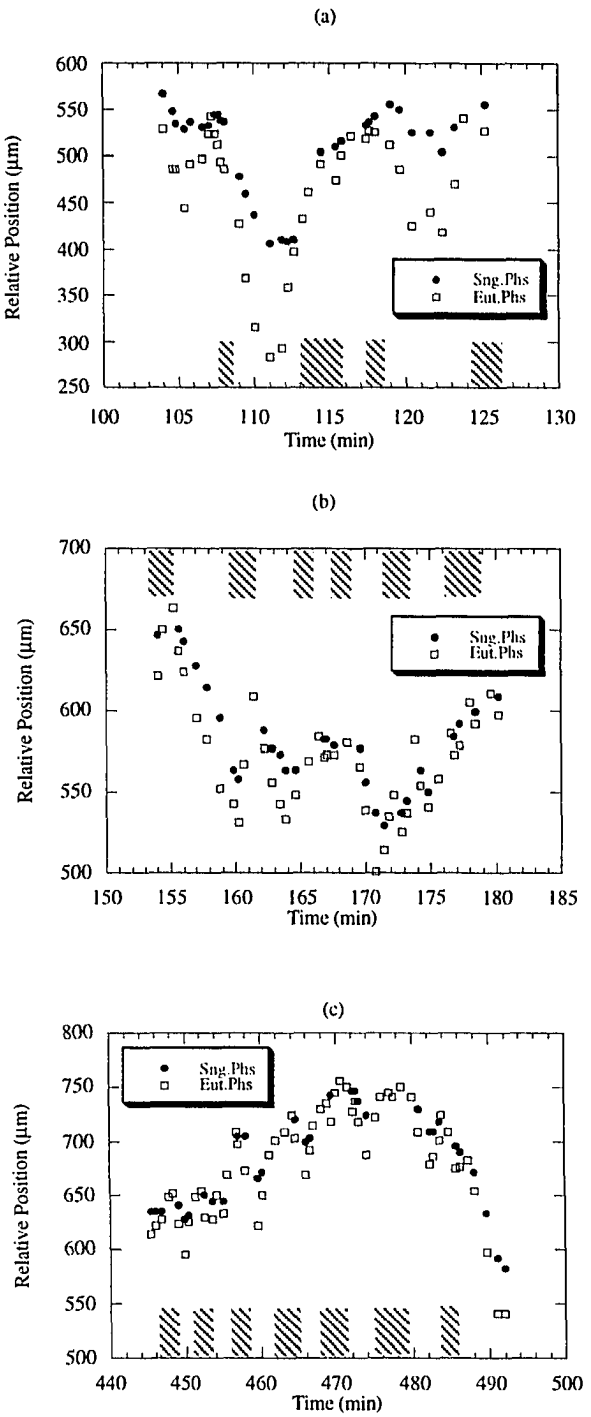

Figure 7. Oscillations between alfa and eutectics in hypoeutectic composition (C=7.96wt%) in the different time periods.

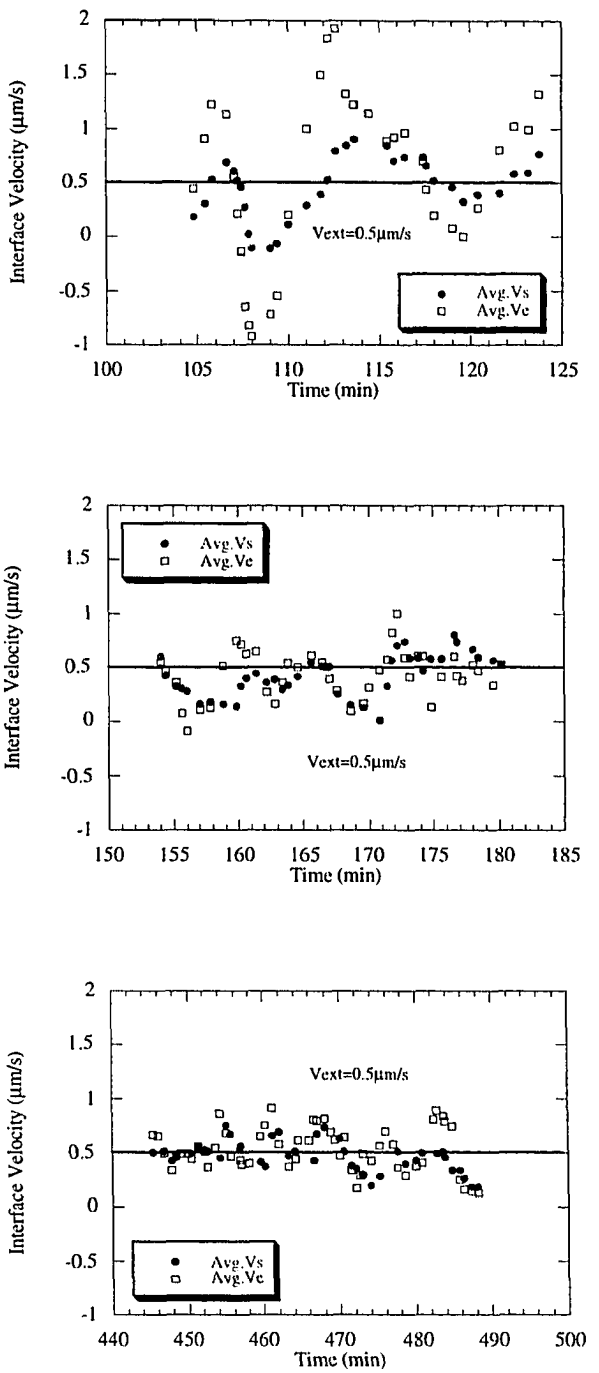

Figure 8. Real velocities in different time frames (external velocity=0.5μm/s, C=7.96wt%). Solid line shows the external velocity.

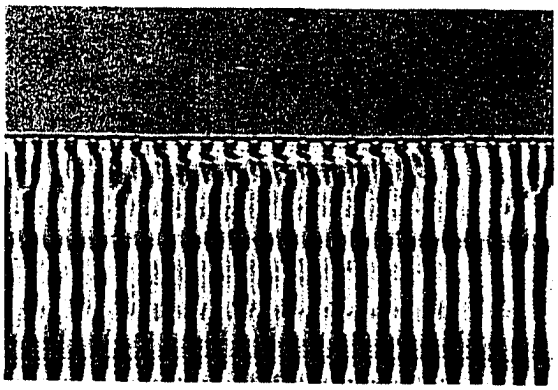

(a) t=73.9 min

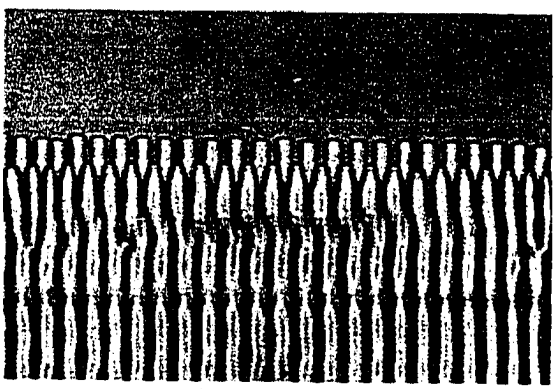

(b) t=75.4 min

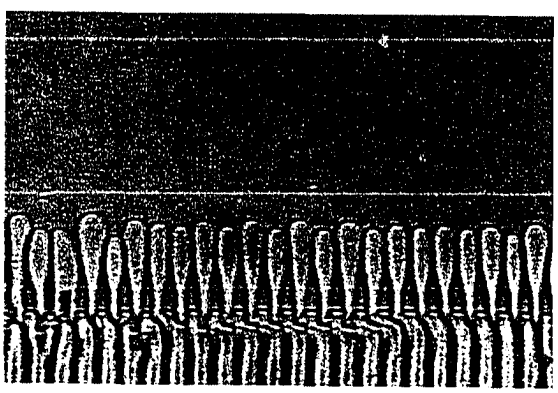

(c) t=78.7 min

Figure 9. Time sequence of oscillations between beta phases and eutectics in hyper eutectic composition (C=8.56wt%, V=0.5μm/s) (a) t=73.9 min (b) t=75.4 min (c) t=78.7 min (d) t=81 min. (e) t=82.8 min (f) t=85.4 min.

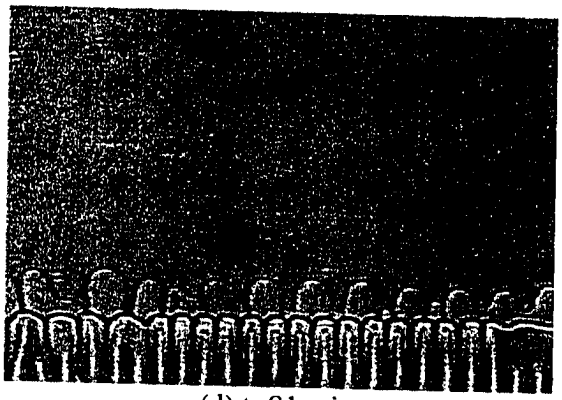

(d) t=81 min

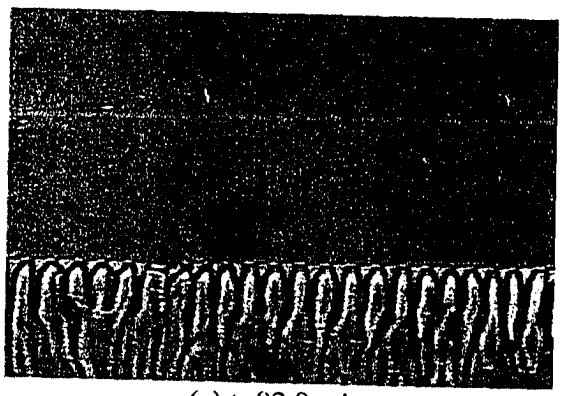

(e) t=82.8 min

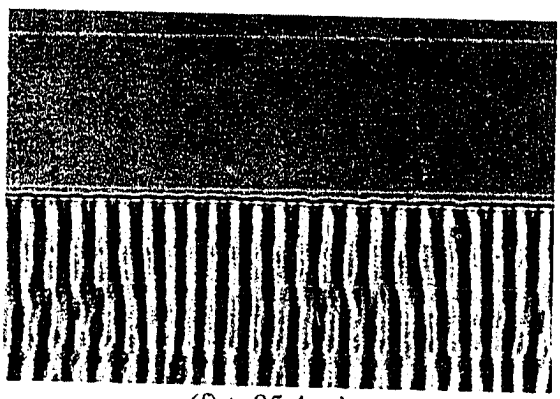

(f) t=85.4 min

Figure 9. Continued.

phases were coarsened with time, the α phases (or the eutectic front) were lagging behind. The coupled growth was recovered by catching up of α phase with the front.

The second case of oscillations is shown in Figure 10 with time sequence from a separate experiment for C=10.85wt%, in which the oscillations lead to the formation of a banded structure between the single phase beta and eutectics. This figure illustrates β phase leadings (b), and subsequent mergings of β lamellae (c). These merged β phases were coarsed and formed a single phase band which can be seen in Figure 10(d) and (e). The coupled growth was then resumed by the α phase nucleations from the single phase band (e).

In order to investigate the effect of compositions on the oscillation behavior, the results on the relative position with time are shown in Figure 11 for two compositions studied. A similar trend can be seen in Figure 11(a) and (b), as in the hypoeutectic case in that larger amplitudes in the relative positon were observed when the composition deviated further from the eutectic composition. In Figure 11(a), no single phase was formed even with the accelerations in the velocity. The β lamellae often outgrew from the coupled growth but the coupled growth was recovered soon. The leading of the β lamellae (or lagging of the α lamellae) was only observed in the hypereutectic compositions. It was also found that the amplitude of the β lamellae was increased more as the compositions were further away from the eutectic composition. Such oscillations were observed at all velocity, until the planar eutectic became unstable and formed colony structures when the velocity was increased to 2μm/s, as shown in Figure 11(a). For a higher composition, Figure 11(b) demonstrates a sudden appearance of the β single phase dendrites after the oscillations between the two morphologies around 400 minutes. Since the β dendrites appeared at V=0.5μm/s in this specific experiment, velocities were decreased with time until the dendrites disappeared. As the dendrites lead the front, all the eutectics were interdendritic eutectics from ~400 minutes to ~1200 minutes. Eventually, the dendrites disappeared by being engulfed with the eutectics at

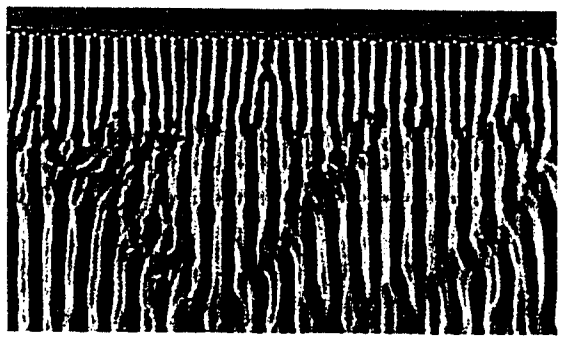

(a)

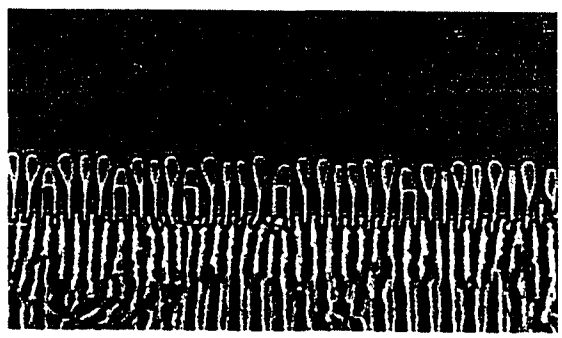

(b)

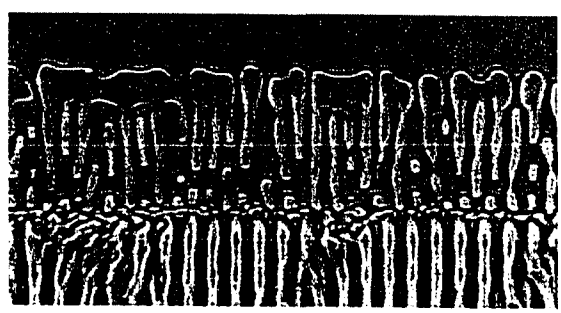

(c)

Figure 10. Time sequence of the oscillation between the beta and eutectic phase (V=0.5μm/s, C=10.85wt%) (a) t=3233.4 sec (b) 3337.7 sec (c) 3402.9 sec (d) 3520.3 sec (e) 3624.6 sec (f) 3754.9 sec.

(d)

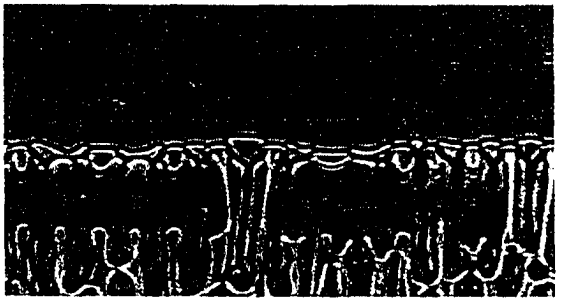

(e)

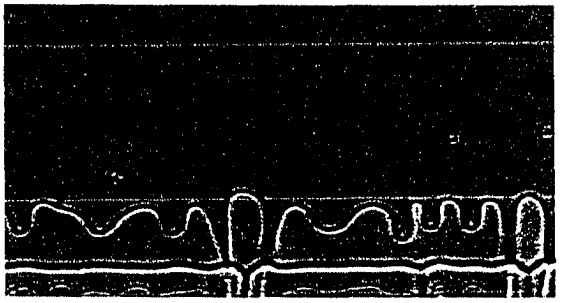

(f)

Figure 10. Continued

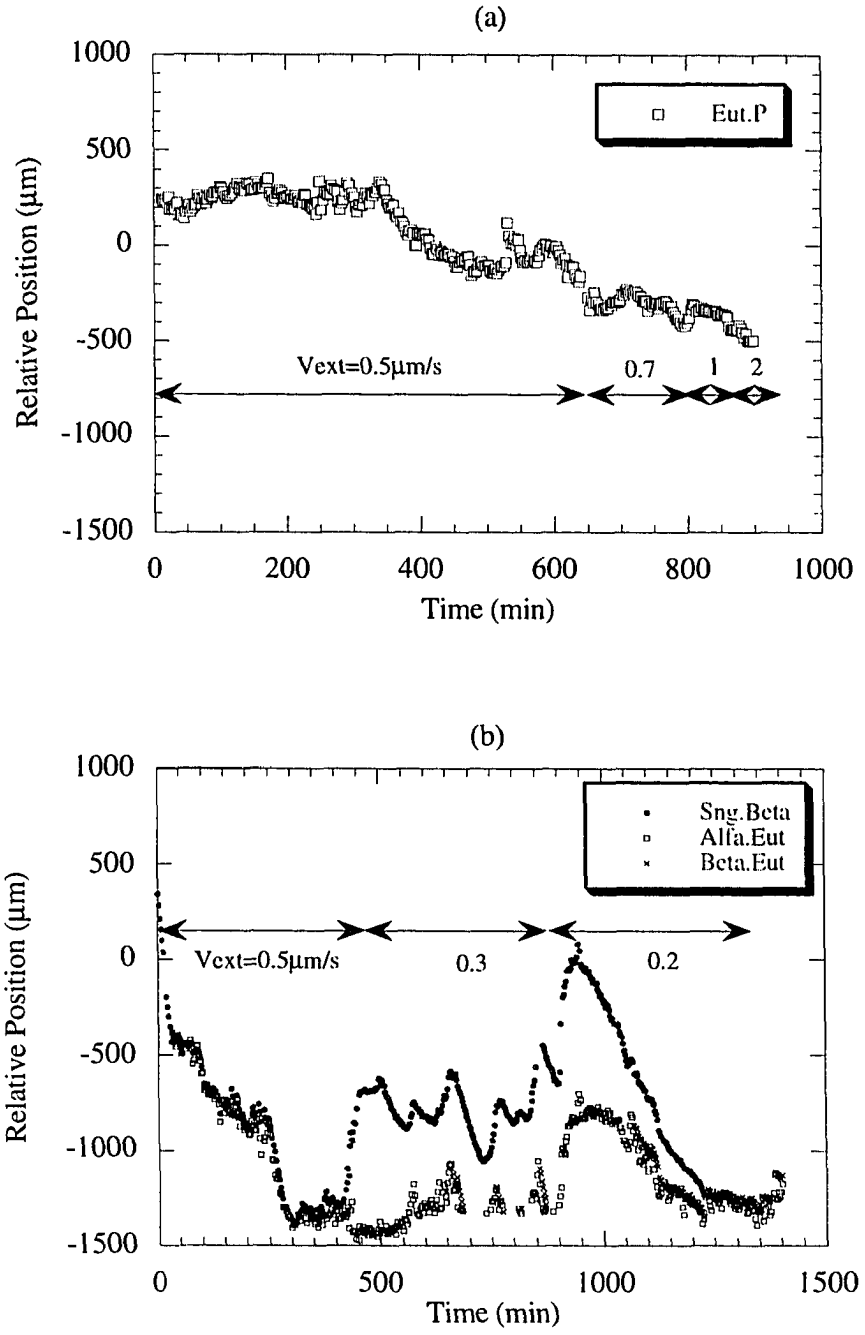

Figure 11. Relative positions with time at the same initial imposed velocity (V=0.5µm/s) in hypereutectic compositions (a) C=8.56wt% (b) C=10.85wt%.

the velocity of 0.2μm/s. The Beta.Eut from the plot represents observed β phase leadings even from the interdendritic eutectics.

To understand the oscillations for the hypereutectic case more systematically, the relative positions between the beta phase and couple growth (eutectic growth) were examined in different time frames, and the results are shown in Figure 12. A similar trend as in hypoeutectic compositions was seen in that eutectic was leading when the slopes of the relative position verses time show the positive values, i.e. the interface is accelerating. The interface velocities are shown in Figure 13. The eutectics again show more variations in the local velocity than the single phases, however, the damping is not that obvious in this figure. Rather, more oscillations were observed in the second time frame than the first one. The big jumps in the eutectic velocities were related with the band formations. The merged β phases were forming thick single phase bands and the α phases were nucleated subsequently to resume the coupled growth. The difference between the hpo and hypereutectic cases, Figure 13 and Figure 8, basically comes from the fact that in Figure 13, the given velocity (V=0.5μm/s) was already high enough to have the full dendrites with the interdendritic eutectics in the later part compared to the former case where only the oscillations were observed without any single phase dendrite formation for given time intervals.

The oscillations shown in Figure 10 were studied in detail and shown in Figures 14(a) and (b) which demonstrate the relative position changes and the corresponding velocity with time. Also shown in the figure is the phase difference between α and β during eutectic oscillation. It is obvious from Figure 14(a) that the β phase leading (or α phase lagging) is attributed to the lagging of the eutectic front. The full eutectic growth was recovered for a short time when the eutectic front caught up the leading β phase. The velocity plot in Figure 14(b) gives a clear picture that the β phase fluctuates less than the eutectic front in the local velocity, even though it looks exactly opposite during the observation. The phase difference was found

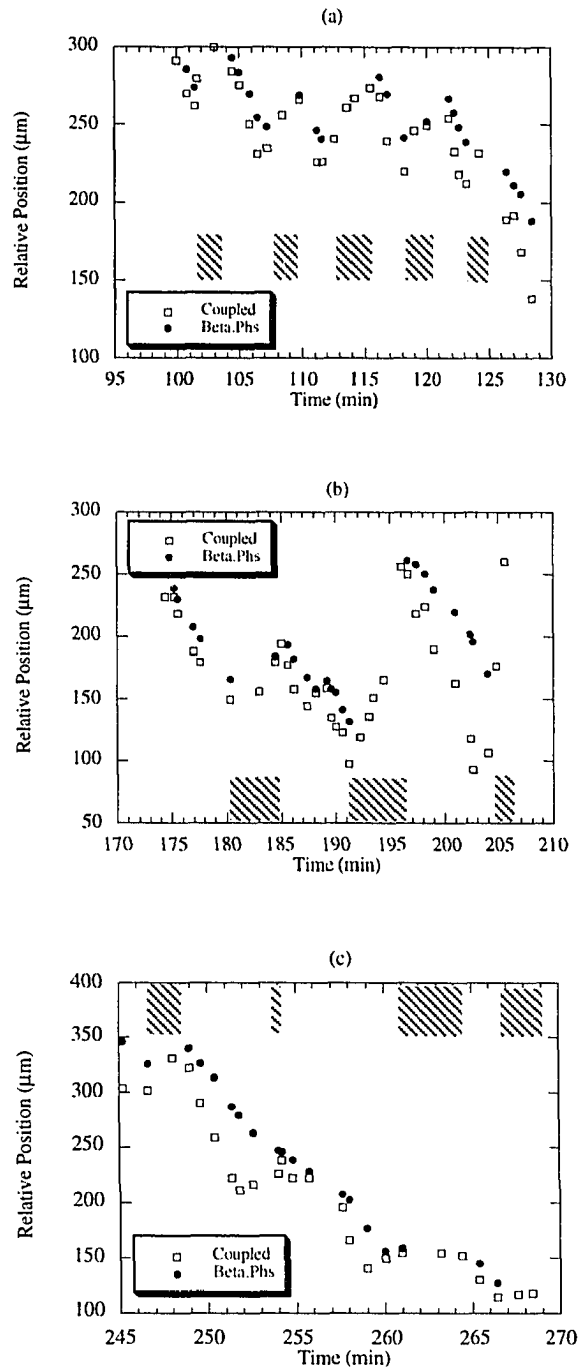

Figure 12. Oscillations between beta phase and eutectics in hypereutectic composition (C=10.85wt%) in different time periods.

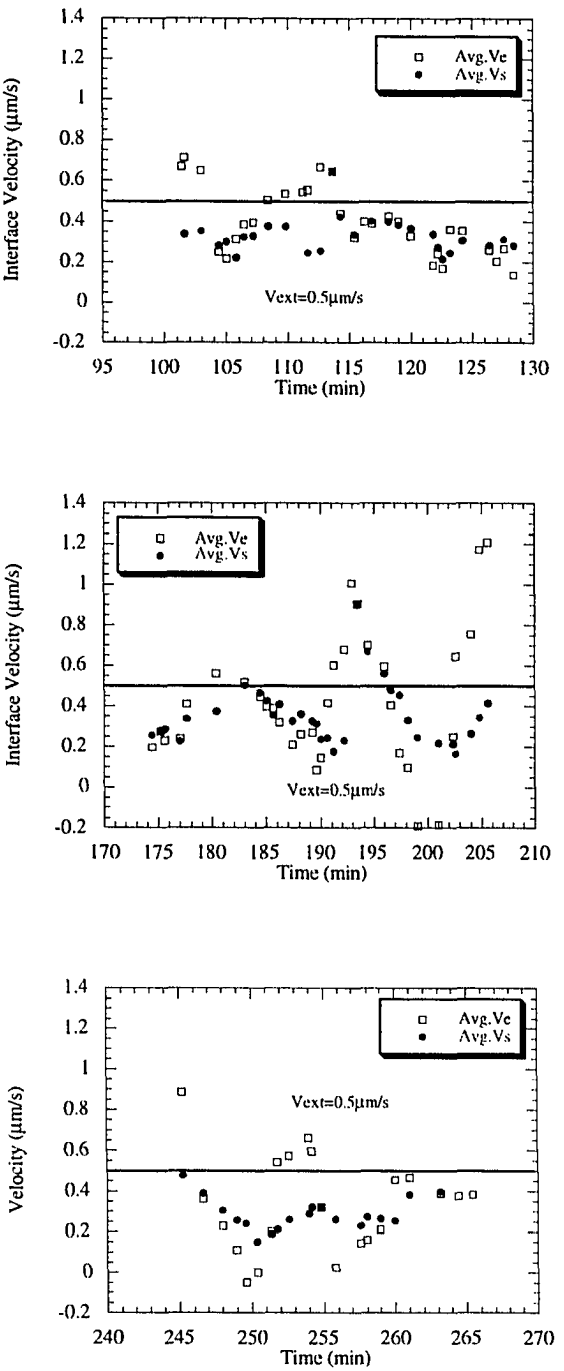

Figure 13. Real velocities in different time frames (external velocity=0.5μm/s, C= 10.85wt%). Solid line shows external velocity.

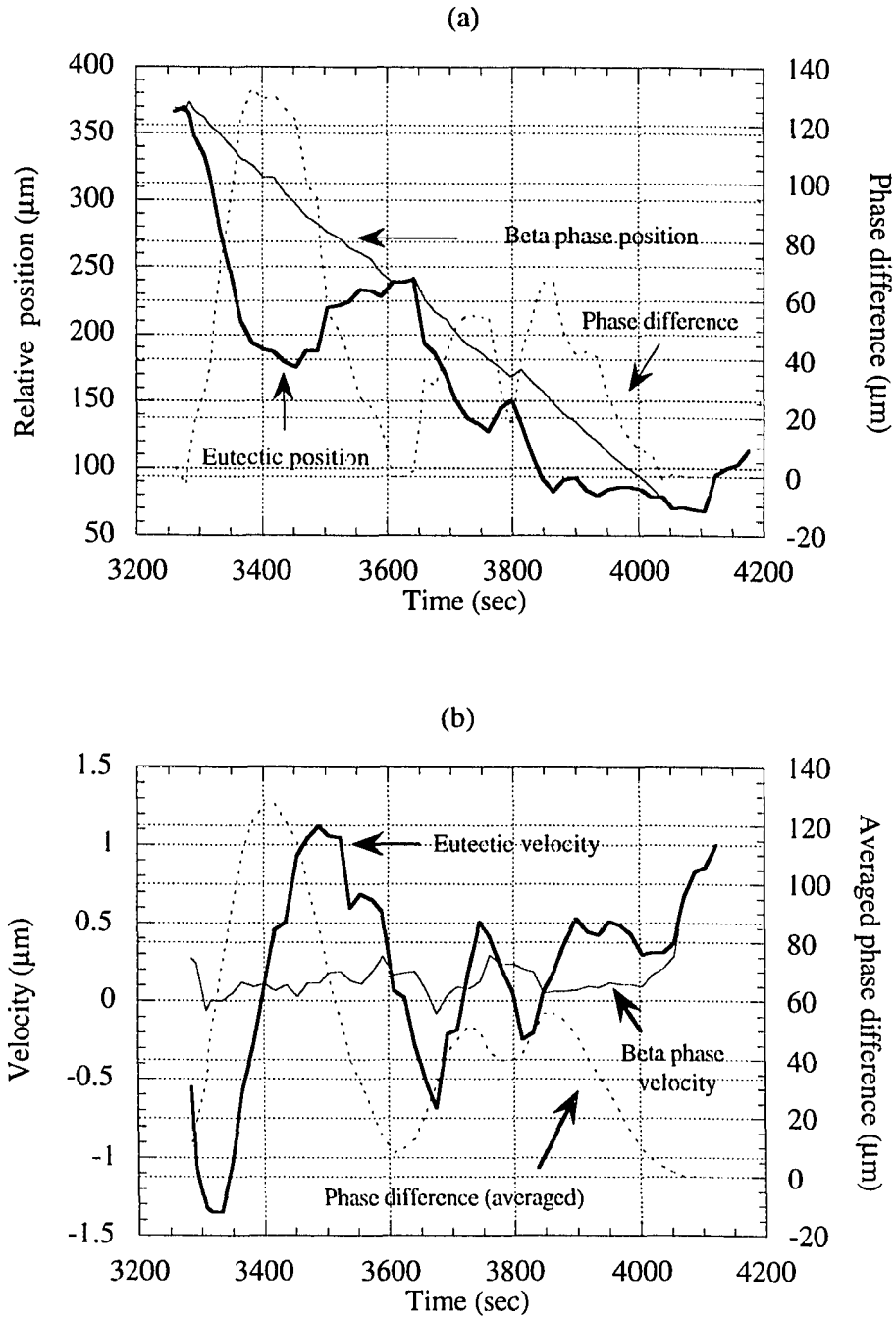

Figure 14. (a) Relative positions and phase differenc between α and β, (b) Local velocity fluctuations under the condition of V=0.5μm/s, G=1.8K/mm, and C=10.85wt%.

to be pronounced when there is a big difference in the actual growth velocity between the two phases.

The effect of compositions on the phase difference in hyper eutectic composition was also studied because the oscillation in hypereutectic composition always accompanied beta phase leadings which cause the phase difference. The phase differences between the beta phase and eutectic front were examined in three compositions such as C=8.56, 9.92, and 10.85wt%. The results are shown in Figure 15. In Figure 15(a), the actual velocities of beta phase (broken line) and eutectics (solid line) were also shown. Since the differences between the two velocities were so small that it looked more like a one line. By comparing the result from Figure 15(a) and (c), it can be seen that the phase difference is proportional to the composition deviation from the eutectic composition. Note that in the case of Figure 15(b), the suppresion in the leading distance is due to a higher temperature gradient (G=3.66K/mm), although the phase differece still shows a larger value than in Figure 15(a). The major peaks were observed to correspond to the times when large differences in the local velocities between the beta phase and eutectics were present.

It was found from the above analyses that the velocity of eutectic interface fluctuates more than that of single phase in both the hypo and hypereutectic compositions. The difference was that the α phase was leading in the hypoeutectic compositions, while the β phase was leading in the hypereutectic compositions. The morphologies of the leading phase were also different between the two sides. In hypoeutectic, α planar single phase was observed at the given velocity. On the other hand, in hypereutectic composition, β cells were observed.

(3) Banded Structures

The oscillations between the single phase and eutectic, discussed above, give rise to a banded structure. The main driving force for the band formation is the fluctuations in the local interface velocity since the single phase layer was formed during the decelerations and the

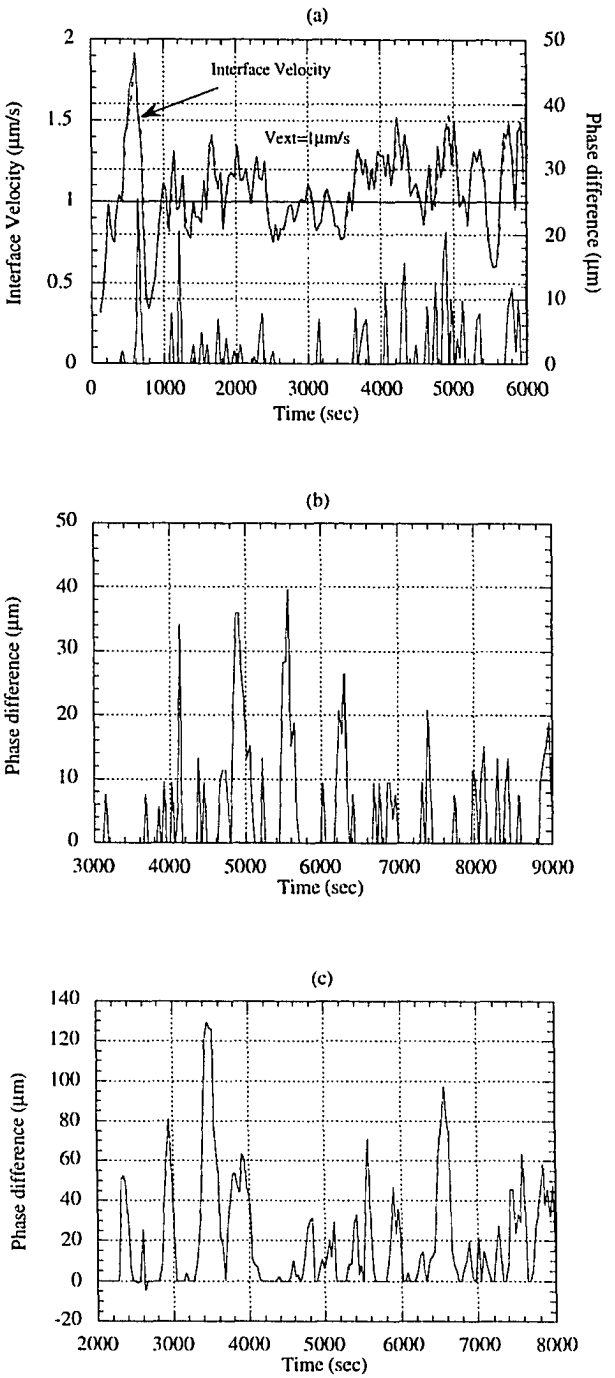

Figure 15. (a) Actual interface velocity with phase difference at V=1μm/s and C=8.56wt% (b) Phase difference at V=0.5μm/s, C=9.92wt%, and G=3.66K/mm (c) Phase difference at V=0.5μm/s and C=10.85wt%.

eutectic phase formed during the accelerations in off eutectic compositions.

In our studies, the band width was separately measured for each morphologies with time and the results are shown in Figure 16. The measurements were made from Exp#20 and Exp#24 (see Table 3) at V=0.5μm/s. Figure 16(a) represents the variation in band width from hypoeutectic composition (C=7.96wt%). The single phase band width is shown to have about the same magnitude during the oscillation whereas the eutectic band width changed in larger amplitude. As was observed in the oscillations with this composition, this banding pattern was maintained throughout this velocity. However, in the hypereutectic composition (C=10.85wt%), the average single phase band width was observed to increase with time. This is shown in Figure 16(b). The variations in the eutectic banding width were still larger than those of single phase, but their magnitude was smaller than the one from the hypoeutectic composition. In addtion to that, the size in band width between the eutectic and single phase became comparable around the end of this measurement. This can be understood because beta dendrites were formed after 400 minutes at this velocity. The increased trend in the single phase band shows more frequent leading of the single phase layers over eutectics.

Comparing the two plots in Figure 16 gives us a clue in the selection of the microstructure that is operating in the system. Conditions closer to the morphological transition make the system oscillate between the two stable state. Depending upon the magnitude of the driving forces which are given by the imposing velocity and the composition in this case, the system seems to approach toward the stable microstructure through the competition. This competition is observed in the form of the oscillations. Such oscillatory structures were not observed previously since either the experiments were carried out slightly away from the transition condition, or after a long run only the quenched region was examined. In our work, experimetns were designed over the transition conditions, and experiments were carried out in a transparent system, so that the oscillations could be observed.

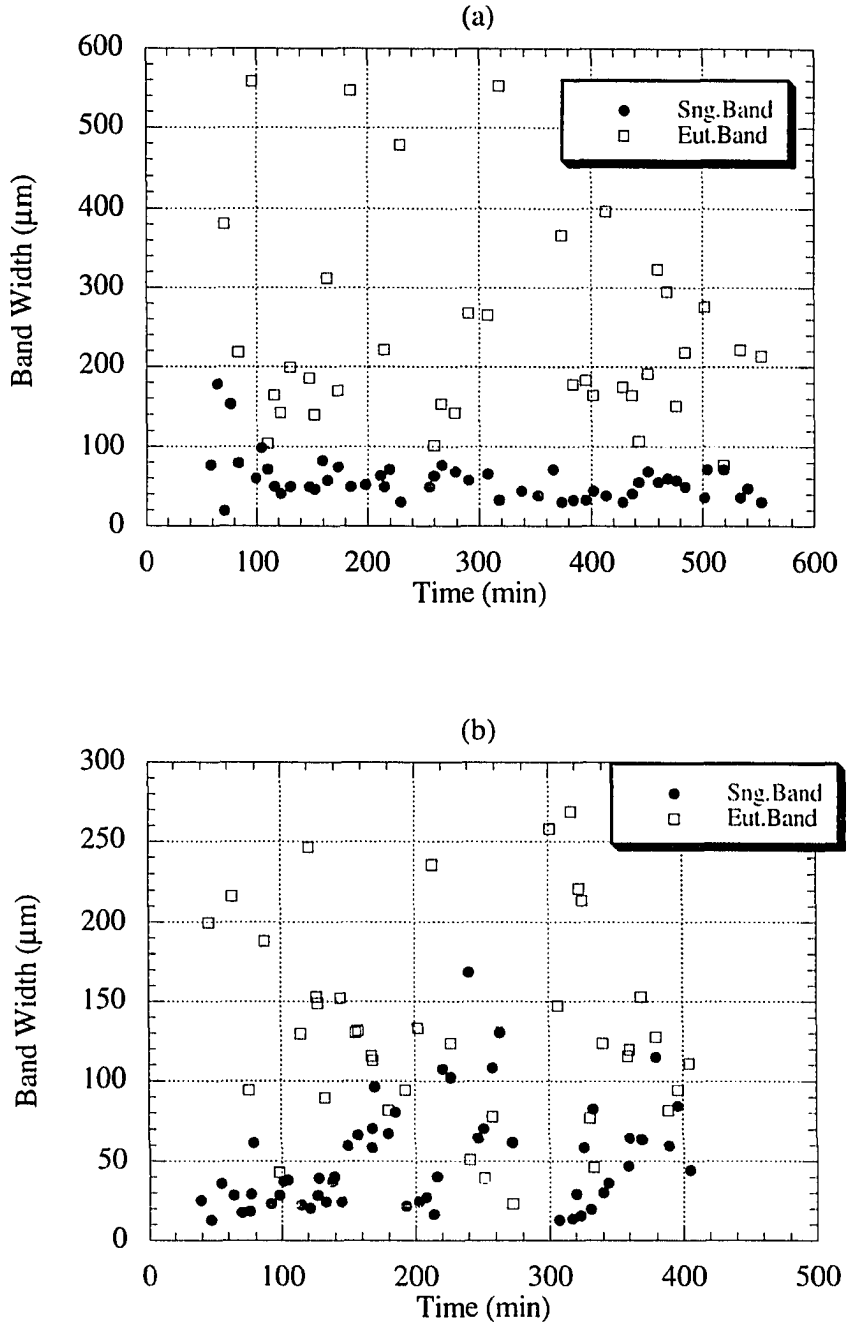

Figure 16. Variations in the band width with time (a) between eutectics and α single phase (C=7.96wt%, V=0.5μm/s) (b) between eutectics and β single phase (C=10.85wt%, V=0.5μm/s).

(4) Morphological Transitions

With the increases in the pulling velocity, it was observed that oscillations became less frequent both in the hypo and hypereutectic compositions. However, the detailed mechanisms by which the eutectics are broken down to the single phases are found to be slightly different from each other. Time sequence of the transition in hypoeutectic composition is shown in Figure 17. The single phase interface is shown to be perturbed at this velocity and then cellular growth was introduced after the oscillations. These cells became sharper in tips and got blunted as the velocity itself fluctuated. At higher velocity (V=1μm/s), the interface was composed of dendrites and interdendritic eutectics at this composition.

The transitions to the single phase dendrites from eutectics were studied by increasing the velocity in off-eutectic compositions. In the hypoeutectic composition of 7.96wt%, the velocity was increased to 0.7μm/s from 0.5μm/s after 14 hours and the relative position was examined with time again. This is shown in Figure 18. The figure shows short period of oscillations in the early part and then single phase started to lead the eutectics. The peak that is shown at around 900 minutes is related to the emergence of the single phase cells. Figure 18(b) illustrates the averaged actual velocities obtained from the relative position. The single phase velocity is found to be larger than that of eutectics with the single phase leading although the velocities were still fluctuating, especially when the single phase cells were appearing.

The transition in hypereutectic composition is shown in Figure 19. The oscillations in this composition were between β cells and eutectics as was mentioned in the previous section. The first micrograph in Figure 19 shows some coarsened and merged β cells after oscillations. Even after eutectics caught up the front, the most leading cell survived and one of them formed a β cell. This cell outgrew the others and eventually, formed a dendrite as shown in Figure 19(f). In this composition, since dendrites appeared at 0.5μm/s, this velocity was decreased step by step so as to study the disappearance of the dendrites. Verhoeven and Gibson [22] studied the hysteresis effect on the eutectic to dendrite transition in off eutectic compositions of

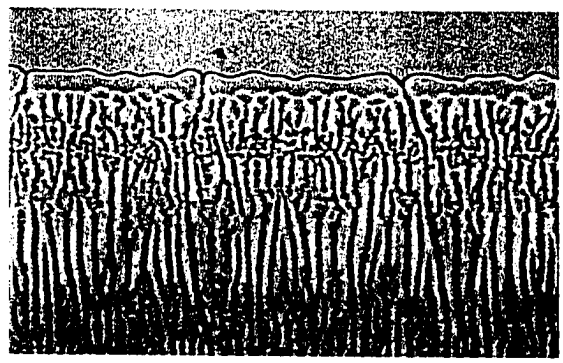

(a) t=862 min

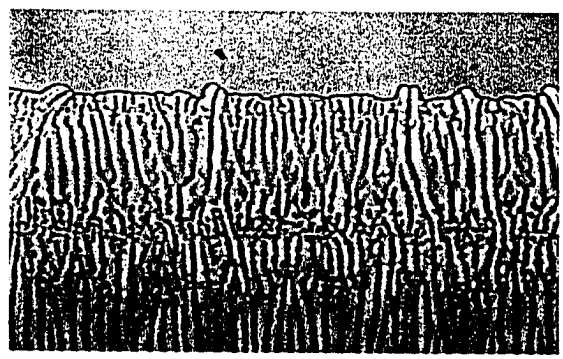

(b) t=871.2 min

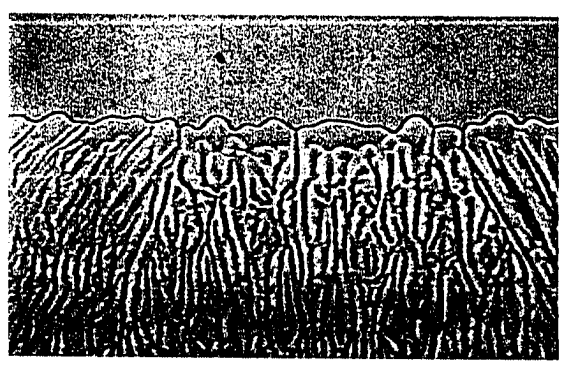

(c) t=875.4 min

Figure 17. Time sequence of dendrite appearance in hypo eutectic composition (C=7.96wt%) at V=0.7μm/s (a) t=862 min (b) t=871.2 min (c) t=875.4 min (d) t=890.6 min (e) t=898.6 min (f) t=904 min.

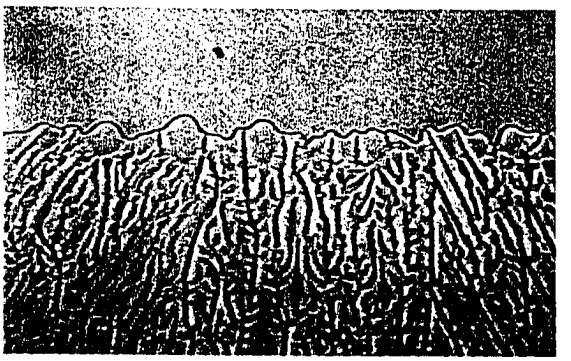

(d) t=890.6 min

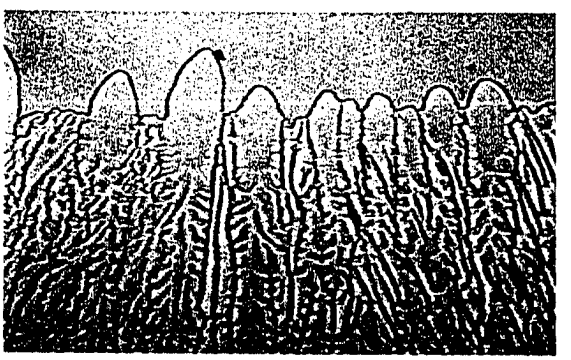

(e) t=898.6 min

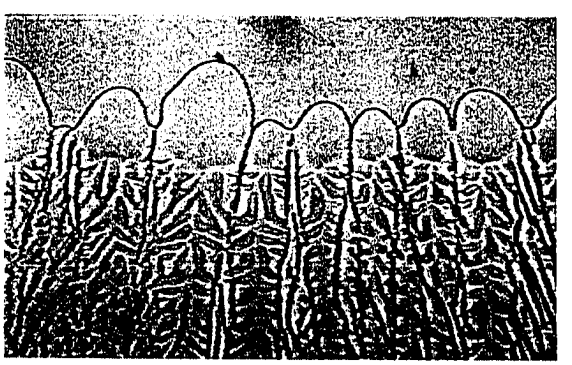

(f) t=904 min

Figure 17. Continued.

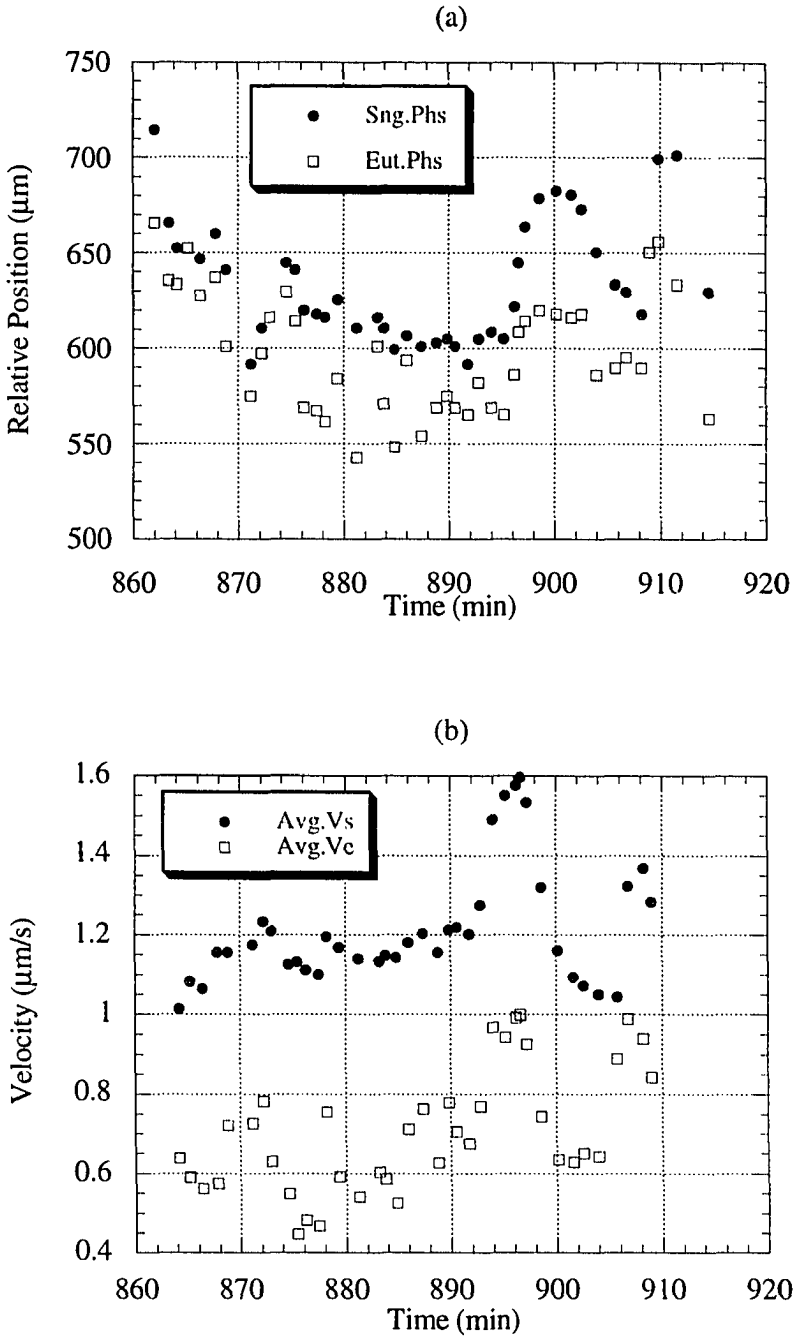

Figure 18. (a) Relative position, (b) Real velocity with time after the change in the velocity to V=0.7μm/s in hypoeutectic compostion (C=7.96wt%).

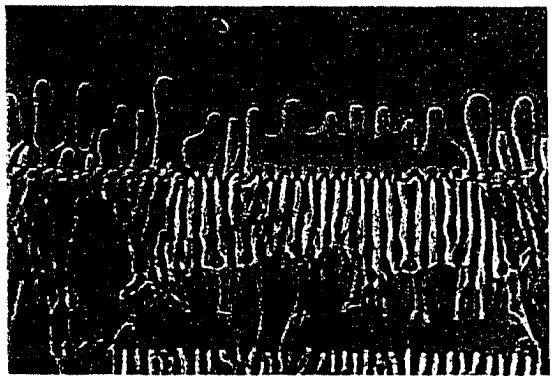

(a) t=395.9 min

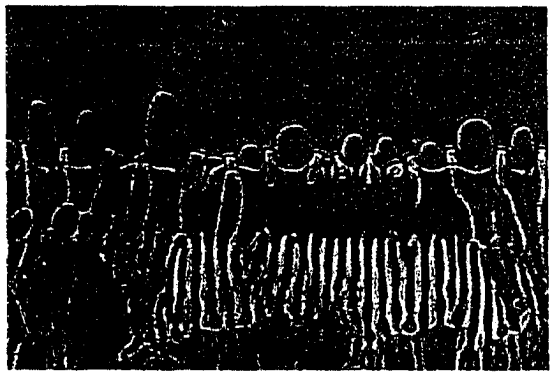

(b) t=398.5 min

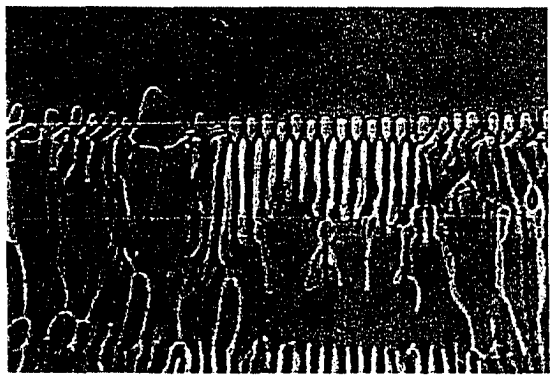

(c) t=403.1 min

Figure 19. Time sequence of dendrite appearance in hyper eutectic composition (C=10.85wt%) at V=0.5μm/s (a) t=395.9 min (b) t=398.5 min (c) t=403.1 min (d) t=411.8 min (e) t=424.4 min (f) t=435.2 min.

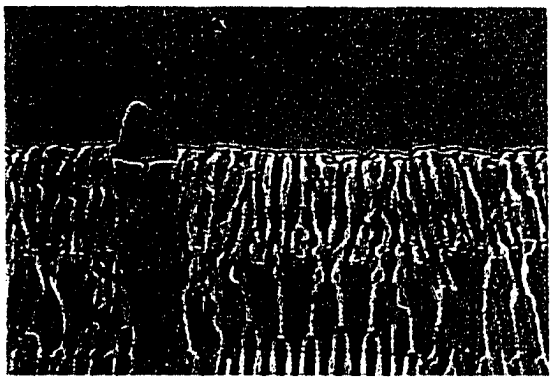

(d) t=411.8 min

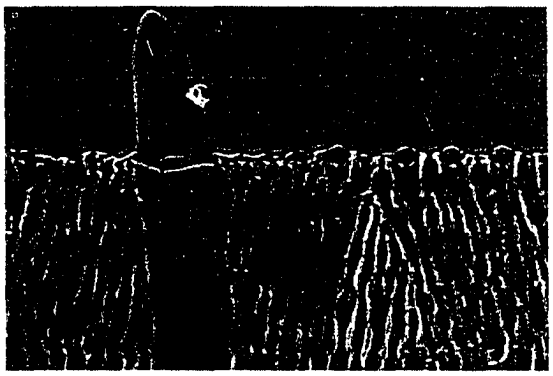

(e) t=424.4 min

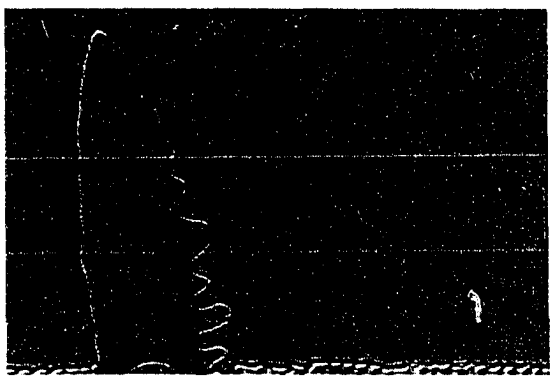

(f) t=435.2 min

Figure 19. Continued.

Sn-Pb alloys. They found that the dendrite appearance velocity was consistently higher than their disappearance velocity. The deceleration study here was aimed to confirm their findings and to examine its mechanism. The velocity was decreased from 0.5μm/s to 0.3μm/s after 8 hours. At V=0.3μm/s, the tips were found to become blunted and the dendrite length was observed to be shortened. This velocity was kept for 6 hours and then the velocity was reduced down to 0.2μm/s. The dendrite disappearance was observed at this velocity and it is shown in Figure 20. As shown in the figure, the dendrite tip was perturbed with short dendrite length. The disappearance was occurring gradually and the dendrite growth velocity became decelerated compared to the eutectic growth velocity. Finally, the dendrites were engulfed by the eutectics. Note the sample position was moved slightly to the left from Figure 20(e). It should be noted that the β phases were still leading even in the interdendritic eutectics as shown in Figure 20(c) in which the liquid composition in front of the growing interface was expected to be much closer to that of eutectic. This experiment confirms the results of Verhoeven and Gibson. However, in their study, most of the dendrites were nucleated from the wall. Therefore, their appearance velocities were not very much reproducible.

From our observations, it can be said that in hypoeutectic compositions, the single phase planar interface led the eutectics during the oscillations and as the velocity went up this planar interface was perturbed into single phase cells. The cells then finally turned into dendrites as the velocity was increased as known from the single phase instability. In hypereutectic sides, the β single phase was leading during the oscillation. These β phases were coarsened with time and some of the coarsened β cells survived the oscillations. These were grown out as dendrites with velocity increases. In these compositions, the single phase instabilities were not observed as in the hypoeutectic compositions.

The true eutectic velocities were compared with different compositions under a constant imposed velocity and the results are shown in Figure 21. It appears that the amplitude of the

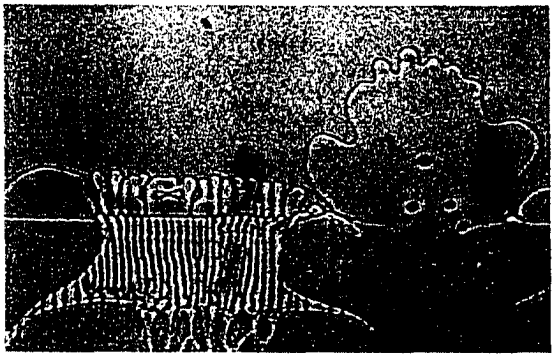

(a) t=1076. 1 min

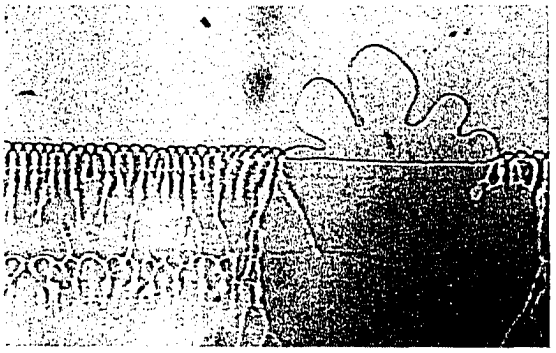

(b) t=1143.4 min

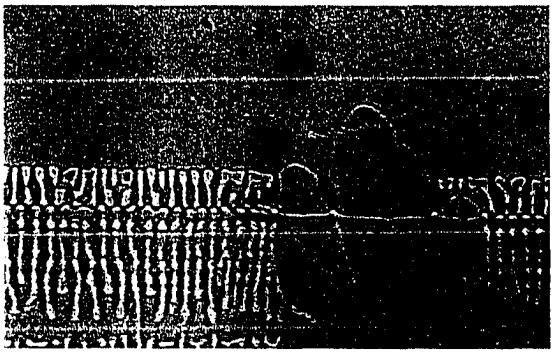

(c) t=1183.4 min

Figure 20. Time sequence of dendrite disappearance in hyper eutectic composition (C=10.85wt%) at V=0.2μm/s (a) t=1076.1 min (b) t=1143.4 min (c) t=1183.4 min (d) t=1222.1 min (e) t=1234.5 min (f) t=1255.1 min.

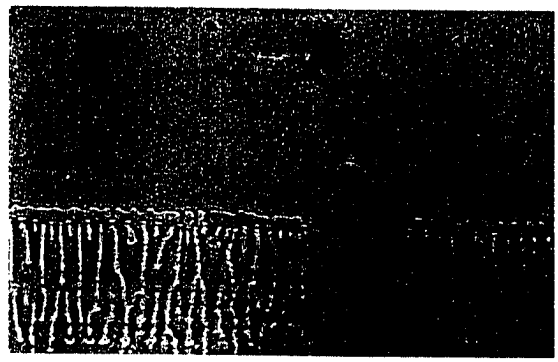

(d) t=1222.1 min

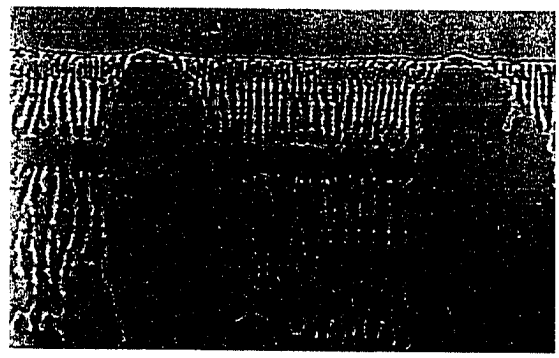

(e) t=1234.5 min

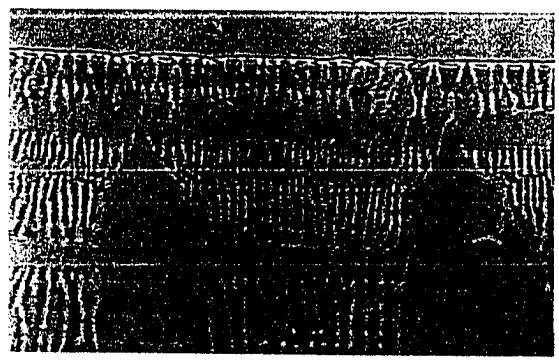

(f) t=1255.1 min

Figure 20. Continued.

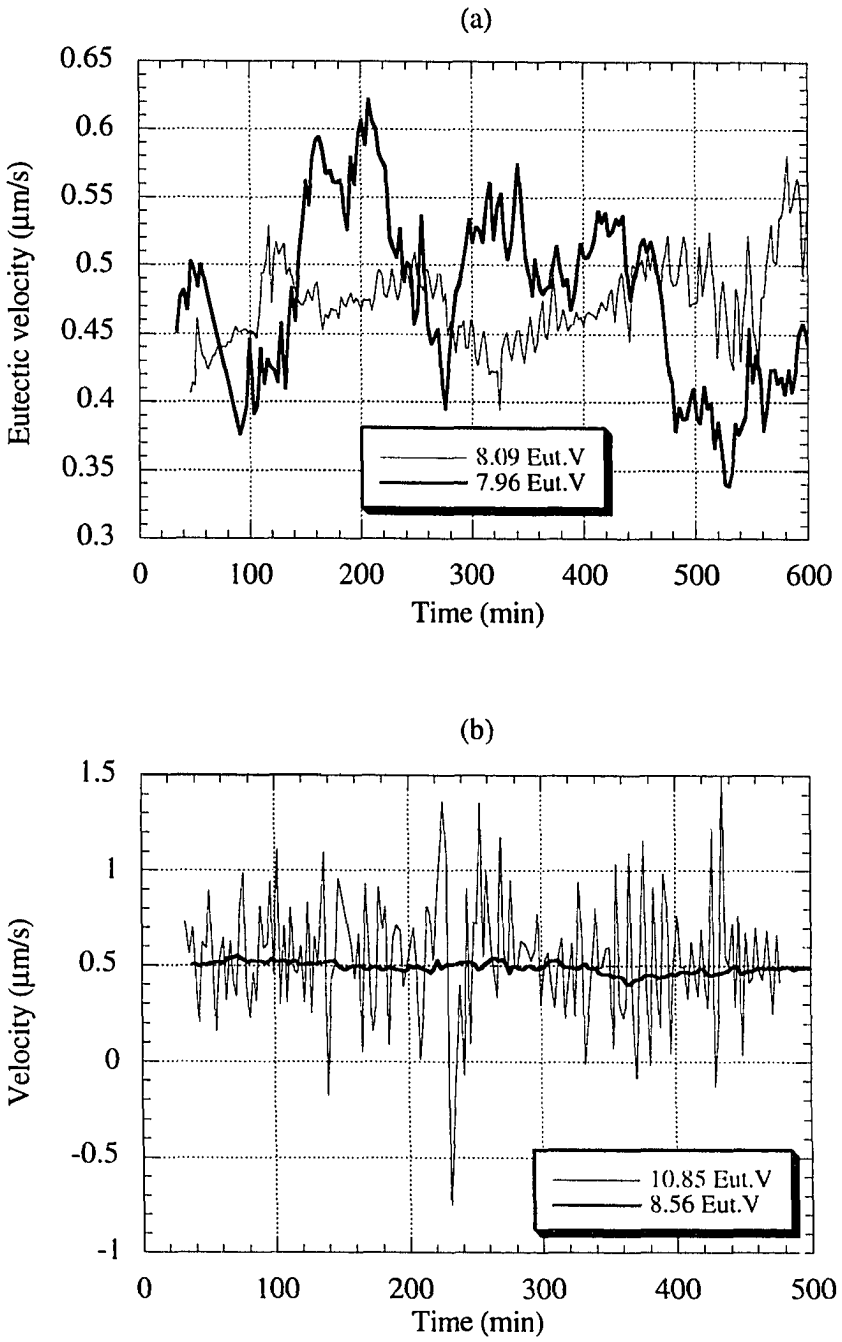

Figure 21. Comparisons of oscillations in the actual eutectic velocities with two different compositions under V=0.5μm/s. (a) hypoeutectic case, (b) hypereutectic case.

oscillation is increasing with the compositions away from the eutectic value. Figure 21(b) shows a distinct difference in the eutectic velocities between the two hypereutectic compositions. The difference in the amplitude seems to be larger in the hyper eutectic case than that in hypo. The reason for the discrepancies in the velocities may come from the competition of two different diffusional modes. As the composition departs from the eutectic value, the tendency toward long range diffusion will increase compared to the short range diffusion once the threshold condition is given. This can be seen clearly in Figure 21(b) in which the composition with thick solid line showed all eutectic microstructures. But the composition with thin line developed dendrites under the same velocity. The effect of the temperature gradient on the fluctuation in the velocity was examined in Figure 22. The temperature gradient used in composition 9.92wt% was 3.66K/mm. Since two parameters were different in this case, it is hard to single out one effect from the other. However, from the observation made so far, it seems that the temperature gradient effect might be smaller than that of composition on the velocity oscillation.

(5) Coupled Zone Concept

Calculated coupled zone and experimental velocity ranges from Table 2 and 3 are shown in Figure 23. The arrows and the bars in the figure represent the velocity ranges for each composition examined. The numbers shown in the figures are the compositions and the corresponding microstructures are written in the figures. E stands for the eutectic microstructure, and D+E represent the dendrites with the interdendritic eutectics. Osc means the oscillating microstructure between the eutectics and single phases. Only in composition of 10.85wt%, the final velocity was lower than the starting velocity. From these experiments, it is found that the oscillations were dominant in the lower velocity region especially in the hypoeutectic composition side. As the velocity increased, the single phase growth became predominant leading the eutectics. When the velocity crossed the coupled zone boundary in a

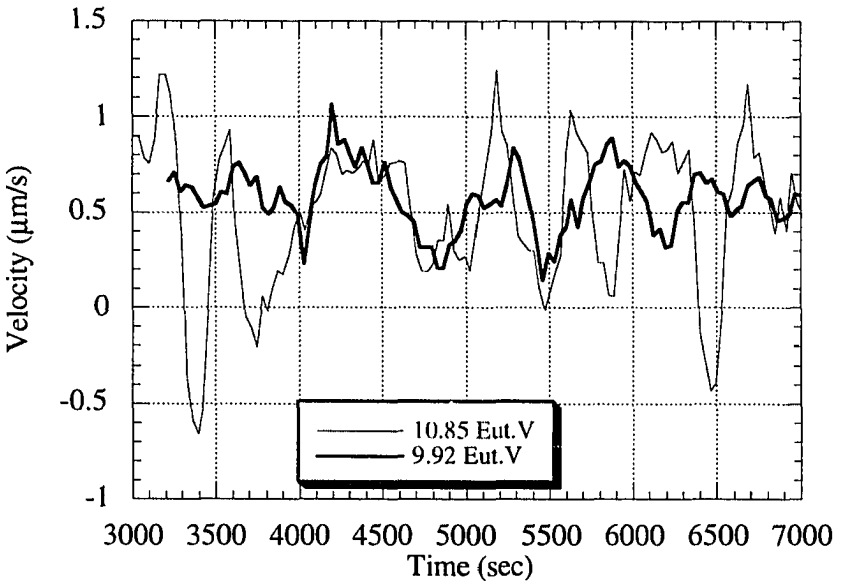

Figure 22. Comparison of the eutectic velocities in two different compositions and temperature gradients (C=9.92wt%, G=3.66K/mm) under the same imposed velocities (V=0.5μm/s).

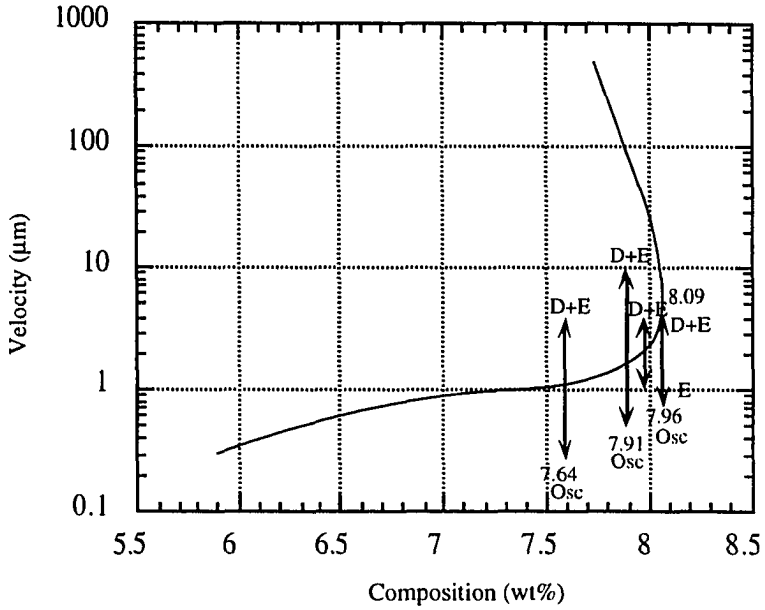

(a)

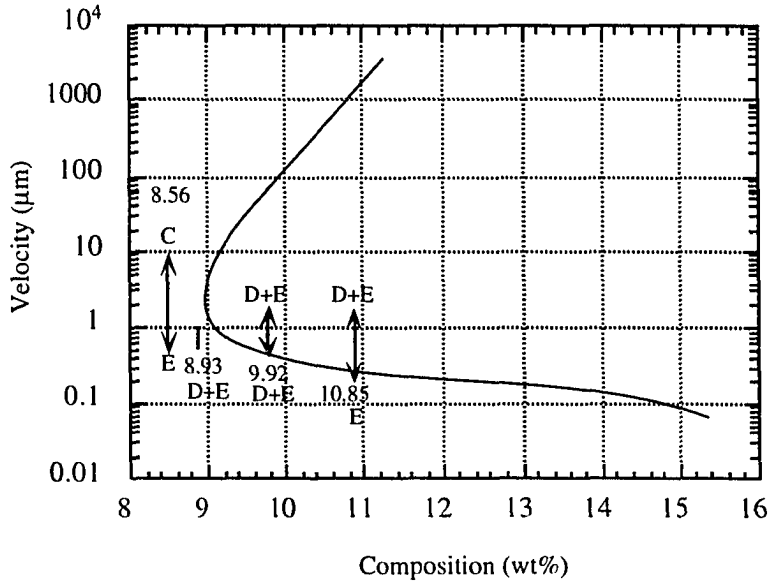

(b)

Figure 23. Calculated coupled zone boundaries with the ranges of compositions and velocities examined (a) in hypoeutectic, (b) in hypereutectic side.

given composition, the microstructure seemed to approach the next steady state condition which is the dendrite growth with the interdendritic eutectics. Therefore, it is expected that the steady state dendrite growth region might be located above the dotted lines in Figure 24. The same reasoning can also be applied to the eutectic growth. Thus, the steady state eutectic growth will be possible belower than the broken lines as can be seen in the figure. These broken lines are drawn lower than V=0.5μm/s in hypoeutectic composition because the oscillation was still existing at this velocity. Most of the oscillations were observed between the starting velocity and the coupled boundary. Therefore, it can be said that the oscillating zone might exist between the coupled zone boundary and above the steady state eutectic lines (broken lines). These velocity regions could be considered in a different way as in Figure 25. Figure 25(a) and (b) represent temperature changes with velocity in the single phase growth as well as the eutectic growth for the compositions of 7.96 and 10.85wt%. The two curves here are based on the steady state growth models of the dendrites and eutectics. The observed oscillating zone was lower than the cross over point in the hypoeutectic composition (a). However, in the hypereutectic composition (b), the observed velocity range was much closer to the crossover point. The plots in Figure 25 illustrate the eutectic growth would lead at lower velocity regions while the dendrite will lead the interface at higher velocity regime as the interface temperature is higher than that of eutectics. The ranges of the oscillation are placed in across the crossover points. These oscillating ranges will have finite sizes of band in the velocity and other single phase temperature curve for different compositions should be considered because there might be compositional changes associated with the velocity fluctuations. In this figure, the observed oscillating zones are marked for each compositions.

In this work, the transitions from the eutectic growth to the single phase dendrites were studied carefully. It was noted that the oscillations existed between the two steady states in the course of the transition and the dendrites were also developed from the instabilities. Conclusively, it seems that the transition is a dynamical process between the two different

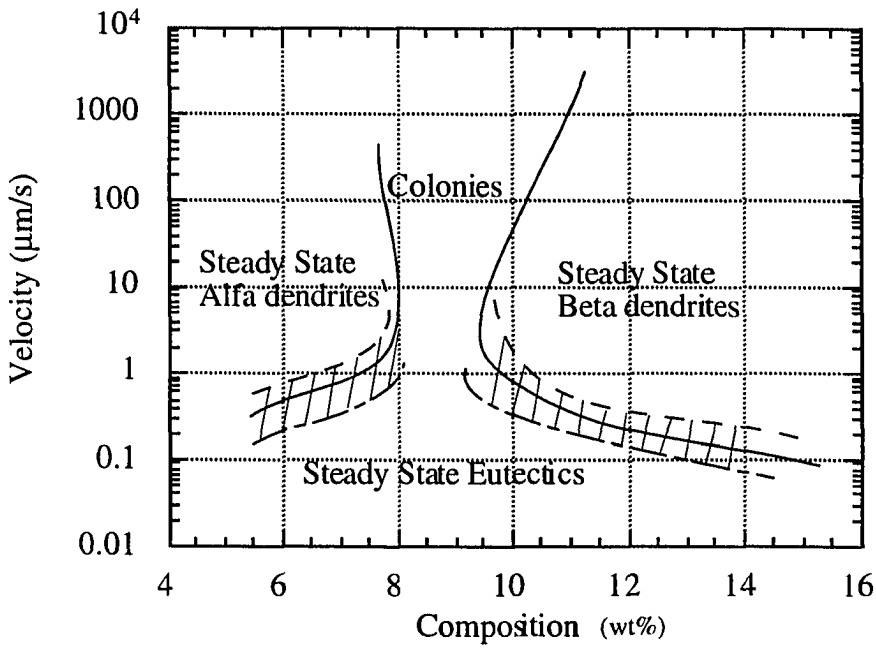

Figure 24. Coupled zone boundary with different microstructural regimes. The hatched regions show where continuous and damped oscillations were observed.

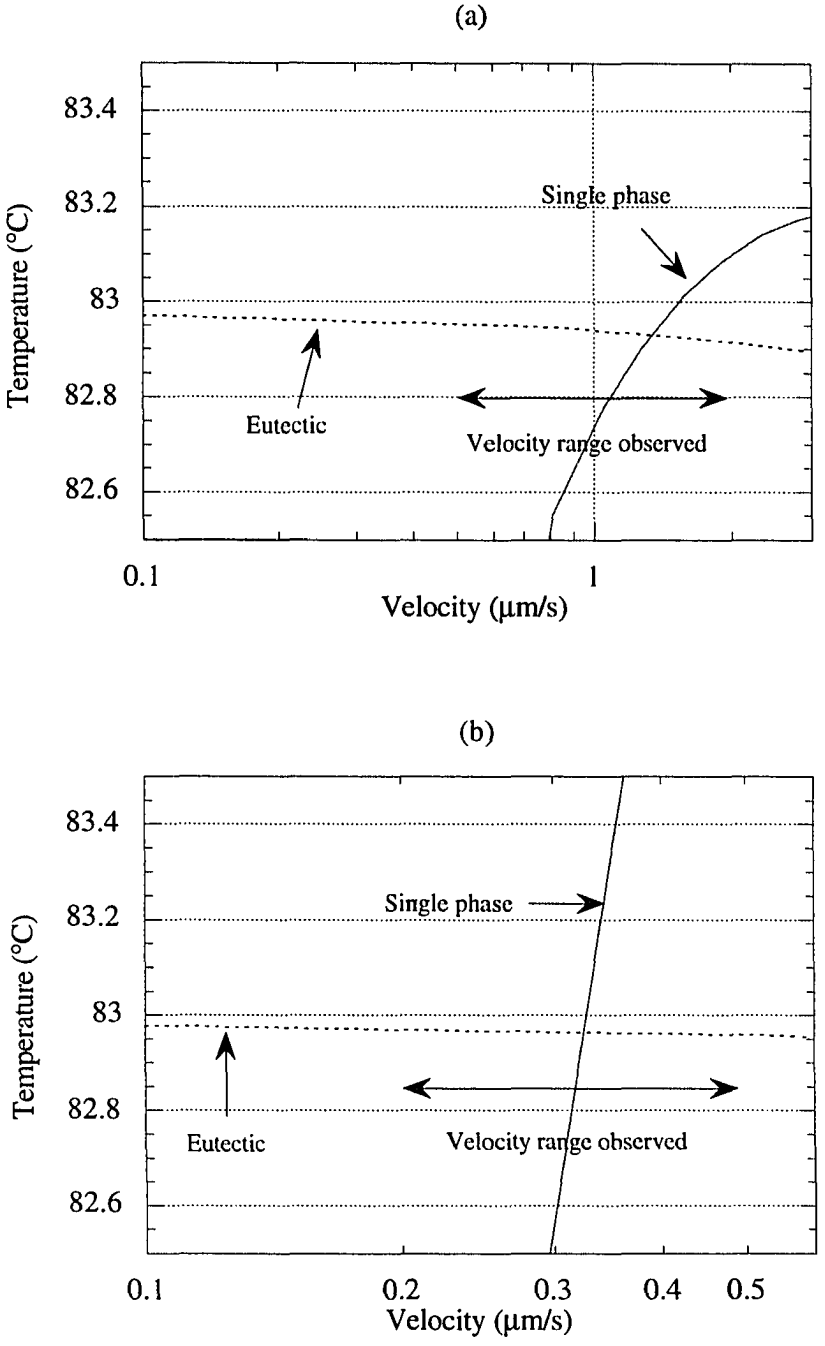

Figure 25. Velocity ranges examined with steady state models on eutectic and dendrite growth for two different compositions (a) C=7.96wt% (b) C=10.85wt%.

steady states in which two different diffusional patterns are competing. Whenever, the short range diffusion is preferred, the eutectics would form in the front. On the other hand, when the long range diffusion is dominant, the single phase growth leads the eutectics.

(6) Comparison with Oscillatory Structures in Other Systems

In this section, the oscillations will be considered first as to why this happens and what might be the driving force of this. Later on, the transition will be also considered in the context of the oscillations.

Recently, Warren and Langer [23] studied charateristic dynamics for the dendritic growth during the directional solidification. Analytical model was proposed showing that the initial motion of the material is proportional to $t^{3/2}$. The main feature of their theoretical work is the prediction of the oscillatory approach to the steady state. However, this theory is restricted in its applications to the earlier part of the initial transient with the planar morphology before the onset of the planar instability.

Park and Trivedi [24] in their recent experimental work observed the fluctuations in the actual interface velocity not only for the planar during the initial transient but also for the cellulars and dendrites throughout the entire period of experiments. The similar observation has been made in our present work. Therefore, this fluctuation in the velocity should be an universal phenomenon regardless of the morphologies. Banded structures have also been observed during the rapid solidification process by several investigators, as described by Zimmermann [10] and Carrard et al. [11]. Similarly, banded structures have been observed in peritectic systems in which alternate bands of primary phase and peritectic phase form. In all these cases, the banded structure is observed at the condition where the competitive growth model shows a transition in phases or microstructures.

IV. Conclusions

The competitive growth model has been critically examined through the careful experiments around the threshold conditions. Coupled zone boundaries were calculated first and the experimental conditions were determined from these. It was observed that oscillations in the morphologies between the two stable microstructures occur when the given condition is close to the critical value for the transition. The actual velocities were measured for the two different morphologies and eutectic velocities were found to be fluctuating more than those of single phases. These fluctuations in the eutectic velocity were also observed to be a strong function of the compositions. Fluctuations increased as composition deviated from the eutectic composition. The oscillations seem to be a procedure through which microstructural selection is made. Therefore, when the given condition is large enough to cause the transition, the duration time for the oscillations is short. Oscillation is considered to be caused by the interaction between the imposed velocity and the diffusion layer in the system. When the given condition is close to the transition, two different types of diffusional patterns are competiting each other resulting in the morphological oscillations.

The transition from the eutectic to single phase dendrites were observed for hypo and hypereutectic compositions. One of the phase outgrew the other through the oscillations. The dendrite appearance velocity was proved to be higher than the disappearance velocity as was previously reported [22].

Associated with oscillations, the bandings between the single phases and eutectics were observed. It was found that the sizes of bandings would be comparable with when the selection was occurring. Otherwise, the magnitudes of the each band were maintained with their oscillations.

Experimental results revealed new observations and facts that were not expected from the well-known Competitive Growth Model (CGM). One of the possible reason why CGM does not predict any of the oscillations and followed single phase instabilities is that the model

was proposed on the bases of two different steady state growth models (Eutectic and Dendrite growth model). When the transition really occurs from the eutectics to single phases, it is found that the steady state growth models could not be applied directly anymore because the actual velocity was not equal to the imposed velocity.

Acknowledgements

The authors would like to thank Philip Gilgien and Professor Wilfred Kurz for providing the program for the coupled zone calculation. The appreciation is also extended to Jeff Jensen and Professor Jang-sik Park for comments on the program and for valuable discussions.

This work was carried out at Ames Laboratory, which is operated for U.S. Department of Energy by Iowa State University under contract No. W-7405-ENG-82. This work was supported by the Office of Basic Energy Sciences, Division of Materials Sciences.

References

1. G. Tammann and A. A. Botschwar: *Z. anaorg. Chem*, 1926, vol. 157, p. 27.
2. A. Kofler: *J. Aust. Inst. Met.*, 1965, vol. 10, pp. 132-39.
3. J. D. Hunt and K. A. Jackson: *Trans. AIME*, 1967, vol. 239, pp. 864-67.
4. K. A. Jackson: *ibid.*, 1968, vol. 242, pp. 1275-79.
5. F. Mollard and M. C. Flemings: *ibid.*, 1967, vol. 239, pp. 1526-46.
6. M. H. Burden and J. D. Hunt: *J. Cryst. Growth*, 1974, vol. 22, pp. 328- 30.
7. D. J. Fisher and W. Kurz: in *Solidification and Casting of Metals*, Metals Soc., London, 1978, p. 57
8. W. Kurz and D. J. Fisher: *Int. Met. Rev.* 1979, p 177
9. R. Trivedi and W. Kurz: in *Solidification Processing of Eutectic Alloys*, D. Stefanescu and G. J. Abbaschian, eds., AIME, Warrendale, PA, 1988.

10. M. Zimmermann, M. Carrard, M. Gremaud, and W. Kurz: *Mater. Sci. Engng.* 1991, vol. A134, p. 1278

11. M. Carrard, M. Gremaud, M. Zimmermann, and W. Kurz:. *Acta. Metall.* 1992, vol. 40, p. 983.

12. M. Zimmermann, M. Carrard, and W. Kurz: *Acta. Metall.*, 1989, vol. 37, pp. 3305-13.

13. W. J. Boettinger: *Metall. Trans.*, 1974, vol. 5, pp. 2023-31.

14. R. Trivedi: *Metall. Trans.*, 1995, vol. 26A, pp. 1583-90.

15. R. Trivedi and W. Kurz: *Int. Met. Rev.*, 1994, vol. 39, pp. 49-74.

16. P. Gilgien and W. Kurz: unpublished work, Swiss Federal Institute of Technology, 1993.

17. L. M. Fabietti: Ph.D. Thesis, Iowa State University, Ames, IA, 1990.

18. W. Kurz and D. J. Fisher: *Fundamentals of Solidification*, Trans Tech Publications, Aedermannsdorf, 1992.

19. J. Mergy, G. Faivre, C. Guthmann, and R. Mellet: *J. Cryst. Growth*, 1993, vol. 134, pp. 353-68.

20. W. F. Kaukler: Ph.D. Thesis, University of Toronto, Toronto, ON, Canada, 1981.

21. V. Seetharaman and R. Trivedi: *Metall. Trans. A*, 1988, vol. 19A, pp. 2955-64.

22. J. D.Verhoeven and E. D. Gibson: *Metall. Trans.*, 1972, vol. 3, p. 1893

23. J. A. Warren and J. S. Langer: *Phys. Rev. E*, 1993, vol. 47, pp. 2702-12.

24. J. S. Park and R. Trivedi: Iowa State University, Ames, IA, unpublished research, 1995.

25. S. H. Han: M. S. Thesis, Iowa State University, 1991.

CHAPTER 5: GENERAL CONCLUSION

Experimental studies have been carried out to examine the transition from a planar to two-phase cellular and dendritic strucutures in a ceramic system of Al_2O_3-ZrO_2 and in the transparent organic system of carbon tetrabromide and hexachloroethane (CBr_4-C_2Cl_6). Several aspects of eutectic interface stability have been examined, and they include the condition for the instability of a planar interface, mechanisms of transition from eutectic to the cellular/dendritic structures, the dynamics of the competition process between the eutectic and the single phase, and the characterization of steady-state spacing and interface temperature of the two-phase cellular/dendritic interface.

I. Alumina-Zirconia Eutectic System

Directional solidification studies in Al_2O_3-ZrO_2 eutectic system shows the eutectic microstructures to consist of rods of ZrO_2 in an Al_2O_3 matrix. Colony growth was found to be prevalent in all samples resulting from the presence of third elements such as Ta, Y_2O_3, and Sc or impurities. In addition to colony formations, faceted Al_2O_3 dendrites and non-faceted ZrO_2 dendrites were observed when the ceramic sample was solidified outside the coupled zone. When the velocity was extended to the rapid solidification regime, the Al_2O_3 dendrties were found to grow in a non-faceted manner due to the formation of metastable Al_2O_3 at large undercoolings. A similar transition in colony structure was also observed in that the colonies became fan like at high velocities.

Eutectic spacings at the center of the colony, measured from the extended velocity regime, showed deviations from the existing model. This departure is due to the presence of a nonplanar eutectic interface which alters the eutectic spacing in the center of the colony. The colony spacing was found to be at least 10 times larger in size than that of eutectic, and showed a spacing variation analogous to that for the single phase dendrite. This is because

both these spacings are governed by the long range diffusion of the third element around nonplanar interfaces. The general trend in eutectic, colony and primary dendrite spacing variation with velocity was found to be similar, and detailed theoretical models are required to quantitatively assess the magnitude of these changes.

II. Colony Formation during Eutectic Growth

The dynamical aspect of colony formation was examined in a transparent organic analog system, and mechanisms by which the planar eutectics broke down to form colonies were examined. Colonies were found to initiate from the grain boundary area, and repeated splittings were observed to lead the morphological change. Two different types of colonies were noted: fan type and needle type. Needle type colonies were found to form along the preferred orientation.

In order to characterize colony growth, the interface temperatures and colony spacings were measured as a function of growth velocity. The interface temperature and the colony spacing both showed maximum in their measured values at about the same velocity. Eutectic spacings were measured from the central parts of the colonies. It was found that when the planar eutectic undergoes the instability to form cellular eutectic, the eutectic spacing increases slightly. The eutectic spacing went through a maximum value, and then decreased as the velocity was increased in the dendritic colony regime. It was postulated that the variation in the eutectic spacing is significantly influenced by the nonplanarity of the interface.

The variations in the interface temperature and colony spacings were very analogous to the case of single phase growth. Thus, the basic ideas of single phase growth were used to explain the experimental results. It is shown that a theoretical model for nonplanar eutectic needs to be developed to examine the temperature and scaling laws for two-phase cellular and eutectic colonies.

III. Oscillating Microstructures in Eutectic Growth

The instability of eutectics into a single phase formation has been studied with critical experiments around the transition conditions. Current models of transitions are based on the competitive growth model which assume that the microstructure that will be stable in the directional solidification is the one that grows with a higher steady-state interface temperature. The relative interface temperatures are calculated under the assumption of steady-state values of each microstructure. When the actual transition occurs, both microstructures are present and near the transition there is a significant interaction between them. In addition, as the velocity of the interface increases near the transition region, dynamical effects of interface motion become important. The increase in velocity gives rise to oscillating behavior which is caused by the solute diffusion constraint. Experimental studies have shown that these interactions give rise to oscillations between the two stable morphologies around the threshold conditions. The effect of velocity on the oscillation has been examined quantitatively, and it was found that the oscillations decrease as the velocity is increased. A finite band of velocity was observed in which oscillating structures were found to exist. Furthermore, the composition of the alloy showed a large effect on the oscillation of the actual interface velocity. The oscillation was found to increase as the alloy composition deviated further from the eutectic composition. Under directional solidification, the microstructure selection is generally based on the steady-state growth condition in which the interface velocity is assumed to be the same as the externally imposed velocity. Our studies have shown that a new class of structures is formed in which there is an oscillation in the interface velocity which can give rise to banded microstructures of two-phases. These studies compliment the studies of banded structures in single phase growth at high velocities and in peritectic alloys at low velocities, and they demonstrate that transition from one phase

(or microstructure) to the other is generally accompanied by the presence of oscillating or banded structures.

ACKNOWLEDGMENT

To the largest degree I am grateful to my major professor, Dr. Rohit K. Trivedi, for giving me the opportunity to work under his guidance. His continuing interest in this work, the constructive criticisms, and valuable suggestions made this work possible. Many years that I spent working with Dr. Trivedi has given me a deep appreciation of his vast knowledge. Further more, and more importantly, he has given me his personal support and encouragement throughout my studies.

I would also like to thank Dr. Iver Anderson, Dr. Chris Schilling, Dr. Palaniappa Molian, Dr. Micheal Tringides, and Dr. John Verhoeven for their service on my graduate committee.

I am indebt to the people in our solidification group who have been providing advice and valuable discussions as well as good laughs during the past few years. Particularly, I would like to thank John Mason, Dr. Luis Fabietti, Dr. Haik Jamgotchian, Dr. Mark Eshelman, and Dr. Jang-sik Park for sharing their knowledge with me. My thanks also go to Dr. Steve Mashl and Dr. Kate Zeisler-Mashal, Edmund Wanut, Chris Boldts, Chris Nodlund, Seong Tcho Kim, David Norman and Andy Flores for their support, and stimulating conversations and friendships.

I also could not forget Patti Boone and Jeff Jensen for answering all my trivial and tedious questions during all this time.

My special thanks are due to the love of my parents and my two brothers who always believe in me and encourage me to carry on my dreams through their uncountable prayers. Without their love and understanding, my studying could not be realized. I am also very grateful to my wife, Seaeun who has been there to rejoice our happy moments and comfort in the difficult times. She made this work possible, necessary, and bearable.

My final appreciation is extended to him who has been always with me and speaks to me "The Lord will keep your going out and your coming in from this time on and forevermore" (Psalm 121:8).

This work was performed at Ames Laboratory under Contract No. W-7405-Eng-82 with the U.S. Department of Energy.